EXPLORING THE ROLES OF NITRIC OXIDE PRODUCTION IN THE COCCOLITHOPHORE *EMILIANIA HUXLEYI*

By

BRITTANY MARIE SCHIELER

A dissertation submitted to the

School of Graduate Studies

Rutgers, The State University of New Jersey

In partial fulfillment of the requirements

For the degree of

Doctor of Philosophy

Graduate Program in Oceanography

Written under the direction of

Kay D. Bidle

And approved by

_____

_____

_____

_____

New Brunswick, New Jersey

May 2019

ABSTRACT OF THE DISSERTATION

Exploring the Roles of Nitric Oxide Production in the Coccolithophore *Emiliania huxleyi*

By BRITTANY MARIE SCHIELER

Dissertation Director:

Kay D. Bidle

Nitric oxide (NO) is a gaseous, membrane-permeable free radical that has emerged in recent decades as a ubiquitous inter- and intra-cellular signaling molecule in all kingdoms of life. Despite the abundance of work elucidating the physiological functions of NO, a number of important open questions remain about its biology, especially in photosynthetic organisms. This dissertation expands the current state of knowledge of NO ecophysiology to the marine phytoplankton *Emiliania huxleyi. E. huxleyi* is a globally important bloom-forming species of coccolithophore, a group of calcifying eukaryotic marine algae. *E. huxleyi* exerts a profound influence on the marine ecosystem in a number of ways including producing a significant portion of marine calcium carbonate, fixing inorganic carbon, modulating biogeochemical cycling of important elements, and impacting climate. *E. huxleyi* is perhaps best known for its vast blooms being routinely infected and terminated by viral infection.

This work shows that NO production is a hallmark of early- to mid-lytic viral infection both in laboratory cultures and in natural *E. huxleyi* populations encountered in the North Atlantic. It provides evidence that NO produced during infection may have an antioxidant function by upregulating and activating the diverse enzymatic

antioxidant machinery, minimizing intracellular oxidative stress during infection so that viruses may replicate and assemble in a redox favorable environment. This dissertation further explores the relationship between NO production, oxidative stress, and antioxidant activity by surveying these traits in various laboratory *E. huxleyi* strains that differ in their inherent susceptibility to viral infection. Significant intra-species variability was observed in the production of NO across a gradient of viral susceptibility, along with gradients in basal antioxidant capacity and production of reactive oxygen species (ROS). The possible relationship between NO, ROS, and antioxidant activity is discussed, as well as implications for costs-of-resistance. An important outcome of this work is the observation that intracellular NO patterns are manifested in the extracellular milieu, indicating that algal diversity and physiology may be important in dictating whether marine microbial populations represent a net source of NO_x to the environment. Lastly, this work sheds light on the possible biosynthetic pathways of NO and the NO-mediated protein post-translational modifications relevant to *E. huxleyi.* This dissertation concludes with a summary of the main findings along with a discussion of the broader impacts, open questions, and future directions.

DEDICATION

To my daughter, Emma Marie, who has made this scientist believe in miracles.

To you I dedicate this dissertation,

which was made possible by the tireless efforts of my mother and

all of the women who came before us.

May you carry on this tradition and follow your dreams fearlessly,

wherever they take you.

ACKNOWLEDGEMENTS

I would like to thank my advisor and mentor, Kay Bidle, for his unwavering support and guidance throughout my graduate career. You took a chance on someone with no background in microbiology and fully welcomed me into your lab and integrated me into your fascinating work. For this, and for all of the wonderful opportunities you have given me, I will be forever grateful.

I would also like to thank the members of my Ph.D. committee, Donald Hirsh, Kim Thamatrakoln, and Adam Kustka for their generosity with their time, scientific knowledge, and laboratory resources. I have truly enjoyed working closely with each of you and collaborating on various aspects of this project.

I was lucky to work with two talented undergraduate students during my graduate work, Carlyn Wefer and Megha Soni, both of whom have been vital to the completion of this dissertation. I am especially grateful to Soni for independently carrying on the mission of this work while I was on maternity leave.

Those lucky enough to become part of the Bidle Lab know that this group of people functions just as much a family as a research group. In the "order of appearance" I would like to thank Chris Brown, Frank Natale, and Liti Haramaty for all of their technical assistance and generosity with their know-how to make this work possible. To Frank, thank you for not only teaching me all you know about flow cytometry, but being a great friend and officemate during this experience. I also want to thank all of the Bidle Lab's post-docs, graduate students, and technicians for their fruitful discussions, friendship, and support over the years: Christien Laber, Mansha Seth-Pasricha, Chris

Johns, Mike Maniscalco, Chris Maniscalco, Jozef Nissimov, Maeve Eason Hubbard, Jason Lathom, Ben Knowles, Chana Kranzler, Austin Grubb, Karen Bondoc, Ben Diaz, and Dina AlRoumi. I especially want to thank Christien for being a dear friend and fieldwork companion from day 1 in the program.

I am extremely grateful to have met so many life-long friends here at Rutgers, especially my cohort. To Alex Lopez, Zoe Vybiral-Bauske, Nicole Waite, Jack McSweeney, Filipa Carvalho, Nicole Couto, and Katie Harazin- thank you so much for all the wonderful memories including our infamous hurricane party, girls' nights, and OTB cocktail hours. To Alex and Zoe- a special thank you for convincing me and Kevin to bring a little fur baby into our life! But no, I still don't want a lizard.

I want to thank all of the wonderful faculty and staff at DMCS who have supported me in so many ways during my time at Rutgers. Thank you to my professors Liz Sikes, Silke Severmann, Gary Taghon, Lee Kerkhof, John Wilkin, Bob Chant, Jim Miller, and Heidi Fuchs for helping me to become a well-rounded oceanographer. Thank you to Sarah, Donna, Patty, and all of the front office staff. Also, thanks to the IT team for helping me with everything catastrophic to silly, including all the times I forgot the password to my WordPress website!

The completion of a Ph.D. would have never been possible without the support of my incredible parents. Mom and Dad- it is only because of your generosity, sacrifices, emphasis on the importance of education, and example of hard work (and babysitting!) that I am here today. I also want to acknowledge my two amazing siblings Allison and C.J., who's own artistic creativity is a constant source of awe and inspiration to me. I also want to thank my family- my loving grandmother, aunts and uncles, and cousins for

always taking an interest in my work and being constantly supportive. I couldn't have made it here without all my "Family Ties."

And finally, I would like to thank my wonderful husband and best friend Kevin. It seems like just yesterday we were two kids at the University of Delaware chasing a crazy dream of becoming marine biologists. Without your constant love, support, and pep talks I know I would not have made it here in one piece. I look forward to all our future has in store for us, especially raising our own little oceanographer!

Funding

This dissertation has been funded in part by graduate and teaching assistantships from the Rutgers' Graduate Program in Oceanography, along with grants from the Gordon and Betty Moore Foundation (grant #3789 to KDB) and the National Science Foundation (grants OCE-1061833 and OCE-1537951 to KBD).

TABLE OF CONTENTS

LIST OF TABLES

Chapter 2

Chapter 3

Chapter 4

LIST OF FIGURES

Chapter 1

Chapter 2

Chapter 4

Chapter 5

CHAPTER 1: Introduction

1.1 *EMILIANIA HUXLEYI*

Marine phytoplankton- single-celled, photosynthesizing oceanic "drifters"- account for nearly 50% of the net global primary production (Field et al. 1998). These microbes, therefore, constitute the majority of the base of marine food webs, fuel oceanic biogeochemical cycling, and significantly alter seawater chemistry. The impact of phytoplankton extends well beyond the ocean. One out of every two breaths of oxygen we take was produced by the photosynthesis of a marine phytoplankter. In fact, marine prokaryotic phytoplankton were the inventors of oxygenic photosynthesis about 3 billion years ago, leading to the oxidation of the atmosphere (Dismukes et al. 2001, Bekker et al. 2004, Kopp et al. 2005).

Coccolithophores are eukaryotic marine phytoplankton that produce intricate calcium carbonate shells called coccoliths. *Emiliania huxleyi* is by far the most abundant coccolithophore species and can be found throughout the world's oceans, excluding polar regions (Paasche 2002, Winter et al. 2014). *E. huxleyi* forms extensive blooms in the North Atlantic that are on the order of hundreds of thousands of square kilometers in area (Holligan et al. 1993, Brown & Yoder 1994, Tyrrell & Merico 2004). These blooms, which can exceed 10^6 cells per liter (Holligan et al. 1993), have a significant impact on biogeochemical cycling of important elements in the ocean, particularly carbon and sulfur, as well as regional climate patterns. As both a fixer of inorganic carbon, as well as one of the dominant calcifiers in the ocean, *E. huxleyi* has a significant, yet poorly constrained, influence on the biological carbon pump (Klaas & Archer 2002, Rost & Riebesell 2004). *E. huxleyi* blooms are also responsible for production of dimethylsulfoniopropionate (DMSP), the biologically-mediated cleavage of which leads

to atmospheric flux of dimethylsulfide (DMS), a trace gas that nucleates to cloud formation (Malin & Steinke 2004). Additionally, *E. huxleyi* blooms cause increased albedo and heating of the surface ocean due to the optical properties of their coccoliths (Tyrrell et al. 1999) .

E. huxleyi is also notable for the fact that its extensive blooms are routinely terminated by viral infection (Bratbak et al. 1993, Brussaard et al. 1996, Schroeder et al. 2002, Martinez et al. 2007, Vardi et al. 2012, Lehahn et al. 2014, Laber et al. 2018). Unlike viral infection in most marine phytoplankton hosts, during which cell lysis is thought to shunt fixed carbon through the microbial loop and away from various export fluxes (Fuhrman 1999, Suttle 2007), recent evidence suggests that infection of *E. huxleyi* by *Coccolithoviruses* (EhVs) may actually facilitate sinking of particulate carbon (Laber et al. 2018, Sheyn et al. 2018). This is believed to be due to the increase in production of transparent exopolymeric particles (TEP) during infection, acting to aggregate cells and the dense calcium carbonate coccoliths (Vardi et al. 2012, Laber et al. 2018). Due to the ubiquity of viral infection in this species, along with the range of molecular tools and laboratory strains available to study infection, the *E. huxleyi*-EhV system has emerged as one of the best-described model systems for viral infection in marine eukaryotic microalgae (Bidle & Vardi 2011, Bidle 2015).

Given their environmental and ecological significance, understanding the molecular processes regulating the growth, death, and fate of *E. huxleyi* cells is an active area of research. One molecular process of interest is the signal transduction coordinated by the free radical nitric oxide (NO). The NO radical is a small, diatomic and reactive gas that has emerged in recent years as an extremely important and surprisingly diverse

signaling molecule in all domains of life (Feelisch & Martin 1995). Once believed to only be a toxic by-product of fossil fuel combustion, the discovery of NO as an endogenous signaling molecule in mammalian endothelial cells lead to the 1998 Nobel Prize in Medicine and Physiology. Since its discovery in mammals, NO has been implicated in a vast list of biological processes including intercellular communication, immunity, programmed cell death, stress surveillance and response, and normal growth and development in animals, plants, unicellular algae, and bacteria (Moncada 1999, Besson-Bard et al. 2008, Gusarov et al. 2009, Kumar et al. 2015). Despite decades of immense focus on the molecular life of *Emiliania huxleyi*, little work has been done to understand the potential roles of this extremely important and versatile molecule in its ecophysiology.

1.2 NITRIC OXIDE BIOCHEMISTRY

Nitric oxide is involved in incredibly diverse, even opposing, cellular functions across biology and this is due to its unique and complex chemistry, some of which is still under debate (Toledo & Augusto 2012). NO has an unpaired electron in the pi antibonding orbital, making it a free radical. It is uncharged, has a relatively poor solubility in aqueous solution, and is more lipohilic in nature, allowing it to readily diffuse across cell membranes. Though the unpaired electron is delocalized between the nitrogen and oxygen atoms, which allows NO to be a relatively stable radical, it has a half-life of just a few seconds in biological systems. This is due to the reactivity of NO with numerous targets within the cell. Unlike many signaling pathways that depend on specific and non-covalent ligand-receptor interactions, NO and related molecules such as

the nitroxyl anion and nitrosonium cation, collectively called reactive nitrogen species (RNS), are unique in that they covalently bind to a wide range of targets. Major biologically relevant reactions of NO are summarized in Figure 1.1.

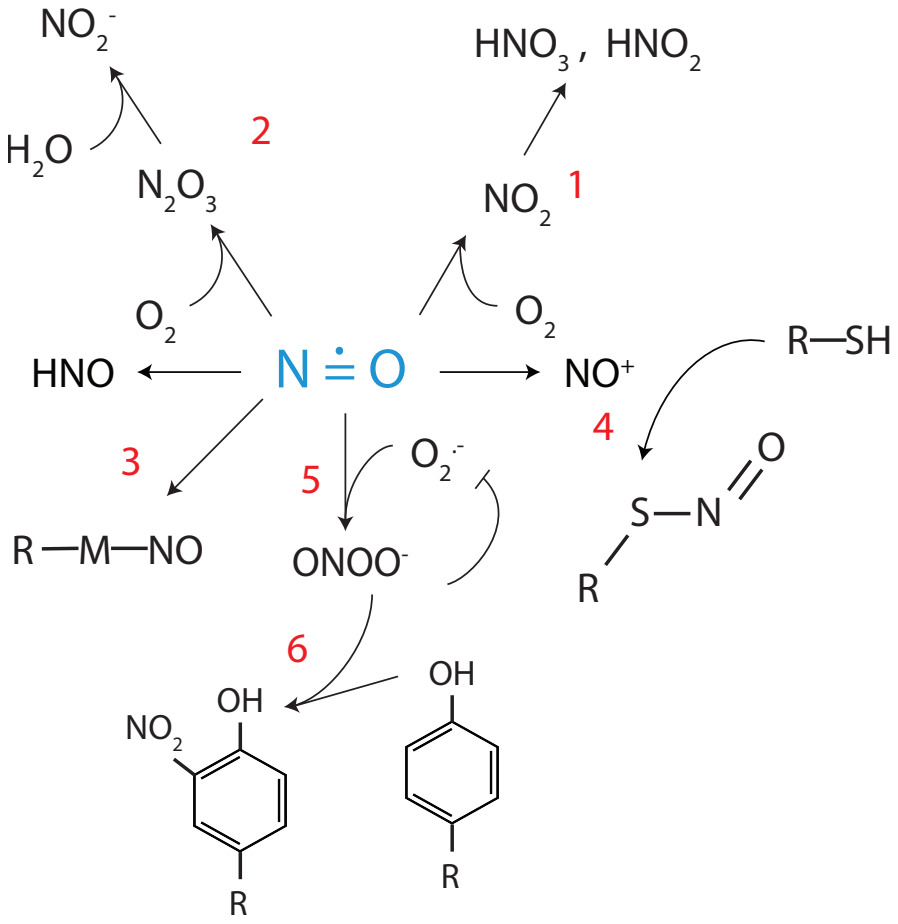

Figure 1.1 Summary of the major, biologically relevant chemical reactions of nitric oxide. Note that major end products of reactions are displayed and some intermediates have been omitted for clarity. M, transition metal; R, generic biomolecule or protein. Pathway 1, oxidation to nitrogen dioxide in gas phase and further formation of nitric and nitrous acids; Pathway 2, oxidation to nitrite in aqueous phase; Pathway 3, metal nitration; Pathway 4; s-nitrosylation of thiols; Pathway 5, reaction with superoxide to form peroxynitritel Pathway 6, protein tyrosine nitration.

NO is quickly oxidized in the presence of oxygen. In the gas phase, NO is oxidized to nitrogen dioxide, a precursor of nitric and nitrous acids in the atmosphere (Pathway 1; Ludwig et al. 2001). In aqueous solutions (Pathway 2), NO oxidizes to nitrite (Spinelli et al. 2011, Toledo & Augusto 2012). In biological systems, however, the NO radical readily reacts with a variety of targets present in the milieu. For example, NO can bind directly to transition metals and prosthetic groups of proteins that contain them, altering their structure and function (Pathway 3). One of the best examples of this is the binding of NO to the iron-containing heme group of soluble guanylate cyclase, stimulating the production of the secondary messenger cGMP from GTP (Murad 1986).

In addition, during a process called s-nitrosylation, NO can covalently bind to thiol groups (-SH), including specific cysteine residues of proteins, to produce S-nitrosothiols and post-translationally modify proteins (Pathway 4). Low molecular weight thiols, such as glutathione (GSH), are common targets of s-nitrosylation in plant and animal cells and are thought to act as an both important intracellular NO reservoirs as well a transport mechanisms in multicellular organisms (Stamler et al. 1992, Feechan et al. 2005). S-nitrosoglutathione also appears to be involved in nitrosylating proteins via trans-nitrosylation. S-nitrosylation of cysteine residues has been extensively documented in animal cells (Stamler et al. 2001) and, to a lesser extent, plant cells (Astier et al. 2011). Studies done in unicellular algae are limited to the freshwater model species *Chlamydomonas reinhardtii* (Morisse et al. 2014).

In addition to directly modifying biomolecules, NO can interact with other radical species and modulate their effects. For example, NO readily reacts with the superoxide radical (O_2^-) to form the potent oxidizing and nitrating agent peroxynitirite ($ONOO^-$)

(Pathway 5). This reaction is extremely quick and irreversible, limited only by the diffusion of each molecule. In fact, formation of peroxynitrite by reaction with NO is the only process that outcompetes detoxification of superoxide by superoxide dismutase (Beckman & Koppenol 1996). Peroxynitrite can react with a variety of macromolecules including proteins, lipids, and nucleic acids. Modification of tyrosine residues in proteins, a process known as tyrosine nitration (Pathway 6), however, has garnered the most attention (Corpas et al. 2009). Much like s-nitrosylation, protein nitration- the addition of a nitro (NO_2) group to specific amino acids- leads to a particular cellular response by causing conformational changes in target enzymes. In animal models, tyrosine nitration is often associated with disease states including Alzheimer's disease (Smith et al. 1997, Castegna et al. 2003), cardiovascular disease (Peluffo & Radi 2007), and cancer (Leon et al. 2008). Work has shown that tyrosine nitration is not just a molecular footprint of oxidative stress in these diseases, but is involved in the disease pathogenesis itself (Souza et al. 2008). In higher plants, crosstalk between NO and reactive oxygen species (ROS) has been implicated in the induction of programmed cell death (PCD) in the hypersensitive response of plants to invading pathogens (Delledonne et al. 2001, Cecconi et al. 2009), and several nitrated tyrosine-containing proteins have been associated with various stress conditions (Corpas et al. 2013).

A major unknown of NO biology in photosynthetic organisms is how it is produced. In animal cells, the main pathway of NO production is via the enzyme nitric oxide synthase (NOS). Mammalian systems have three NOS isoforms, endothelial (eNOS), neuronal (nNOS), and inducible (iNOS). Though they differ in localization, regulation, and expression, all NOSs work by facilitating the five-electron- NADPH- and

oxygen-dependent oxidation of L-arginine to NO and citrulline (Alderton et al. 2001). NOSs have also been described in several prokaryote systems (Crane et al. 2010). While NOS *activity* has been extensively demonstrated in plant cells (Cueto et al. 1996, Corpas et al. 2006, Flores et al. 2008), no true plant NOS gene has been identified, with the notable exception of the green picoeukaryote *Ostreococcus tauri* (Foresi et al. 2010, Correa-Aragunde et al. 2013). While a NOS in *Arabidopsis thaliana* (AtNOS1) was previously described (Guo et al. 2003), the NOS activity of this gene was called into question by numerous labs (Zemojtel et al. 2006, Moreau et al. 2008) and was later renamed to *Arabidopsis thaliana* nitric oxide-associated protein 1 (AtNOA1). AtNOA1 was instead shown to be a GTPase localized to the chloroplast, with strong homology to the bacterial YqeH family that is involved in ribosome synthesis/stability (Moreau et al. 2008). The model pennate diatom *Phaeodactylum tricornutum* was shown to contain two orthologs to AtNOA1 (named PtNOA) that demonstrate a strong relationship to NO production and NO-mediated stress responses in this species (Vardi et al. 2008). The exact relationship of NOAs to NO production remains elusive, however, and Moreau et al. 2008 hypothesizes a role for enhanced ROS production in the chloroplast of AtNOA1 mutants in its NO-related phenotypes.

In addition to a potential NOS, it has been shown that nitrate reductase (NR), a key enzyme in nitrogen assimilation in photosynthetic organisms, can be an important source of NO by catalyzing the reduction of cellular nitrite to NO when nitrite accumulates in the cell, such as when photosynthesis is inhibited and during anaerobic conditions (Yamasaki & Sakihama 2000, Yu et al. 2014). In addition, NO can be formed non-enzymatically via the reduction of nitrite in acidic conditions or in the presence of

ascorbic acid. To date, at least seven different putative NO production pathways, both reductive and oxidative, as well as both enzymatic and non-enzymatic, have been proposed in plants (reviewed in Mur et al., 2012 and Yu et al., 2014), though the NR and NOS enzymatic pathways continue to receive the most attention.

The biological relevance of NO and RNS can be easily appreciated by a literature search with the terms 'nitric oxide.' Since its discovery as the elusive endothelial derived relaxation factor in the 1980's (Ignarro et al. 1987), the known biological roles of NO in animal cells (e.g. Toledo & Augusto 2012) and in higher plants (Mur et al. 2013; Yu et al. 2014) has been quickly growing. The most striking feature of NO signaling that emerges in the literature is the seemingly contradictory outcomes NO production can elicit within a cell. This is probably best illustrated by the confusion in the literature regarding the pro- vs. anti-apoptotic actions of NO in cancer cells (Burke et al. 2013). It is now appreciated that this perplexing aspect of NO biology is not only due to the presence of specific targets near the site of NO production, such as metals or other radicals, but also the route of its production (NOS *vs* NR *vs* another mechanism), the dynamics of its production (steady, constitutive production *vs* rapid bursts), the concentrations of NO produced (picomolar *vs* nanomolar), and the cellular site of its production (mitochondria vs. peroxisomes vs. chloroplasts) (Mur et al. 2012).

1.3 NITRIC OXIDE IN PHYTOPLANKTON

Investigations into nitric oxide production and functioning in phytoplankton are relatively recent. A comprehensive review has recently been published that outlines the current state of knowledge of NO in marine photosynthetic organisms and, interestingly,

it appears that the dichotomous nature of NO that has been observed in both animals and higher plants is also a feature of NO in phytoplankton (Kumar et al. 2015). Much of the NO research has centered on the dinoflagellate group *Symbiodinium* with respect to the breakdown of their symbiosis with their hosts corals during bleaching events, as well as various aspects of diatom physiology. Work has shown that NO is produced by both the algal symbiont and the cnidarian coral host upon exposure to high-heat stress (Trapido-Rosenthal et al. 2005, Perez & Weis 2006, Bouchard & Yamasaki 2008, Hawkins & Davy 2012). Furthermore, increased NO production has been linked to caspase activity and PCD in *Symbiodinium,* a processes that has been hypothesized to initiate bleaching events (Bouchard & Yamasaki 2009).

In diatoms, NO production has also been linked to both PCD as well as stress acclimation pathways in several species. For example, the model pennate diatom *Phaeodactylum tricornutum* employs an NO and Ca^{2+} based stress-surveillance system in response to exposure to toxic polyunsaturated aldehydes (PUAs) (Vardi et al. 2006, Gallina et al. 2014) that involves nitric oxide-associated protein (PtNOA). *P. tricornutum* lines over-expressing PtNOA, which displays enhanced NO production, are hyper-sensitive to the PUA decadienal (Vardi et al. 2008). Furthermore, the concentration and type of PUA leads to unique NO production signatures that ultimately result in species-specific responses (Gallina et al. 2014). NO has been shown to be involved in the up-regulation of the death-specific protein (ScDSP) in the diatom *Skeletonema costatum* and may be a critical signal in its physiological response to low-light stress (Chung et al. 2008).

Alternative to its role in PCD, NO has also been shown to be involved in the normal growth and physiology of several different phytoplankton species including the tiny green alga *Ostreococcus tauri* (Foresi et al. 2010), freshwater Antarctic *Chlorella sp.* (Estevez & Puntarulo 2005), the harmful algal species *Chattonella marina* (Kim et al. 2008), and the cyanobacterium *Microcystis aerugrinosa* (Tang et al. 2011). NO has also been implicated in the adhesion of cells to appropriate substratum in benthic diatoms (Thompson et al. 2008), *P. tricornutum* (Vardi et al. 2008), and the zoospores of the green alga *Ulva* (Thompson et al. 2009) with increased intracellular NO levels being associated with decreased adhesion strength and settlement in these groups. In addition, NO has been shown to mediate cell survival in the face of several abiotic stressors including in *Chlorella vulgarus* in response to copper stress (Singh et al. 2004), protection of *Scenedesmus obliquus* against H_2O_2 (Mallick et al. 2002), and reduction of UV-B damage in the cyanobacterium *Spirulina platensis* (Xue et al. 2007).

In addition to being an intracellular signaling molecule, NO may also act as a diffusible messenger involved in "communication" between neighboring cells in tissue or individuals in a population or bloom. Indeed, the first physiological role ever ascribed to NO was as the molecule produced by endothelial cells that acted on smooth muscle cells in the vicinity that leads to blood vessel dilation, certainly a type of "communication" relevant to multicellular organisms. Based on the measured diffusion coefficient of NO (~3300 $\mu m^2/s$), along with its typical half-life *in vivo* (5-15 s), it has been predicted that an individual NO molecule can travel at least 150-300 μm from its site of production in aqueous solution (Lancaster 1997). Some *in situ* studies have measured a longer half-life in seawater, leading to even longer potential travel distances (Zafiriou & Mcfarland 1981,

Olasehinde et al. 2010). For the size ranges of the types of organisms under consideration here (1-10 μm) that often bloom to relatively high densities (10^5-10^6 cells per L), it is possible that NO may act as an "infochemical," transmitting information about the physiological state of an individual cell to its neighbors to elicit a response. Work by Vardi *et al*. (2006) has provided convincing evidence that diatoms can sense stressed individuals in their vicinity and that a diffusible signal, which may possibly be NO, is responsible for subsequent cellular responses.

Besides having a multitude of physiological functions *in vivo*, the NO free radical also has important impacts on the climate and the environment. Though NO is an overall minor component of the elemental N budget, the concentration of NO_x (NO and its oxidation products such as nitrogen dioxide, NO_2) present in the atmosphere plays a critical role in balancing the destruction and accumulation of tropospheric ozone (O_3), an important contributor to positive radiative forcing. NO can also lead to production of hydroxyl radicals, altering the oxidizing capacity of the atmosphere. In addition, NO_x can lead to the formation of nitric and nitrous acids (HNO_3 and HNO_2 respectively; Figure 1.1 Pathway 1), an increasingly important component of acid precipitation (Ludwig et al. 2001).

It was once thought that emissions of nitric oxide were exclusively of anthropogenic origin, such as fossil fuel combustion and biomass burning. However, several studies have demonstrated that natural abiotic and biotic processes in soils can be major contributors to global NO_x emissions. NO_x release is particularly prevalent over highly fertilized, cultivated agricultural lands (Davidson & Kingerlee 1997, Pilegaard 2013), and is thought to be due mostly to the microbial activities of nitrification and

denitrification in which NO is an intermediate. Though global estimates of soil NO_x emissions are still under debate, even less is known about the propensity for the oceans to be a source of atmospheric NO_x. A few investigations have suggested that the ocean is a net source of NO_x to the atmosphere, generally via the photolysis of nitrite to NO in surface waters (Zafiriou & Mcfarland 1981, Olasehinde et al. 2010, Anifowose et al. 2015). Whether large blooms of phytoplankton producing NO at physiological levels can also act as a transient NO_x source remains an important open question.

1.4 DISSERTATION QUESTIONS

Despite the increase in research on NO in phytoplankton within the last decade, investigations in *Emiliania huxleyi* have been notably absent. The only mention of NO function in *E. huxleyi* was by Zhang *et al*. (2003) who observed an increase in the growth rate of *E. huxleyi* cultures treated with an exogenously added NO saturated solution. This led the authors to conclude that NO may act as a growth factor (Zhang et al. 2003). Virtually nothing is known about the production dynamics, ecophysiological roles, or biosynthetic pathways of NO in *E. huxleyi*. This represents a critical gap in our knowledge of the biology of this ecologically and environmentally important model organism. *E. huxleyi* and their viruses have also become one of the best systems to study the subcellular processes that govern viral infection of eukaryotic microalgae and its environmental implications (Bidle & Vardi 2011, Bidle 2015). Since successful infection of *E. huxleyi* appears to be predicated on viral takeover of host PCD pathways, including ROS production, metacaspase expression and caspase activity (Evans et al. 2006, Bidle et

al. 2007, Sheyn et al. 2016), it is conceivable that NO may be an important component of the subcellular mechanisms regulating infection.

The overall goal of this dissertation is to shed light on the function of this enigmatic molecule in the life and death of the cosmopolitan coccolithophore *Emiliania huxleyi*, with a particular emphasis on elucidating its role during viral infection. In Chapter 2, the dynamics of NO production during viral infection of a model laboratory strain are presented and a potential antioxidant function for this molecule is discussed. Hypotheses presented in Chapter 2 are further supported by field data from the *North Atlantic Viral Infection of Coccolithophores Expedition* (NA-VICE) during which natural *E. huxleyi* populations at various stages of viral infection were studied. Additionally, Chapter 2 presents important control experiments for two methods to detect and quantify NO production utilized throughout this dissertation. In Chapter 3 variability in NO production, basal reactive oxygen stress, and antioxidant capacity of various strains of *E. huxleyi* that differ in their susceptibility to viral infection is shown and possible implications for understanding the costs of resistance to host cells is discussed. Finally, Chapter 4 aims to elucidate the broader pathways NO is involved in by uncovering the mechanisms of NO production in *E. huxleyi* as well as identifying the proteins in the *E. huxleyi* proteome that may be regulated by NO-mediated post-translational modification. The dissertation concludes with a summary of the main findings, broader impacts for the field, and avenues for future work.

1.5 REFERENCES

Alderton WK, Cooper CE, Knowles RG (2001) Nitric oxide synthase: structure, function and inhibition. Biochemical Journal 357:593-615

Anifowose AJ, Takeda K, Sakugawa H (2015) Photoformation rate, steady-state concentration and lifetime of nitric oxide radical (NO.) in a eutrophic river in Higashi-Hiroshima, Japan. Chemosphere 119:302-309

Astier J, Rasul S, Koen E, Manzoor H, Besson-Bard A, Lamotte O, Jeandroz S, Durner J, Lindermayr C, Wendehenne D (2011) S-nitrosylation: an emerging post-translational protein modification in plants. Plant science : an international journal of experimental plant biology 181:527-533

Beckman JS, Koppenol WH (1996) Nitric oxide, superoxide, peroxynitrite: The good, the bad, and the ugly. The American Journal of Physiology 271:C1424-C1437

Bekker A, Holland HD, Wang P-L, Rumble III D, Stein HJ, Hannah JL, Coetzee LL, Beukes NJ (2004) Dating the rise of atmospheric oxygen. Nature 427:117-120

Besson-Bard A, Pugin A, Wendehenne D (2008) New insights into nitric oxide signaling in plants. Annual review of plant biology 59:21-39

Bidle KD (2015) The molecular ecophysiology of programmed cell death in marine phytoplankton. Annual review of marine science 7:341-375

Bidle KD, Haramaty L, Barcelos ERJ, Falkowski P (2007) Viral activation and recruitment of metacaspases in the unicellular coccolithophore, *Emiliania huxleyi*. Proceedings of the National Academy of Sciences of the United States of America 104:6049-6054

Bidle KD, Vardi A (2011) A chemical arms race at sea mediates algal host-virus interactions. Current opinion in microbiology 14:449-457

Bouchard JN, Yamasaki H (2008) Heat stress stimulates nitric oxide production in *Symbiodinium microadriaticum*: a possible linkage between nitric oxide and the coral bleaching phenomenon. Plant & cell physiology 49:641-652

Bouchard JN, Yamasaki H (2009) Implication of nitric oxide in the heat-stress-induced cell death of the symbiotic alga *Symbiodinium microadriaticum*. Marine Biology 156:2209-2220

Bratbak G, Egge JK, Heldal M (1993) Viral mortality of the marine alga Emiliania huxleyi (Haptophyceae) and termination of algal blooms. Marine Ecology Progress Series 93:39-58

Brown CW, Yoder JA (1994) Coccolithophorid blooms in the global ocean. Journal of Geophysical Research 99:7467-7482

Brussaard CPD, Kempers RS, Kop AJ, Riegman R, Heldal M (1996) Virus-like particles in a summer bloom of *Emiliania huxleyi* in the North Sea. Aquatic Microbial Ecology 10:105-113

Castegna A, Thongboonkerd V, Klein JB, Lynn B, Markesbery WR, Butterfield DA (2003) Proteomic identification of nitrated proteins in Alzheimer's disease brain. Journal of Neurochemistry 85:1394-1401

Cecconi D, Orzetti S, Vandelle E, Rinalducci S, Zolla L, Delledonne M (2009) Protein nitration during defense response in Arabidopsis thaliana. Electrophoresis 30:2460-2468

Chung CC, Hwang SP, Chang J (2008) Nitric oxide as a signaling factor to upregulate the death-specific protein in a marine diatom, Skeletonema costatum, during blockage of electron flow in photosynthesis. Applied and environmental microbiology 74:6521-6527

Corpas FJ, Barroso JB, Carreras A, Valderrama R, Palma JM, Leon AM, Sandalio LM, del Rio LA (2006) Constitutive arginine-dependent nitric oxide synthase activity in different organs of pea seedlings during plant development. Planta 224:246-254

Corpas FJ, Chaki M, Leterrier M, Barroso JB (2009) Protein tyrosine nitration: A new challenge in plants. Plant Signaling & Behavior 4:920-923

Corpas FJ, Palma JM, Del Rio LA, Barroso JB (2013) Protein tyrosine nitration in higher plants grown under natural and stress conditions. Frontiers in plant science 4:1-4

Correa-Aragunde N, Foresi N, Lamattina L (2013) Structure diversity of nitric oxide synthases (NOS): the emergence of new forms in photosynthetic organisms. Frontiers in plant science 4:232

Crane BR, Sudhamsu J, Patel BA (2010) Bacterial nitric oxide synthases. Annual review of biochemistry 79:445-470

Cueto M, Hernández-Perera O, Martín R, Bentura ML, Rodrigo J, Lamas S, Golvano MP (1996) Presence of nitric oxide synthase activity in roots and nodules of *Lupinus albus*. FEBS letters 398:159-164

Davidson EA, Kingerlee W (1997) A global inventory of nitric oxide emissions from soils. Nutrient Cycling in Agroecosystems 48:37-50

Delledonne M, Zeier J, Marocco A, Lamb C (2001) Signal interactions between nitric oxide and reactive oxygen intermediates in the plant hypersensitive disease

resistance response. Proceedings of the National Academy of Sciences of the United States of America 98:13454-13459

Dismukes GC, Klimov VV, Baranov SV, Kozlov YN, DasGupta J, Tyryshkin A (2001) The origin of atmospheric oxygen on Earth: the innovation of oxygenic photosynthesis. Proceedings of the National Academy of Sciences of the United States of America 98:2170-2175

Evans C, Malin G, Mills GP, Wilson WH (2006) Viral Infection of *Emiliania Huxleyi* (Prymnesiophyceae) Leads to Elevated Production of Reactive Oxygen Species. Journal of Phycology 42:1040-1047

Feechan A, Kwon E, Yun BW, Wang Y, Pallas JA, Loake GJ (2005) A central role for S-nitrosothiols in plant disease resistance. Proceedings of the National Academy of Sciences of the United States of America 102:8054-8059

Feelisch M, Martin JF (1995) The early role of nitric oxide in evolution. Trends in Ecology and Evolution 10:496-499

Field CB, Behrenfeld MJ, Randerson JT, Falkowski P (1998) Primary production of the biosophere: Integrating terrestrial and oceanic components Science 281:237-240

Flores T, Todd CD, Tovar-Mendez A, Dhanoa PK, Correa-Aragunde N, Hoyos ME, Brownfield DM, Mullen RT, Lamattina L, Polacco JC (2008) Arginase-negative mutants of *Arabidopsis* exhibit increased nitric oxide signaling in root development. Plant physiology 147:1936-1946

Foresi N, Correa-Aragunde N, Parisi G, Calo G, Salerno G, Lamattina L (2010) Characterization of a nitric oxide synthase from the plant kingdom: NO generation from the green alga *Ostreococcus tauri* is light irradiance and growth phase dependent. The Plant cell 22:3816-3830

Fuhrman JA (1999) Marine viruses and their biogeochemical effects. Nature 399:541-548

Gallina AA, Brunet C, Palumbo A, Casotti R (2014) The effect of polyunsaturated aldehydes on *Skeletonema marinoi* (Bacillariophyceae): the involvement of reactive oxygen species and nitric oxide. Marine drugs 12:4165-4187

Guo FQ, Okamoto M, Crawford NM (2003) Identification of a plant nitric oxide synthase gene invoved in hormonal signaling. Science 302:100-103

Gusarov I, Shatalin K, Starodubtseva M, Nudler E (2009) Endogenous nitric oxide protects bacteria against a wide sprectrum of antibiotics. Science 235:1380-1384

Hawkins TD, Davy SK (2012) Nitric oxide production and tolerance differ among *Symbiodinium* types exposed to heat stress. Plant & cell physiology 53:1889-1898

Holligan PM, Fernández E, Aiken J, Balch WM, Boyd P, Burkill PH, Finch M, Groom SB, Malin G, Muller K, Purdie DA, Robinson C, Trees CC, Turner SM, van der Wal P (1993) A biogemical study of the coccolithophore, *Emiliania huxleyi,* in the North Atlantic Global Biogeochemical Cycles 7:879-900

Kim D, Kang YS, Lee Y, Yamaguchi K, Matsuoka K, Lee KW, Choi KS, Oda T (2008) Detection of nitric oxide (NO) in marine phytoplankters. Journal of bioscience and bioengineering 105:414-417

Klaas C, Archer DE (2002) Association of sinking organic matter with various types of mineral ballast in the deep sea: Implications for the rain ratio. Global Biogeochemical Cycles 16:63-61-63-14

Kopp RE, Kirschvink JL, Hilburn IA, Nash CZ (2005) The Paleoproterozoic snowball Earth: a climate disaster triggered by the evolution of oxygenic photosynthesis. Proceedings of the National Academy of Sciences of the United States of America 102:11131-11136

Kumar A, Castellano I, Patti FP, Palumbo A, Buia MC (2015) Nitric oxide in marine photosynthetic organisms. Nitric oxide : biology and chemistry 47:34-39

Laber CP, Hunter JE, Carvalho F, Collins JR, Hunter EJ, Schieler BM, Boss E, More K, Frada M, Thamatrakoln K, Brown CM, Haramaty L, Ossolinski J, Fredricks H, Nissimov JI, Vandzura R, Sheyn U, Lehahn Y, Chant RJ, Martins AM, Coolen MJL, Vardi A, DiTullio GR, Van Mooy BAS, Bidle KD (2018) *Coccolithovirus* facilitation of carbon export in the North Atlantic. Nature microbiology 3:537-547

Lancaster JR (1997) A tutorial on the diffusibility and reactivity of free nitric oxide. Nitric Oxide: Biology and Chemistry 1:18-30

Lehahn Y, Koren I, Schatz D, Frada M, Sheyn U, Boss E, Efrati S, Rudich Y, Trainic M, Sharoni S, Laber C, DiTullio GR, Coolen MJ, Martins AM, Van Mooy BA, Bidle KD, Vardi A (2014) Decoupling physical from biological processes to assess the impact of viruses on a mesoscale algal bloom. Current biology : CB 24:2041-2046

Leon L, Jeannin JF, Bettaieb A (2008) Post-translational modifications induced by nitric oxide (NO): implication in cancer cells apoptosis. Nitric oxide : biology and chemistry 19:77-83

Ludwig J, Meixner FX, Vogel B, Förstner J (2001) Soil-air exchange of nitric oxide: An overview of processes, environmental factors, and modeling studies. Biogeochemistry 52:225-257

Malin G, Steinke M (2004) Dimethyl sulfide production: what is the contribution of the coccolithophores? In: Thierstein HR, Young JR (eds) Coccoltihophores: From Molecular Processes to Global Impact. Springer, Germany

Mallick N, Mohn FH, Soeder CJ, Grobbelaar JU (2002) Ameliorative role of ntiric oxide on H2O2 toxicity to a chlorophycean alga *Scenedesmus obliquus*.

Martinez JM, Schroeder DC, Larsen A, Bratbak G, Wilson WH (2007) Molecular dynamics of *Emiliania huxleyi* and cooccurring viruses during two separate mesocosm studies. Applied and environmental microbiology 73:554-562

Moncada S (1999) Nitric oxide: discovery and impact on clinical medicine. Journal of the Royal Society of Medicine 92:164-169

Moreau M, Lee GI, Wang Y, Crane BR, Klessig DF (2008) AtNOS/AtNOA1 is a functional *Arabidopsis thaliana* cGTPase and not a nitric-oxide synthase. The Journal of biological chemistry 283:32957-32967

Morisse S, Zaffagnini M, Gao XH, Lemaire SD, Marchand CH (2014) Insight into protein S-nitrosylation in *Chlamydomonas reinhardtii.* Antioxidants & redox signaling 21:1271-1284

Mur LA, Mandon J, Persijn S, Cristescu SM, Moshkov IE, Novikova GV, Hall MA, Harren FJ, Hebelstrup KH, Gupta KJ (2012) Nitric oxide in plants: an assessment of the current state of knowledge. AoB PLANTS 5:pls052

Murad F (1986) Cyclic guanosine monophosphate as a mediator of vasodilation. Journal of Clinical Investigation 78:1-5

Olasehinde EF, Takeda K, Sakugawa H (2010) Photochemical production and consumption mechanisms of nitric oxide in seawater. Environmental science & technology 44:8403-8408

Paasche E (2002) A review of the coccolithophorid *Emiliania huxleyi* (Prymnesiophyceae) with particular reference to growth, coccolith formation, and clacification-photosynthesis intercations. Phycologia 40:503-529

Peluffo G, Radi R (2007) Biochemistry of protein tyrosine nitration in cardiovascular pathology. Cardiovascular research 75:291-302

Perez S, Weis V (2006) Nitric oxide and cnidarian bleaching: an eviction notice mediates breakdown of a symbiosis. The Journal of experimental biology 209:2804-2810

Pilegaard K (2013) Processes regulating nitric oxide emissions from soils. Philosophical transactions of the Royal Society of London Series B, Biological sciences 368:20130126

Rost B, Riebesell U (2004) Coccolithophores and the biological pump: responses to environmental changes. In: Thierstein HR, Young JR (eds) Coccolithophores: from molecular processes to global impact. Springer, Berlin

Schroeder DC, Oke J, Malin G, Wilson WH (2002) *Coccolithovirus* (*Phycodnaviridae*): characterisation of a new large dsDNA algal virus that infects *Emiliana huxleyi*. Archives of virology 147:1685-1698

Sheyn U, Rosenwasser S, Ben-Dor S, Porat Z, Vardi A (2016) Modulation of host ROS metabolism is essential for viral infection of a bloom-forming coccolithophore in the ocean. The ISME journal 10:1742-1754

Sheyn U, Rosenwasser S, Lehahn Y, Barak-Gavish N, Rotkopf R, Bidle KD, Koren I, Schatz D, Vardi A (2018) Expression profiling of host and virus during a coccolithophore bloom provides insights into the role of viral infection in promoting carbon export. The ISME journal 12:704-713

Singh A, Sharma L, Mallick N (2004) Antioxidative role of nitric oxide on copper toxicity to a chlorophycean alga, *Chlorella*. Ecotoxicology and environmental safety 59:223-227

Smith MA, Harris PLR, Sayre LM, Beckman JS, Perry G (1997) Widespread peroxynitrite-mediated damage in Alzheimer's disease. The Journal of Neuroscience 17:2653-2657

Souza JM, Peluffo G, Radi R (2008) Protein tyrosine nitration--functional alteration or just a biomarker? Free radical biology & medicine 45:357-366

Spinelli F, Cellini A, Marchetti L, Nagesh KM, Piovene C (2011) Emission and function of volatile organic compounds in response to abiotic stress. In: Shanker A, Venkateswarlu B (eds) Abiotic Stress in Plants - Mechanisms and Adaptations IntechOpen

Stamler JS, Lamas S, Fang FC (2001) Nitrosylation: The prototypic redox-based signaling mechansim. Cell 106:675-683

Stamler JS, Singel DJ, Loscalzo J (1992) Biochemistry of nitric oxide and its redox-activated forms. Science 258:1898-1902

Suttle CA (2007) Marine viruses--major players in the global ecosystem. Nature reviews Microbiology 5:801-812

Tang X, Chen J, Wang WH, Liu TW, Zhang J, Gao YH, Pei ZM, Zheng HL (2011) The changes of nitric oxide production during the growth of *Microcystis aerugrinosa*. Environmental pollution 159:3784-3792

Thompson SEM, Callow ME, Callow JA (2009) The effects of nitric oxide in settlement and adhesion of zoospores of the green alga *Ulva*. Biofouling 26:167-178

Thompson SEM, Taylor AR, Brownlee C, Callow ME, Callow JA (2008) The Role of Nitric Oxide in Diatom Adhesion in Relation to Substratum Properties(1). J Phycol 44:967-976

Toledo JC, Jr., Augusto O (2012) Connecting the chemical and biological properties of nitric oxide. Chemical research in toxicology 25:975-989

Trapido-Rosenthal H, Zielke S, Owen R, Buxton L, Boeing B, Bhagooli R, Archer J (2005) Increased zooxanthellae nitric oxide synthase activity is associated with coral bleaching. The Biological Bulletin 208:3-6

Tyrrell T, Holligan PM, Mobley CD (1999) Optical impacts of oceanic coccolithophore blooms. Journal of Geophysical Research 104:3223-3241

Tyrrell T, Merico A (2004) Emiliania huxleyi: bloom observations and the conditions that induce them. In: Thierstein HR, Young JR (eds) Coccolithophores: From Molecular Processes to Global Impact. Springer, Germany

Vardi A, Bidle KD, Kwityn C, Hirsh DJ, Thompson SM, Callow JA, Falkowski P, Bowler C (2008) A diatom gene regulating nitric-oxide signaling and susceptibility to diatom-derived aldehydes. Current biology : CB 18:895-899

Vardi A, Formiggini F, Casotti R, De Martino A, Ribalet F, Miralto A, Bowler C (2006) A stress surveillance system based on calcium and nitric oxide in marine diatoms. PLoS biology 4:e60

Vardi A, Haramaty L, Van Mooy BAS, Fredricks HF, Kimmance SA, Larsen A, Bidle KD (2012) Host-virus dynamics and subcellular controls of cell fate in a natural coccolithophore population. Proceedings of the National Academy of Sciences of the United States of America 109:19327-19332

Winter A, Henderiks J, Beaufort L, Rickaby REM, Brown CW (2014) Poleward expansion of the coccolithophore *Emiliania huxleyi*. Journal of Plankton Research 36:316-325

Xue L, Li S, Sheng H, Feng H, Xu S, An L (2007) Nitric oxide alleviates oxidative damage induced by enhanced ultraviolet-B radiation in cyanobacterium. Current microbiology 55:294-301

Yamasaki H, Sakihama Y (2000) Simultaneous production of nitric oxide and peroxynitrite by plant nirate reductase: in vitro evidence for the NR-dependent formation of active nitrogen species. FEBS letters 468:89-92

Yu M, Lamattina L, Spoel SH, Loake GJ (2014) Nitric oxide function in plant biology: a redox cue in deconvolution. The New phytologist 202:1142-1156

Zafiriou OC, Mcfarland M (1981) Nitric-oxide from nitrite photolysis in the central Equatorial Pacific. Journal of Geophysical Research-Oceans 86:3173-3182

Zemojtel T, Frohlich A, Palmieri MC, Kolanczyk M, Mikula I, Wyrwicz LS, Wanker EE, Mundlos S, Vingron M, Martasek P, Durner J (2006) Plant nitric oxide synthase: a never-ending story? Trends in plant science 11:524-525; author reply 526-528

Zhang Z, Lin C, Liu C, Sun M, Ding H (2003) The effect of nitric oxide on the growth of marine phytoplankton. Journal of Ocean University of Qingdao 2:185-188

CHAPTER 2: Nitric Oxide Production and Antioxidant Function During Viral Infection of the Coccolithophore *Emiliania huxleyi* [*]

[*] This chapter has been published as: **Schieler, B.M.**, Soni, M.V., Brown, C.M., Coolen, M.J.L., Fredricks, H., Van Mooy, B.A.S., Hirsh, D.J. and K.D. Bidle (2019) Nitric oxide production and antioxidant function during viral infection of the coccolithophore *Emiliania huxleyi*. *The ISME Journal* 13:1019-1031.

2.1 ABSTRACT

Emiliania huxleyi is a globally important marine phytoplankton that is routinely infected by viruses. Understanding the controls on the growth and demise of _E. huxleyi_ blooms is essential for predicting the biogeochemical fate of their organic carbon and nutrients. In this study, we show that the production of nitric oxide (NO), a gaseous, membrane-permeable free radical, is a hallmark of early-stage lytic infection in _E. huxleyi_ by Coccolithoviruses, both in culture and in natural populations in the North Atlantic. Enhanced NO production was detected both intra- and extra-cellularly in laboratory cultures, and treatment of cells with an NO scavenger significantly reduced viral production. Pre-treatment of exponentially growing _E. huxleyi_ cultures with the NO donor S-nitroso-N-acetylpenicillamine (SNAP) prior to challenge with hydrogen peroxide (H_2O_2) led to greater cell survival, suggesting that NO may have a cellular antioxidant function. Indeed, cell lysates generated from cultures treated with SNAP and undergoing infection displayed enhanced ability to detoxify H_2O_2. Lastly, we show that fluorescent indicators of cellular ROS, NO, and death, in combination with classic DNA- and lipid-based biomarkers of infection, can function as real-time diagnostic tools to identify and contextualize viral infection in natural _E. huxleyi_ blooms.

2.2 INTRODUCTION

Emiliania huxleyi is a cosmopolitan species of coccolithophore, a group of unicellular, eukaryotic marine phytoplankton that produces intricate shells (coccoliths) of calcium carbonate. As both a dominant calcifier and a bloom-forming photoautotroph, *E. huxleyi* exerts a profound influence on marine biogeochemical cycles (particularly of carbon and sulfur) and food web dynamics. *E. huxleyi* is known for forming large annual blooms in the North Atlantic, often spanning $>10^5$ km^2 with cell densities exceeding 10^6 cells l^{-1} (Holligan et al. 1993, Brown & Yoder 1994, Tyrrell & Merico 2004). These blooms are associated with dimethyl sulfide production in the surface ocean and flux into the atmosphere (Malin & Steinke 2004), increased albedo and heating of the surface ocean due to their coccoliths (Tyrrell et al. 1999), and enhanced export flux of carbonate to the deep ocean (Klaas & Archer 2002).

Understanding the mechanisms of *E. huxleyi* bloom termination is necessary for predicting the fate of its calcium carbonate and fixed organic carbon in the ocean. *E. huxleyi* is often infected by large, double stranded DNA viruses belonging to the group *Phycodnaviridae* (Bratbak et al. 1993, Brussaard et al. 1996, Schroeder et al. 2002). These *Coccolithoviruses*, known as EhVs, have been shown to cause the termination of *E. huxleyi* in culture (Bidle et al. 2007, Vardi et al. 2009) and natural blooms (Martinez et al. 2007, Vardi et al. 2012, Lehahn et al. 2014, Laber et al. 2018, Sheyn et al. 2018). One paradigm holds that viral lysis shunts fixed carbon away from downward vertical flux or transfer to higher trophic levels by stimulating cell lysis and bacterial respiration of dissolved organic carbon in the surface ocean (Fuhrman 1999, Suttle 2007). However, the biogeochemical and ecosystem consequences of infection

could vary among different phytoplankton species. Recent evidence suggests that infection of *E. huxleyi* may actually facilitate aggregation and sinking of particulate carbon into the mesopelagic where it is subsequently respired (Laber et al. 2018, Sheyn et al. 2018). This may be a result of increased cellular production of transparent exopolymeric particles (TEP) during infection, which acts to enhance particle aggregation and couple infection with microzooplankton grazing (Frada et al. 2014).

Due to the ecological significance of *E. huxleyi* blooms and the range of recently developed diagnostic tools for studying infection, *E. huxleyi* and EhVs have emerged as one of the best described systems for understanding the molecular mechanisms of infection in marine eukaryotic microalgae (Bidle & Vardi 2011). During infection, EhVs co-opt and rewire cellular lipid biosynthetic machinery, producing viral-specific classes of glycosphingolipids (vGSLs) (Vardi et al. 2009, Vardi et al. 2012, Rosenwasser et al. 2014) and betaine-like lipids (Hunter et al. 2015). Accumulation of these polar lipids during infection occur concomitant with a late stage increase in production of reactive oxygen species (ROS; (Evans et al. 2006, Martinez Martinez et al. 2011, Sheyn et al. 2016)), particularly hydrogen peroxide (H_2O_2; (Sheyn et al. 2016)), caspase activity, and metacaspase expression (Bidle et al. 2007, Vardi et al. 2012), ultimately leading to programmed cell death (PCD; (Bidle 2015)) in the form of autophagy (Schatz et al. 2014) .

The dynamics of ROS production during viral infection are well described (Evans et al. 2006, Vardi et al. 2012, Sheyn et al. 2016). Little is known, however, about the role(s) of reactive nitrogen species (RNS), such as nitric oxide (NO), in modulating subcellular redox pathways and associated cellular responses. NO is a

small, uncharged free radical gas that has been shown to be involved in a myriad of biological functions, including immunity, stress adaptation, and normal growth in all branches of life (Moncada 1999, Gusarov et al. 2009, Mur et al. 2012, Martens-Habbena et al. 2015). The foundation for this breadth of action rests on the broad reactivity of NO with various cellular targets, as well as its ability to diffuse across membranes to act both intra- and extra-cellularly. Of particular interest is the role of NO in modifying cellular ROS pools, either via radical–radical reactions or indirectly through the regulation of pro- or anti-oxidant pathways (Toledo & Augusto 2012, Groß et al. 2013, Begara-Morales et al. 2016). Although the sources(s) of NO synthesis in plants and photosynthetic protists is still unresolved (Frohlich & Durner 2011), its signaling function during cellular response to diverse biotic and abiotic stressors is well known and summarized in several in-depth reviews (Besson-Bard et al. 2008, Kumar et al. 2015). In diatoms, for instance, NO is part of a stress-surveillance system that senses and responds to the toxic polyunsaturated aldehyde decadeinal (Vardi et al. 2006, Vardi et al. 2008, Gallina et al. 2014).

To date, investigations on the role(s) of NO in *E. huxleyi* physiology have been limited. One study demonstrated *E. huxleyi* growth rate and maximum cell densities increased in response to low levels of exogenously added NO (Zhang et al. 2003). In addition, we have previously shown that *E. huxleyi* cell lysates possess the enzymatic capacity to produce NO from nitrite and NADH via nitrate reductase ((Hirsh et al. 2016) and Chapter 4). There is, however, a notable gap in our knowledge of the mechanistic roles of this ubiquitous signaling molecule in *E. huxleyi* ecophysiology, including during viral infection. Given EhV infection induces PCD through elevated

ROS production, it stands to reason that NO may play an important interactive role in infection dynamics. Here, we demonstrate that elevated intracellular NO production is a hallmark of early-stage lytic viral infection of *E. huxleyi* both in culture and in natural populations in the North Atlantic. Scavenging of intracellular NO leads to a dose-dependent reduction in viral burst sizes, indicating that NO is critical for maximal viral production in lab conditions. Using a novel liposome-enabled electron paramagnetic resonance (EPR) spectroscopy method (Hirsh et al. 2016), we also show that elevated extracellular NO is observed during infection. Our work further suggests that intracellular NO production upregulates cellular antioxidant activity during the early stages of infection, keeping the cellular redox state favorable for viral replication.

2.3 MATERIALS & METHODS

2.3.1 Culture conditions and viral infections

Emiliania huxleyi strain CCMP1516 was obtained from the Provasoli-Guillard National Center for Marine Algae and Microbiota and grown in batch culture in f/2 (minus Si) media at 18 °C on a 14:10 light:dark cycle at a light intensity of 250 µmol $m^{-2}s^{-1}$. Virus strain EhV201 (obtained courtesy of W. Wilson, Marine Biological Association, Plymouth, UK) was propagated in batch cultures of *E. huxleyi* CCMP1516. Viral lysates were passed through a 0.45 µm pore-size PVDF syringe filter to remove cell debris. For infection experiments, *E. huxleyi* was inoculated with EhV during mid-exponential growth (~5.0×10^5 cells ml^{-1}) at a virus-to-host ratio of 5:1. Uninfected *E. huxleyi* cultures served as controls.

2.3.2 Enumeration of cells and viruses

E. huxleyi cell abundances were quantified using either a BD InFlux Mariner 209S flow cytometer or a BD Accuri C6 flow cytometer. Cell abundances were determined based on the chlorophyll autofluorescence (E_x/E_m: 488 nm, 692 nm) vs. forward scatter signature. Free viruses were quantified by flow cytometry according to (Brussaard et al. 2000). See Supplementary Information for additional flow cytometry methods.

2.3.3 Intracellular NO detection

Semi-quantitative measurements of intracellular NO were made using the NO specific fluorescent probe DAF-FM Diacetate (DAF-FM DA; Thermo Fisher, Waltham, MA). DAF-FM DA passes through cell membrane, is cleaved by intracellular esterases to DAF-FM, and accumulates inside the cell. DAF-FM is non-fluorescent until it binds to NO or its oxidized products to form a fluorescent triazole product, DAF-FM-T (Kojima et al. 1999). Stocks of DAF-FM DA were made to 5 mM in DMSO (Sigma-Aldrich, St. Louis, MO) and used at a final concentration of 5 μM. Stained samples were incubated in the dark at RT for 45 min. Mean fluorescence intensity per cell was determined by flow cytometry (E_x/E_m: 488 nm, 520 nm). An unstained sample was run to account for background autofluorescence. Several controls were run to contextualize DAF-FM DA results and are described below.

2.3.4 Chemical identification of DAF-FM-T in cells

The presence of the fluorescent DAF-FM-T triazole product in cells treated with NO donors was chemically confirmed using high performance liquid chromatography (HPLC) and ion-trap mass spectrometry (MS). Cultures of *E. huxleyi* CCMP1516 were treated with the NO donors S-nitroso-N-acetylpenicillamine (SNAP; Thermo Fisher) and sodium nitroprusside (SNP; Sigma-Aldrich) at 100 µM and 1 mM, respectively, and stained with 5 µM DAF-FM DA. A DAF-FM-T standard was generated in vitro by exposing 50 µM DAF-FM (Thermo Fisher) to an excess (> 50 mM) of SNP. Identification of DAF-FM and DAF-FM-T was confirmed by MS^2 spectra of the 413 *m/z* and 424 *m/z* molecular ions, which showed diagnostic neutral loss of CO_2 (44 *m/z*) as previously characterized (Cortese-Krott et al. 2012). See Supplementary Information for full description.

2.3.5 Intracellular esterase activity

Intracellular esterase activity was measured in infected and uninfected cells using a general fluorogenic esterase substrate. Cell lysates were generated and protein was quantified (see Supplementary Information). A total of 2 µg of protein was incubated with 25 µM 4-Methylumbelliferyl butyrate (Sigma-Aldrich). The time course of fluorescence (E_x/E_m: 365 nm, 440 nm) was measured every 2 min for 1 h using a SpectraMax M3 microplate reader. Esterase activity is expressed as the rate of change in fluorescence (RFU) per µg protein.

2.3.6 Intracellular ROS and cell death analysis

Cellular ROS production was assessed using the fluorescent probe CM-H_2DCFDA (Thermo Fisher), which has a broad reactivity with a variety of ROS.

Stocks of CM-H_2DCFDA were made up to 1 mM in DMSO and used at a final concentration of 5 µM. Samples were incubated in the dark at RT for 60 min. The percentage of dead cells in cultures was determined using SYTOX Green (Thermo Fisher). SYTOX Green (5 mM stock solution in DMSO) was used at a final concentration of 1 µM and incubated in the dark at RT for 10–15 min. Stained samples (E_x/E_m: 488 nm, 520 nm), along with an unstained control, were analyzed by flow cytometry.

2.3.7 Extracellular NO measurements

In situ, cell-derived NO produced during infection and present in the surrounding media was monitored using liposome-encapsulated spin trap (LEST) and electron paramagnetic resonance (EPR) spectroscopy, as previously described (Hirsh et al. 2016). In brief, liposomes were prepared from a 9:1 molar ratio of the phospholipids POPC and DPPG (Avanti Polar Lipids, Alabaster, AL) in chloroform containing 10 mM of the NO spin trap N-methyl-D-glucamine dithiocarbamate (MGD) and 2 mM ammonium iron (II) sulfate. See Supplementary Information for more details.

LEST (25 µL) was incubated in 10 ml of triplicate infected and uninfected cultures adjusted to equal cell densities with f/2 (minus Si) media for 3 h in the dark at RT. LEST incubated in f/2 (minus Si) served as a negative control; LEST incubated in the presence of 200 µM of the NO donor NOC-9 (Sigma-Aldrich) served as a positive control. After incubation, LEST was pelleted by centrifugation (20,000 × *g*, 30 min, 4 °C). The supernatant was removed such that 30 µL of LEST pellet and buffer remained. The pellet and buffer were homogenized, flash frozen in liquid nitrogen, and

stored at −80 °C. For EPR analysis, frozen LEST was thawed and drawn up into microcapillary tubes. EPR spectra were collected and the signal from spin-trapped NO quantified as described previously (Hirsh et al. 2016). See Supplementary Information for more details.

2.3.8 NO donor, NO scavenger, and hydrogen peroxide treatments

To further investigate the cellular role of NO during infection, the following experiments were conducted: (1) *E. huxleyi*-EhV infection in the presence of an NO scavenger, (2) monitoring physiology of *E. huxleyi* pre-treated with various concentrations of an NO donor and subsequently challenged with hydrogen peroxide (H_2O_2), and (3) determination of the total antioxidant capacity of *E. huxleyi* cell lysates both treated with an NO donor and undergoing infection. The NO donor used was S-nitroso-N-acetylpenicillamine (SNAP) and treatments were done at concentrations empirically determined to be non-lethal (up to 100 µM; Figure S7) for at least 16 h prior to H_2O_2 treatment or biomass harvest. Given SNAP has a donor half-life of ~6 h, this time period represents >2 half-lives. The NO scavenger used was carboxy-PTIO potassium salt (c-PTIO; Thermo Fisher) and was applied to cells at the time of infection at a range of concentrations (250 µM–1 mM dissolved in MilliQ). Treatments with H_2O_2 (30% w/w; Sigma-Aldrich) were performed between 10 and 100 µM. Cell abundance, percent dead cells, intracellular NO and ROS, and the photochemical quantum yield of photosystem II (F_v/F_m; see Supplementary Information) were monitored for these experiments.

2.3.9 Total antioxidant capacity

E. huxleyi cell lysates were generated and protein concentration was determined (see Supplementary Information). The total enzymatic and non-enzymatic antioxidant capacity (TAC) of the extracts was determined using the Antioxidant Assay Kit (Cayman Chemical, Ann Arbor, MI), which measures the capacity of cell extracts to prevent the oxidation of ABTS (2,2'-azino-di-[3-ethylbenzthiazoline sulphonate]) in the presence of H_2O_2compared to a standard of the vitamin E analog Trolox (6-hydroxy-2,5,7,8-tetramethylchroman-2-carboxylic acid). The assay and standard curve were run according to the manufacturer's instructions. Absorbance at 750 nm was measured using a SpectraMax M3 microplate reader. TAC is expressed as the concentration (mM) of antioxidants in equivalents of Trolox normalized to the total protein concentration of the sample.

2.3.10 Fieldwork

Intracellular NO, ROS, and cell death were assessed for open ocean, EhV-infected *E. huxleyi* populations in the Northeast Atlantic during the North Atlantic Virus Infection of Coccolithophores Expedition (http://www.bco-dmo.org/project/2136) aboard the R/V Knorr. The NA-VICE traversed a 2000 nautical mile transect from the Azores to Iceland and identified *E. huxleyi* blooms at different stages of bloom formation and viral infection (Lehahn et al. 2014, Laber et al. 2018, Sheyn et al. 2018). Individual CTD casts were characterized and grouped into stations-"early infection (EI)", "early infection revisited (EI_R)", "late infection (LI)", and "post infection (PI)"—using a combination of MODIS/AQUA satellite imagery, a suite of diagnostic lipid- and gene-based molecular biomarkers, analytical flow cytometry, in situ optical sensors, and sediment traps (methods described by (Laber et al. 2018)).

Here we further divided the "early infection" population into "EI_1" and "EI_2" given the greater number of samples available at this site for analysis and to provide higher temporal resolution to the trends. In order to explore the robustness of the patterns observed, we explored additional data from three CTD casts not analyzed in the aforementioned study (Laber et al. 2018), along with an individual CTD cast (cast 92) from EI_1 to illustrate a comparative signal for an early infected population. See Supplementary Information for a list of casts in each station.

Water was collected at six depths—extending from the subsurface, through the mixed layer encompassing the chlorophyll maximum, and down to 150 m—using Niskin bottles mounted on a 24-position rosette equipped with a Seabird SBE conductivity-temperature-depth (CTD) profiler. Sub-samples were stained with DAF-FM Diacetate, CM-H_2DCFDA, and SYTOX Green (5 μM) as described above. Stained samples, along with an unstained control, were run on a Guava flow cytometer (EMD Millipore, Burlington, MA) in duplicate. We present data from three depths per cast corresponding to the depth at which *E. huxleyi* cell abundance was highest, along with one sampling depth above and one sampling depth below the *E. huxleyi* maximum, in box-and-whisker plots. These depths generally ranged from 8 to 40 m and are listed in Table S2.

2.3.11 Data analysis and statistics

Flow cytometry data collected for laboratory experiments were analyzed using FlowJo (v. 10.2). Statistics (counts and mean fluorescence) were based on at least 1000 *E. huxleyi* events. Mean fluorescence per cell for DAF-FM Diacetate and CM-H_2DCFDA stained samples are reported as the difference between the mean 520 nm

fluorescence per cell of the stained sample and an unstained control. Percent SYTOX Green positive cells are reported as the percent of the total *E. huxleyi* population that has elevated 520 nm fluorescence relative to an unstained control.

Flow cytometry data for fieldwork were analyzed using GuavaSoft InCyte (v. 2.2.2). *E. huxleyi* was distinguished by pre-gating all events by chlorophyll and gating the *E. huxleyi* population off side scatter and forward scatter signatures corresponding to a reference culture. Statistics (counts and mean fluorescence) were based on at least 50 *E. huxleyi*events, with most samples encompassing 100–400 events, and averaged between two replicates per depth.

Statistically significant differences between infected and uninfected cultures for the parameters measured in this study were determined with Student's *t*-tests ($p < 0.05$). To test differences between multiple means, a one-way ANOVA with a Tukey HSD post hoc test was used. Error bars on all graphs are ± standard error of the mean (se). Linear regression analysis was used to explore relationships between various parameters in the NA-VICE dataset. All statistical tests were performed in R and plots were generated using the ggplot2 package.

2.4 RESULTS

2.4.1 Intracellular NO production increases during viral infection

The onset of cell lysis by EhV infection at 48–72 h post infection (hpi) was marked by 12.5 and 60% decreases in cell abundance between 24–48 hpi and 48–72 hpi, respectively (Fig. 2.1a), coinciding with EhV production (Fig. 2.1b). Cell decline was concomitant with increases in both the proportion of dead or dying cells indicated

by SYTOX Green (26% of culture at 48 hpi and 58% culture at 72 hpi; Fig. 2.1c) and intracellular ROS indicated by CM-H_2DCFDA, increasing ~3-fold at 48 hpi and ~17-fold at 72 hpi (Fig. 2.1d). Both SYTOX and CM-H_2DCFDA signals were strongest at 72 hpi. Notably, intracellular NO production did not follow these trends. Enhanced intracellular NO, assessed with DAF-FM DA, was observed earlier than the burst of ROS, increasing 1.5- to 2-fold above uninfected controls at 24 hpi (Fig. 2.1e, f). Intracellular NO production in infected cultures remained elevated compared to uninfected controls throughout the course of infection. A steady decrease in basal intracellular NO production was observed in uninfected control cells over the same time frame (Fig. 2.1e).

Intracellular esterase activity in infected cells remained unchanged during infection, while control cells displayed an increase in esterase activity during growth (Figure S2.1), suggesting that changes in intracellular esterase activity were not responsible for the higher DAF-FM DA fluorescence observed in infected cells. Furthermore, treatment of *E. huxleyi* with the NO donor SNAP increased DAF-FM DA cellular fluorescence, while the NO scavenger diminished fluorescence (Figure S2.2). The presence of the NO-bound, fluorescent DAF-FM-T product was also chemically confirmed using HPLC MS/MS in cells treated with two NO donors in a dose-dependent manner (Figures S2.3 and S2.4).

2.4.2 Viral infection triggers enhanced extracellular NO

Statistically significant differences in extracellular NO production were observed between infected and uninfected cultures at 48 hpi, 24 h after peak

intracellular NO production (Fig. 2.2). Four-fold higher cell-normalized extracellular NO was observed at 48 hpi in the infected cultures relative to uninfected controls. A control experiment in which cells were incubated with LEST for 3 h found no impacts of LEST on cell survival, intracellular NO production, intracellular ROS production, or photochemical quantum yield of photosystem II (Fv/Fm) (Table S2.1).

2.4.5 NO scavenging decreases viral burst size

EhV infection proceeded similarly in cells treated with the NO scavenger c-PTIO as that observed for untreated cells across a range of concentrations, with the onset of cell lysis and viral production occurring 48–72 hpi (Figure S2.5). There was, however, a statistically significant, dose-dependent decrease in viral burst size (the number of viruses produced per cell lysed between the 24–72 hpi) in c-PTIO-treated cells undergoing infection (Fig. 2.3). Exposure of uninfected control *E. huxleyi* cells to c-PTIO yielded no significant differences in cellular growth rates or Fv/Fm compared to untreated cells over the course of 72 h (Figure S2.6).

2.4.6 NO production stimulates antioxidant activity

Cells that were pre-treated with the NO donor SNAP prior to challenge with H_2O_2 (100 μM) had enhanced growth compared to cells treated with H_2O_2 only over the course of 72 h (Fig. 2.4a). Additionally, none of the SNAP pre-treated cultures experienced net cell death in the first 24 h of the experiment, though growth rates were diminished (Fig. 2.4a). In contrast, cells treated with H_2O_2 only experienced net cell decline within the first 24 h of treatment. SNAP pre-treated cultures were also able to maintain higher Fv/Fm values over the course of 72 h compared to the H_2O_2-only

control (Fig. 2.4b). No effect was observed in DMSO-only pre-treated cultures (SNAP is dissolved in DMSO) in their response to H_2O_2 treatment (Figure S2.8).

Cell lysates from cultures treated with SNAP exhibited significantly elevated protein-normalized total enzymatic and non-enzymatic antioxidant capacity (TAC) (Fig. 2.5). The protein-normalized TAC of cells also increased in cells undergoing viral infection, with statistically significant differences between infected and uninfected cells beginning at 24 hpi. Little to no change was detected in uninfected control cultures during this same time period (Fig. 2.6).

2.4.7 NO, ROS, and cell death in natural *E. huxleyi* blooms

Open ocean *E. huxleyi* blooms were encountered during the NA-VICE cruise in the eastern North Atlantic that were at different stages of viral infection ((Lehahn et al. 2014, Laber et al. 2018, Sheyn et al. 2018); Fig. 2.7a–c). Stations were designated as "early infection" (EI_1, EI_2, EI_R), "late infection" (LI), and "post infection" (PI) by (Laber et al. 2018) based on the relative abundance of *E. huxleyi* (Fig. 2.7b) and cell-associated EhV populations (i.e., the number of copies of major capsid protein (MCP) per host cell) (Fig. 2.7c), as well as the inventories of diagnostic glycosphingolipid (such as vGSLs and sGSLs) and betaine-like lipid biomarkers, all of which are indicative of these stages of infection ((Vardi et al. 2009, Vardi et al. 2012, Fulton et al. 2014, Hunter et al. 2015); see Discussion). The abundance of *E. huxleyi* cells ranged from ~1000–3000 cells ml^{-1} in early infection stations and decreased in late (~1300 cells ml^{-1}) and post (~800 cells ml^{-1}) infection stations (Fig. 2.7b). Early infection stations had low copy numbers of EhV-derived MCP (mean of 44 copies

cell^{-1}). MCP copy number increased in late (mean of 120 copies cell^{-1}) and post (mean of 800 copies cell^{-1}) infection (Fig. 2.7c), indicative of an increased degree of infection.

Intracellular NO production was elevated in EI_2, EI_R, LI, and PI, relative to the initial occupation of EI_1, with a 5.2, 2.8, 3.0, and 5.0-fold higher mean per cell DAF-FM DA fluorescence, respectively (Fig. 2.7d). Intracellular ROS of *E. huxleyi* at these stations was generally low and not statistically different from each other. ROS was elevated only in *E. huxleyi* cells found in the PI populations (Fig. 2.7e), with an average 3.5-fold higher mean per cell CM-H_2DCFDA fluorescence than the other stations, consistent with observations of a late phase infected culture (Fig. 2.1). Similarly, cell death was moderately elevated in LI populations and significantly higher in PI populations; *E. huxleyi* cells averaged about 6-fold higher mean per cell SYTOX Green fluorescence in PI casts (Fig. 2.7f) above cells in early infection populations. Taken together, the levels of cellular NO, ROS, and death of *E. huxleyi* cells undergoing different stages of infection generally reflected the patterns observed in lab cultures (Fig. 2.1).

These diagnostic parameters were examined for three additional *E. huxleyi* populations (CTD 29, 40, and 89) that were outside of the aforementioned characterized water masses. An individual cast (CTD 92) from the collection of casts performed and characterized at EI_1 with DNA- and lipid-based biomarkers was also included for comparison (Fig. 2.8; (Laber et al. 2018)). While not all biomarkers showed statistically significant differences, likely due to low sample size per station, trends in the data nonetheless suggest that these populations were in distinct phases of

infection. CTD casts 29 and 40 appeared most similar to a late infection or post infection scenario, respectively, with high ROS, NO, and cell death signatures. Specifically, CTD cast 29 had median DAF-FM DA, CM-H_2DCFDA, and SYTOX Green fluorescence values of 20.1, 22.4, and 25.8 RFU, respectively. CTD cast 40 had median DAF-FM DA, CM-H_2DCFDA, and SYTOX Green fluorescence values of 14.1, 34.1, and 74.9 RFU, respectively. These casts also had high EhV-derived MCP copies *E. huxleyi* cell^{-1} (mean of 170 and 230 copies cell^{-1} for cast 29 and 40), and low host cell abundance (mean less than 450 cells ml^{-1}). Cast 29 also had a high vGSL:sGSL ratio (mean ratio of 2.4 across all depths, with a $\log_{10}$ depth integrated inventory ratio of −0.042), further indicating active viral infection.

On the other hand, *E. huxleyi* populations sampled at CTD casts 89 and 92 were characterized by lower ROS, NO, and cell death signatures. Cast 89 had median DAF-FM DA, CM-H_2DCFDA, and SYTOX Green fluorescence values of 6.7, 12.9, and 5.6 RFU, respectively. CTD cast 89 also had moderate EhV-derived MCP copies (mean of 98 copies cell^{-1}) and low cell abundance (mean of 460 cells ml^{-1}), along with a much lower vGSL:sGSL ratio (mean ratio of 0.60 across all depths, with a log10 depth integrated inventory of −0.35). Cells at CTD cast 92 had the lowest comparative DAF-FM DA, CM-H_2DCFDA, and SYTOX Green fluorescence with median values of 2.4, 10.7, and 1.9 RFU, respectively. These populations also had very low incidence of EhV-derived MCP (mean of only 8 copies cell^{-1}) and high host cell abundance (~2000 cells ml^{-1}).

Relationships among these diagnostic stains across the cruise were explored using linear regression analysis. There was a significant positive correlation

($r^2 = 0.4337$, $p = 1.21e^{-7}$) between the levels of intracellular ROS and cell death (mean SYTOX fluorescence) in *E. huxleyi* cells across all CTD casts (Fig. 2.9a). In addition, there was a positive correlation ($r^2 = 0.510$, $p = 1.39e^{-7}$) between cell death and EhV-derived MCP copies *E. huxleyi* cell^{-1} (Fig. 2.9b). There were weak or non-significant relationships observed between intracellular NO and: intracellular ROS ($r^2 = 0.0696$, $p = 0.0266$); cell death ($r^2 = -0.0049$, $p = 0.386$); and EhV-derived MCP copies *E. huxleyi*cell^{-1} ($r^2 = -0.00684$, $p = 0.414$) across the stations.

2.5 DISCUSSION

The production of reactive oxygen species (ROS)—radical and non-radical molecules known to have toxic cellular effects such as hydrogen peroxide (H_2O_2), superoxide ($O_2^{\cdot -}$), and the hydroxyl radical ($HO^{\cdot}$)—is a well-documented feature of lytic viral infection in *E. huxleyi* (Evans et al. 2006, Vardi et al. 2012, Sheyn et al. 2016). Unlike in host-pathogen systems of higher plants in which a ROS burst often occurs rapidly following pathogen invasion in order to prevent the spread of infection (Lamb & Dixon 1997), cellular ROS production in the *E. huxleyi*-EhV system is not observed until late stages of infection occurring at the onset of lysis. These ROS, specifically H_2O_2, appear to be required for the induction of the PCD cascade in the host and subsequent cell lysis (Sheyn et al. 2016).

Little is known about the function of reactive nitrogen species, such as NO, in *E. huxleyi* physiology or in the emerging picture of the molecular pathways governing viral infection. Our previous work demonstrated that *E. huxleyi* cell lysates possess the ability to produce NO via nitrate reductase (NR) and hinted at the

possibility of elevated NO production during infection (Hirsh et al. 2016). It remains unclear, however, whether cellular nitrite levels reach sufficient concentrations during infection to drive NR-dependent NO production. Here, we demonstrate that enhanced intracellular NO production is a hallmark of viral infection in this species and does not occur simultaneously with the accumulation of ROS, indicating an independent function. Statistically significant differences in intracellular NO between infected and non-infected control cells were seen as early as 24 hpi, when there is ~2-fold higher DAF-FM DA fluorescence in infected cells. NO in cells remains elevated throughout the course of infection, relative to uninfected controls. Additionally, we detected an increase in extracellular NO in cultures during infection. These results provide an interesting framework for further exploring the role of NO in viral infection within a population. The ability of NO to act as a diffusible extracellular signal has been previously demonstrated in diatoms where it was shown to be a critical component in the stress perception of *Phaeodactylum tricornutum* (Vardi et al. 2006). Given our results, it is conceivable that NO produced during viral infection of *E. huxleyi* may serve a similar extracellular signaling role, possibly communicating infection to neighboring cells.

Both the early production and apparent requirement of NO for optimal viral production does suggest a potential cyto-protective role. NO has been shown in both plants and algae to have a broad antioxidant function, allowing cells to cope with various stressors that elicit ROS (Li et al. 2013). For example, NO has been implicated in the response of *Chlorella vulgarus* to copper stress (Singh et al. 2004), protection of *Scenedesmus obliquus* against H_2O_2 (Mallick et al. 2002), and reduction of UV-B

damage in the cyanobacterium *Spirulina platensis* (Xue et al. 2007). Our findings show that NO may be responsible for similar antioxidant activity in *E. huxleyi*. Pre-treatment of cells with an NO donor increased survival upon subsequent challenge with H_2O_2, the main ROS produced during infection. Additionally, exogenously added NO led to an increase in the ability of *E. huxleyi* cell lysates to detoxify H_2O_2, a feature of cells also undergoing viral infection.

The antioxidant function of NO in early-infected *E. huxleyi* supports previous observations of antioxidant changes that occur in this system. Sheyn et al. (Sheyn et al. 2016) showed that significant changes in the expression of antioxidant related genes and metabolites occur in the early stages of infection. Specifically, despite downregulation of some genes involved in ROS detoxification (such as ascorbate peroxidase and catalase) and upregulation of others, net H_2O_2 accumulation and cell death induction was not observed until late stages of the infection. *E. huxleyi* is also able to maintain high levels of both total and reduced glutathione pools (Sheyn et al. 2016), suggesting a maintenance of antioxidant capacity. Additionally, viral infection has been shown to induce production of the volatile organic sulfur compound dimethyl sulfide (DMS), along with its byproduct acrylic acid (Evans et al. 2007), both of which are believed to also have an antioxidant function (Sunda et al. 2002, Evans et al. 2007). Therefore, there is evidence to support our observation that increased antioxidant function is a hallmark of infection, and we suggest that that NO may be crucial player in this induction.

Surprisingly, we observed a continued enhancement of cellular antioxidant capacity well into the late stages of infection, when oxidative stress and cell death

became apparent. Previous work has demonstrated that prior exposure of the green alga *Chlamydomonas reinhardtii* and the dinoflagellate *Peridinium gatunense* to H_2O_2 increases both cellular antioxidant enzyme activity and the cell's ability to detoxify ROS, but, paradoxically, it also increases sensitivity to subsequent sub-lethal doses of ROS (Murik & Kaplan 2009). This sensitivity has been attributed to accumulation of certain metabolites of antioxidant pathways during the initial stress, specifically the metabolite dehydroascorbate (Murik & Kaplan 2009, Murik et al. 2014), which acts as a stress-surveillance system. It is feasible that a similar mechanism occurs in *E. huxleyi* during viral infection, in which increased NO production and antioxidant capacity during the early stages of infection act to sensitize cells to oxidative stress and ROS-induced PCD later on.

The mechanism(s) by which NO production may lead to increased cellular antioxidant capacity in algae is unknown. However, work in plant systems suggest that a major mechanism of NO function is by post-translational modification of antioxidant proteins, particularly s-nitrosylation of cysteine residues (Begara-Morales et al. 2016). For example, it has been shown that NO binds to the ascorbate peroxidase of *Arabidopsis thaliana*, upregulating its H_2O_2-scavenging activity during stress (Yang et al. 2015). Other possible points of NO involvement during viral infection include regulation of metacaspases, the activity of which has been demonstrated to be essential for viral infection of *E. huxleyi* (Bidle et al. 2007). In *Arabidopsis*, for example, NO is a critical regulator of type-II metacaspase 9 (Belenghi et al. 2007). Future work in the *E. huxleyi*-EhV system should explore potential host and/or viral proteins that are targets of NO-mediated post-translational modification in order to get a complete

understanding of the role of NO in infection and the antioxidant changes that occur. Our observation that extracellular NO does not accumulate until 48 hpi (24 h after intracellular increases are seen) does point to the existence of intracellular NO sinks during infection.

Our findings also demonstrate NO production by naturally occurring *E. huxleyi* populations undergoing various stages of viral infection in the eastern North Atlantic (Lehahn et al. 2014, Laber et al. 2018, Sheyn et al. 2018). These populations were characterized as either early, late, or post infection based on an array of diagnostic lipid (glycosphingolipid and betaine-like lipids) and gene-based (EhV-derived MCP) biomarkers, along with the abundance of host *E. huxleyi* (Laber et al. 2018, Sheyn et al. 2018). We were able to ground-truth the diagnostic stains used in our lab cultures in natural populations across a dynamic range of infection states. We observed that intracellular ROS production and cell death generally show similar trends in the field to those in laboratory (Fig. 2.1; (Evans et al. 2006, Martinez Martinez et al. 2011, Sheyn et al. 2016)) and mesocosm (Vardi et al. 2012) studies. Both are significantly elevated only in the post infection scenario where the abundance of replicating EhVs was high, *E. huxleyi* abundance was low, and lipid biomarkers indicated active infection. When all stations are taken together, a statistically significant linear relationship between cell death and intracellular ROS, as well as between cell death and EhV copy number, is observed, supporting multiple laboratory studies showing that the accumulation of ROS within cells occurs concurrently with initiation of cell death.

Patterns of intracellular NO in *E. huxleyi* at these stations also support our lab-based results. Elevated NO occured in relatively early infection and remains elevated in *E. huxleyi* cells encountered at both the late and post infection scenarios. We identified three distinct early infection phases where EhV-derived MCP copy number was low and *E. huxleyi* cell concentrations were high: EI_1, EI_2, and EI_R. Populations at EI_2 and EI_Rwere characterized by elevated NO production relative to EI_1. It may be that the populations sampled at the EI_1 were early enough in infection that virus-induced NO production had not yet occurred, as illustrated by CTD cast 92.

Finally, data from additional casts reinforced the robustness and predictive power of the relationships that emerged between diagnostic stain data and other established biomarkers of viral infection. The combination of very low levels of cellular NO, ROS, death, virus-specific lipid signatures (vGSL:sGSL), and EhV-derived MCP copy numbers per *E. huxleyi* cell at CTD casts 89 and 92 was indicative infection was either in its beginning stages or was occurring at a low level at these two casts. Furthermore, the relatively high abundances of *E. huxleyi* cells found in CTD cast 92 further suggests that this was a relatively healthy bloom with little to no lytic viral infection occurring. *E. huxleyi* at CTD casts 29 and 40 were marked by relatively high levels of intracellular NO, ROS, and cell death in resident *E. huxleyi* populations. As expected, these populations showed strong evidence of a late or post stage viral infection with high virus-specific lipids (cast 29), high EhV-derived MCP reads, and low abundances of *E. huxleyi*.

Fluorescent dyes targeting cellular lipids have been previously used to quickly and efficiently diagnose viral infection in lab studies (Martinez Martinez et al. 2011).

Our field observations suggest that NO production, determined through the DAF-FM DA staining, can also be a useful early indicator of the onset of lytic viral infection in natural *E. huxleyi* populations. NO can be assessed in real-time and its increase occurs prior to the emergence of other fluorescent signatures and biomarkers, many of which can only be analyzed on shore. Combined with classic and previously established infection biomarkers, fluorescent intracellular NO, ROS, and death indicators can provide an in situ, high-resolution assessment of the stage of lytic viral infection and physiological status of natural blooms.

2.6 CONCLUSION

Our work implicates the free radical NO as a crucial player in the molecular pathways governing the viral infection of *E. huxleyi*, distinct from ROS production. Furthermore, intracellular NO may have an antioxidant function, keeping ROS accumulation low so that viruses can replicate and assemble in a redox favorable environment. The application of an exogenous NO donor to *E. huxleyi* cultures enhanced survival in the face of subsequent H_2O_2 stress. Similarly, cultures undergoing infection and treated with a low dose of exogenous NO exhibited enhanced ability to detoxify H_2O_2. Additionally, the patterns of NO production, ROS production, and cell death seen in the laboratory were observed across a dynamic range of infection states for natural *E. huxleyi* populations sampled in the North Atlantic. Taken together, our culture studies and fieldwork demonstrate that the use of this suite of stains, along with classic lipid- and gene-based biomarkers, helps to more fully describe and diagnose viral infection status in natural *E. huxleyi* populations.

2.7 ACKNOWLEDGEMENTS

We would like to thank K. Thamatrakoln and A. Kustka for feedback and fruitful discussion. We also thank the captain and crew of the *R/V Knorr* for their assistance during the NA-VICE. This work was funded by grants from the National Science Foundation (OCE-1061833 and OCE-1537951 to KBD) and the Gordon and Betty Moore Foundation (GBMF#3301 to BASVM and GBMF#3789 to KDB).

2.8 REFERENCES

Begara-Morales JC, Sanchez-Calvo B, Chaki M, Valderrama R, Mata-Perez C, Padilla MN, Corpas FJ, Barroso JB (2016) Antioxidant Systems are Regulated by Nitric Oxide-Mediated Post-translational Modifications (NO-PTMs). Frontiers in plant science 7:152

Belenghi B, Romero-Puertas MC, Vercammen D, Brackenier A, Inze D, Delledonne M, Van Breusegem F (2007) Metacaspase activity of *Arabidopsis thaliana* is regulated by S-nitrosylation of a critical cysteine residue. The Journal of biological chemistry 282:1352-1358

Besson-Bard A, Pugin A, Wendehenne D (2008) New insights into nitric oxide signaling in plants. Annual review of plant biology 59:21-39

Bidle KD (2015) The molecular ecophysiology of programmed cell death in marine phytoplankton. Annual review of marine science 7:341-375

Bidle KD, Haramaty L, Barcelos ERJ, Falkowski P (2007) Viral activation and recruitment of metacaspases in the unicellular coccolithophore, *Emiliania huxleyi*. Proceedings of the National Academy of Sciences of the United States of America 104:6049-6054

Bidle KD, Vardi A (2011) A chemical arms race at sea mediates algal host-virus interactions. Current opinion in microbiology 14:449-457

Bratbak G, Egge JK, Heldal M (1993) Viral mortality of the marine alga *Emiliania huxleyi* (Haptophyceae) and termination of algal blooms. Marine Ecology Progress Series 93:39-58

Brown CW, Yoder JA (1994) Coccolithophorid blooms in the global ocean. Journal of Geophysical Research 99:7467-7482

Brussaard CPD, Kempers RS, Kop AJ, Riegman R, Heldal M (1996) Virus-like particles in a summer bloom of *Emiliania huxleyi* in the North Sea. Aquatic Microbial Ecology 10:105-113

Brussaard CPD, Marie D, Bratbak G (2000) Flow cytometric detection of viruses. Journal of Virological Methods 85:175-182

Cortese-Krott MM, Rodriguez-Mateos A, Kuhnle GG, Brown G, Feelisch M, Kelm M (2012) A multilevel analytical approach for detection and visualization of intracellular NO production and nitrosation events using diaminofluoresceins. Free radical biology & medicine 53:2146-2158

Evans C, Kadner SV, Darroch LJ, Wilson WH, Liss PS, Malin G (2007) The relative significance of viral lysis and microzooplankton grazing as pathways of dimethylsulfoniopropionate (DMSP) cleavage: An *Emiliania huxleyi* culture study Limnology and Oceanography 52:1036-1045

Evans C, Malin G, Mills GP, Wilson WH (2006) Viral Infection of *Emiliania Huxleyi* (Prymnesiophyceae) Leads to Elevated Production of Reactive Oxygen Species. Journal of Phycology 42:1040-1047

Frada MJ, Schatz D, Farstey V, Ossolinski JE, Sabanay H, Ben-Dor S, Koren I, Vardi A (2014) Zooplankton may serve as transmission vectors for viruses infecting algal blooms in the ocean. Current biology : CB 24:2592-2597

Frohlich A, Durner J (2011) The hunt for plant nitric oxide synthase (NOS): is one really needed? Plant science : an international journal of experimental plant biology 181:401-404

Fuhrman JA (1999) Marine viruses and their biogeochemical effects. Nature 399:541-548

Fulton JM, Fredricks HF, Bidle KD, Vardi A, Kendrick BJ, DiTullio GR, Van Mooy BA (2014) Novel molecular determinants of viral susceptibility and resistance in the lipidome of Emiliania huxleyi. Environmental microbiology 16:1137-1149

Gallina AA, Brunet C, Palumbo A, Casotti R (2014) The effect of polyunsaturated aldehydes on Skeletonema marinoi (Bacillariophyceae): the involvement of reactive oxygen species and nitric oxide. Marine drugs 12:4165-4187

Groß F, Durner J, Gaupels F (2013) Nitric oxide, antioxidants and prooxidants in plant defence responses. Frontiers in plant science 4:419

Gusarov I, Shatalin K, Starodubtseva M, Nudler E (2009) Endogenous nitric oxide protects bacteria against a wide sprectrum of antibiotics. Science 235:1380-1384

Hirsh DJ, Schieler BM, Fomchenko KM, Jordan ET, Bidle KD (2016) A liposome-encapsulated spin trap for the detection of nitric oxide. Free radical biology & medicine 96:199-210

Holligan PM, Fernández E, Aiken J, Balch WM, Boyd P, Burkill PH, Finch M, Groom SB, Malin G, Muller K, Purdie DA, Robinson C, Trees CC, Turner SM, van der Wal P (1993) A biogemical study of the coccolithophore, *Emiliania huxleyi,* in the North Atlantic Global Biogeochemical Cycles 7:879-900

Hunter JE, Frada MJ, Fredricks HF, Vardi A, Van Mooy BAS (2015) Targeted and untargeted lipidomics of Emiliania huxleyi viral infection and life cycle phases highlights molecular biomarkers of infection, susceptibility, and ploidy. Frontiers in Marine Science 2

Klaas C, Archer DE (2002) Association of sinking organic matter with various types of mineral ballast in the deep sea: Implications for the rain ratio. Global Biogeochemical Cycles 16:63-61-63-14

Kojima H, Urano Y, Kikuchi K, Higuchi T, Hirata Y, Nagano T (1999) Fluorescent indicators for imaging nitric oxide production. Angewandte Chemie 38:3209-3212

Kumar A, Castellano I, Patti FP, Palumbo A, Buia MC (2015) Nitric oxide in marine photosynthetic organisms. Nitric oxide : biology and chemistry 47:34-39

Laber CP, Hunter JE, Carvalho F, Collins JR, Hunter EJ, Schieler BM, Boss E, More K, Frada M, Thamatrakoln K, Brown CM, Haramaty L, Ossolinski J, Fredricks H, Nissimov JI, Vandzura R, Sheyn U, Lehahn Y, Chant RJ, Martins AM, Coolen MJL, Vardi A, DiTullio GR, Van Mooy BAS, Bidle KD (2018) *Coccolithovirus* facilitation of carbon export in the North Atlantic. Nature microbiology 3:537-547

Lamb C, Dixon RA (1997) The oxidative burst in plant disease response. Annu Rev Plant Physiol Plant Mol Biol 48:251-275

Lehahn Y, Koren I, Schatz D, Frada M, Sheyn U, Boss E, Efrati S, Rudich Y, Trainic M, Sharoni S, Laber C, DiTullio GR, Coolen MJ, Martins AM, Van Mooy BA, Bidle KD, Vardi A (2014) Decoupling physical from biological processes to assess the impact of viruses on a mesoscale algal bloom. Current biology : CB 24:2041-2046

Li P, Liu CY, Liu H, Zhang Q, Wang L (2013) Protective function of nitric oxide on marine phytoplankton under abiotic stresses. Nitric oxide : biology and chemistry 33:88-96

Malin G, Steinke M (2004) Dimethyl sulfide production: what is the contribution of the coccolithophores? In: Thierstein HR, Young JR (eds) Coccoltihophores: From Molecular Processes to Global Impact. Springer, Germany

Mallick N, Mohn FH, Soeder CJ, Grobbelaar JU (2002) Ameliorative role of ntiric oxide on H2O2 toxicity to a chlorophycean alga *Scenedesmus obliquus*.

Martens-Habbena W, Qin W, Horak RE, Urakawa H, Schauer AJ, Moffett JW, Armbrust EV, Ingalls AE, Devol AH, Stahl DA (2015) The production of nitric oxide by marine ammonia-oxidizing archaea and inhibition of archaeal ammonia oxidation by a nitric oxide scavenger. Environmental microbiology 17:2261-2274

Martinez JM, Schroeder DC, Larsen A, Bratbak G, Wilson WH (2007) Molecular dynamics of *Emiliania huxleyi* and cooccurring viruses during two separate mesocosm studies. Applied and environmental microbiology 73:554-562

Martinez Martinez J, Poulton NJ, Stepanauskas R, Sieracki ME, Wilson WH (2011) Targeted sorting of single virus-infected cells of the coccolithophore *Emiliania huxleyi.* PloS one 6:e22520

Moncada S (1999) Nitric oxide: discovery and impact on clinical medicine. Journal of the Royal Society of Medicine 92:164-169

Mur LA, Mandon J, Persijn S, Cristescu SM, Moshkov IE, Novikova GV, Hall MA, Harren FJ, Hebelstrup KH, Gupta KJ (2012) Nitric oxide in plants: an assessment of the current state of knowledge. AoB PLANTS 5:pls052

Murik O, Elboher A, Kaplan A (2014) Dehydroascorbate: a possible surveillance molecule of oxidative stress and programmed cell death in the green alga *Chlamydomonas reinhardtii*. The New phytologist 202:471-484

Murik O, Kaplan A (2009) Paradoxically, prior acquisition of antioxidant activity enhances oxidative stress-induced cell death. Environmental microbiology 11:2301-2309

Rosenwasser S, Mausz MA, Schatz D, Sheyn U, Malitsky S, Aharoni A, Weinstock E, Tzfadia O, Ben-Dor S, Feldmesser E, Pohnert G, Vardi A (2014) Rewiring Host Lipid Metabolism by Large Viruses Determines the Fate of *Emiliania huxleyi*, a Bloom-Forming Alga in the Ocean. The Plant cell 26:2689-2707

Schatz D, Shemi A, Rosenwasser S, Sabanay H, Wolf SG, Ben-Dor S, Vardi A (2014) Hijacking of an autophagy-like process is critical for the life cycle of a DNA virus infecting oceanic algal blooms. The New phytologist 204:854-863

Schroeder DC, Oke J, Malin G, Wilson WH (2002) *Coccolithovirus* (*Phycodnaviridae*): characterisation of a new large dsDNA algal virus that infects Emiliana huxleyi. Archives of virology 147:1685-1698

Sheyn U, Rosenwasser S, Ben-Dor S, Porat Z, Vardi A (2016) Modulation of host ROS metabolism is essential for viral infection of a bloom-forming coccolithophore in the ocean. The ISME journal 10:1742-1754

Sheyn U, Rosenwasser S, Lehahn Y, Barak-Gavish N, Rotkopf R, Bidle KD, Koren I, Schatz D, Vardi A (2018) Expression profiling of host and virus during a coccolithophore bloom provides insights into the role of viral infection in promoting carbon export. The ISME journal 12:704-713

Singh A, Sharma L, Mallick N (2004) Antioxidative role of nitric oxide on copper toxicity to a chlorophycean alga, *Chlorella*. Ecotoxicology and environmental safety 59:223-227

Sunda W, Kieber DJ, Kiene RP, Huntsman S (2002) An antioxidant function for DMSP and DMS in marine algae. Nature 418:31-320

Suttle CA (2007) Marine viruses--major players in the global ecosystem. Nature reviews Microbiology 5:801-812

Toledo JC, Jr., Augusto O (2012) Connecting the chemical and biological properties of nitric oxide. Chemical research in toxicology 25:975-989

Tyrrell T, Holligan PM, Mobley CD (1999) Optical impacts of oceanic coccolithophore blooms. Journal of Geophysical Research 104:3223-3241

Tyrrell T, Merico A (2004) *Emiliania huxleyi*: bloom observations and the conditions that induce them. In: Thierstein HR, Young JR (eds) Coccolithophores: From Molecular Processes to Global Impact. Springer, Germany

Vardi A, Bidle KD, Kwityn C, Hirsh DJ, Thompson SM, Callow JA, Falkowski P, Bowler C (2008) A diatom gene regulating nitric-oxide signaling and susceptibility to diatom-derived aldehydes. Current biology : CB 18:895-899

Vardi A, Formiggini F, Casotti R, De Martino A, Ribalet F, Miralto A, Bowler C (2006) A stress surveillance system based on calcium and nitric oxide in marine diatoms. PLoS biology 4:e60

Vardi A, Haramaty L, Van Mooy BAS, Fredricks HF, Kimmance SA, Larsen A, Bidle KD (2012) Host-virus dynamics and subcellular controls of cell fate in a natural coccolithophore population. Proceedings of the National Academy of Sciences of the United States of America 109:19327-19332

Vardi A, Van Mooy BA, Fredricks HF, Popendorf KJ, Ossolinski JE, Haramaty L, Bidle KD (2009) Viral glycosphingolipids induce lytic infection and cell death in marine phytoplankton. Science 326:861-865

Xue L, Li S, Sheng H, Feng H, Xu S, An L (2007) Nitric oxide alleviates oxidative damage induced by enhanced ultraviolet-B radiation in cyanobacterium. Current microbiology 55:294-301

Yang H, Mu J, Chen L, Feng J, Hu J, Li L, Zhou JM, Zuo J (2015) S-nitrosylation positively regulates ascorbate peroxidase activity during plant stress responses. Plant physiology 167:1604-1615

Zhang Z, Lin C, Liu C, Sun M, Ding H (2003) The effect of nitric oxide on the growth of marine phytoplankton. Journal of Ocean University of Qingdao 2:185-188

2.9 FIGURES

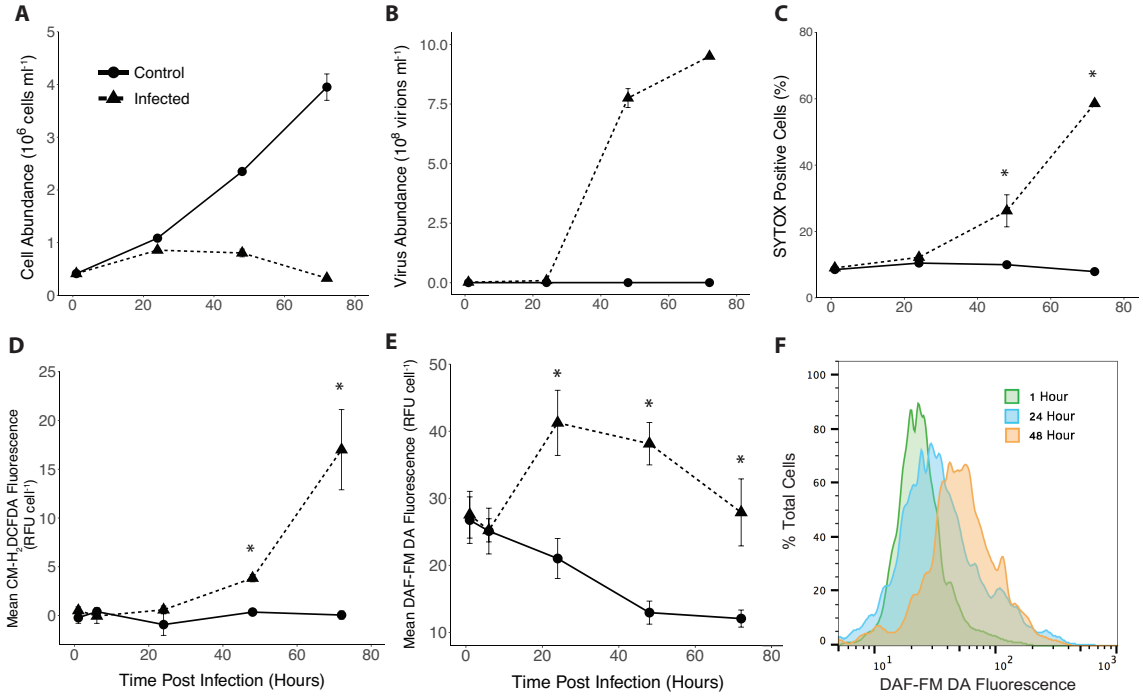

Figure 2.1 Physiological dynamics of viral infection of *E. huxleyi* CCMP1516 by EhV201. **a** Cell abundance and **b** viral abundance of infected (triangles/dashed line) and uninfected (circles/solid line) cultures are a mean of $n = 2$ (±se) from one representative viral infection experiment. **c** Percent dead cells assessed by SYTOX Green, **d** intracellular ROS assessed by CM-H_2DCFDA, and **e** intracellular NO assessed by DAF-FM DA. Values represent the mean of at least $n = 4$ (±se) across at least 3 distinct infection experiments. Statistically significant differences between infected and control cultures were determined using unpaired Student's *t*-test (*$p < 0.05$). **f** Histogram overlay of DAF-FM DA fluorescence values of one representative infected culture at 1, 24, and 48 hpi

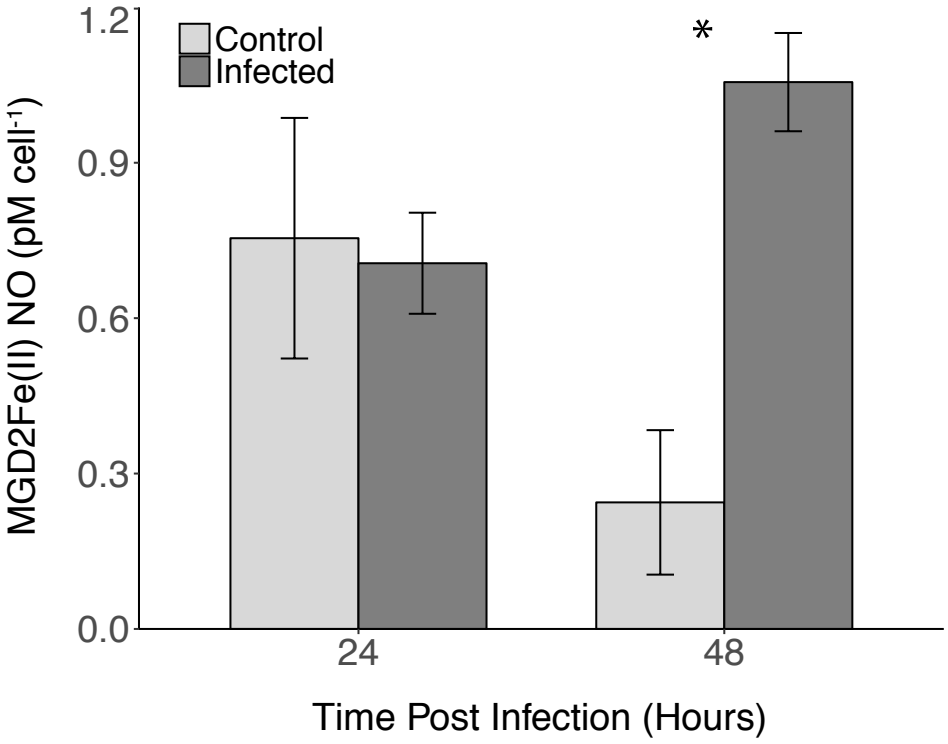

Figure 2.2 Concentration of extracellular NO in *E. huxleyi* CCMP1516 infected with EhV201 (dark gray bars) and control cultures (light gray bars). Values represent the mean concentration of spin trap bound NO per cell over a 3 h incubation period ($n = 3$, ±se). Statistically significant differences between infected and control cultures were determined using unpaired Student's *t*-test (*$p < 0.05$)

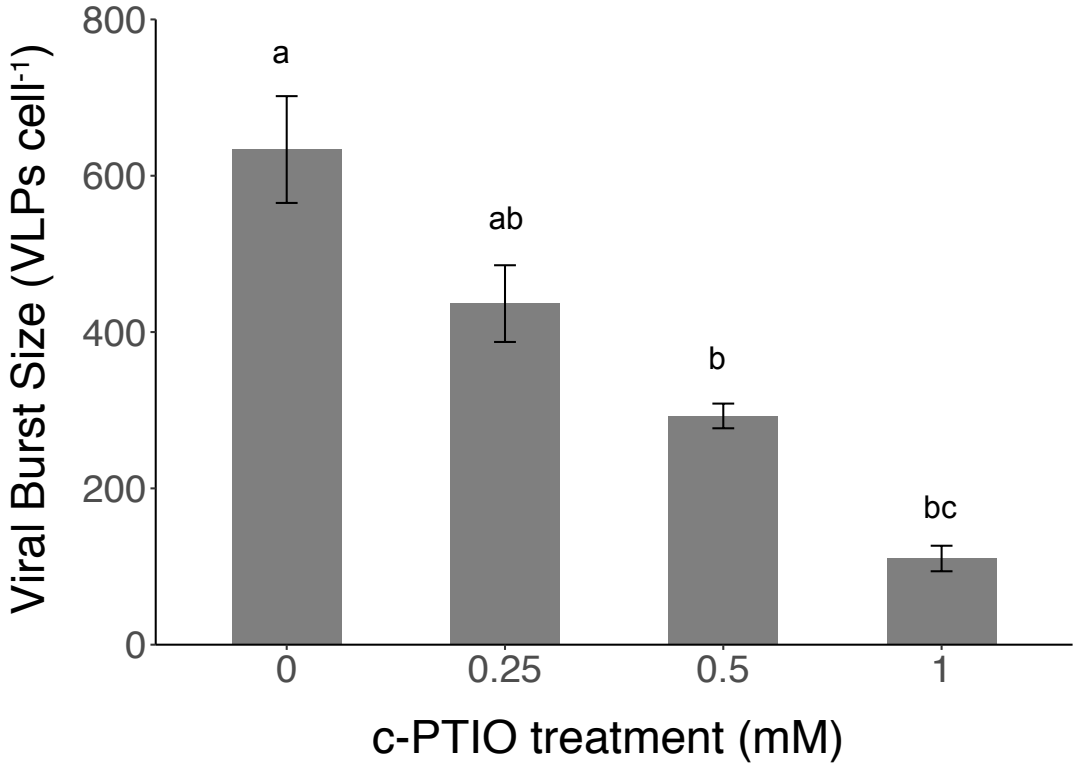

Figure 2.3 Viral burst sizes of infected *E. huxeyi* CCMP1516 treated with the NO scavenger c-PTIO, represented as the number of viral particles produced per cell lysed between 24 and 72 h post infection. Data are the mean of $n = 2$ (±se) and are a representative subset of multiple experiments. Statistically significant differences were determined using one-way ANOVA with the Tukey HSD post hoc test (letters denote statistically different subgroups; $p < 0.05$)

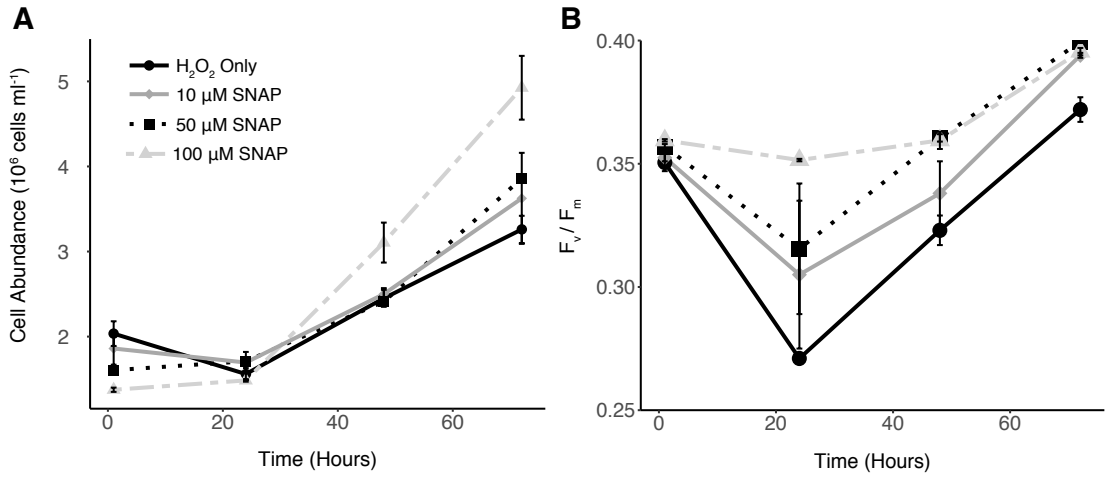

Figure 2.4 Response of cells pre-treated with exogenous NO to H_2O_2. **a** Cell abundance and **b** Fv/Fm of H_2O_2 treated (100 µM) *E. huxleyi* CCMP1516 pre-treated with different concentrations (10 µM, 50 µM, and 100 µM) of the NO donor SNAP. Data are a representative subset of multiple experiments and values represent the mean of $n = 2$ (±se)

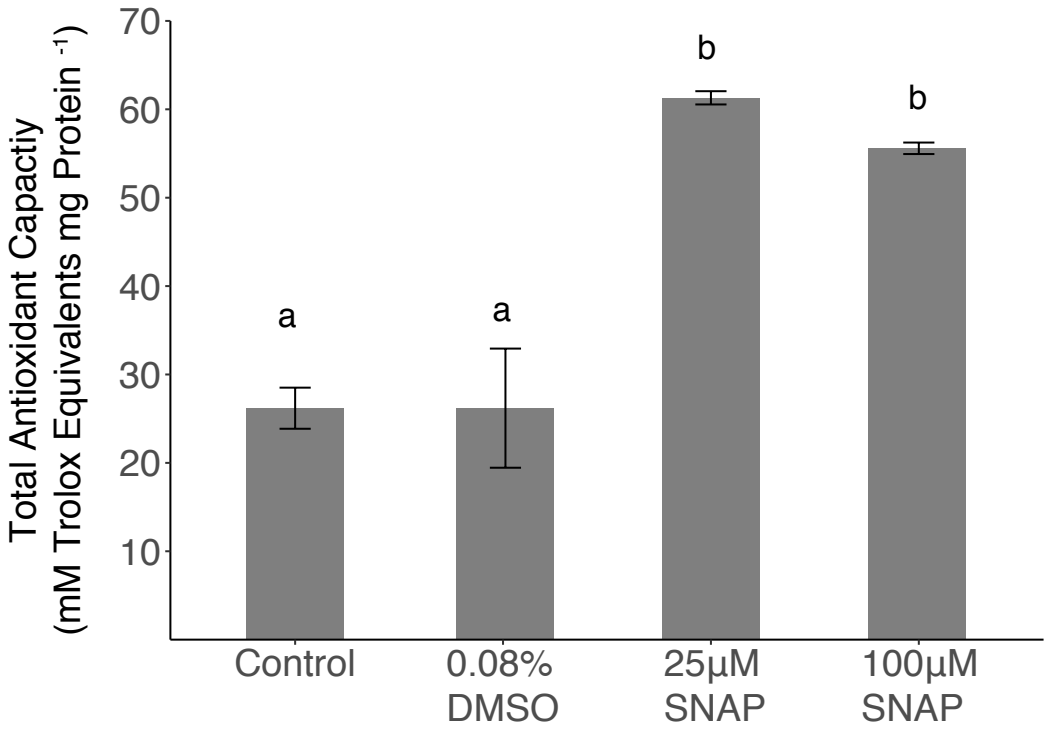

Figure 2.5 Protein-normalized, cellular antioxidant capacity of lysates from *E. huxleyi* CCMP1516 cultures treated with SNAP, along with a DMSO only and untreated controls. Statistically significant differences were determined using one-way ANOVA with the Tukey HSD post hoc test (letters denote statistically different subgroups, $p < 0.05$). Data shown are a representative subset of multiple experiments and are the mean of $n = 2$ (±se) per treatment

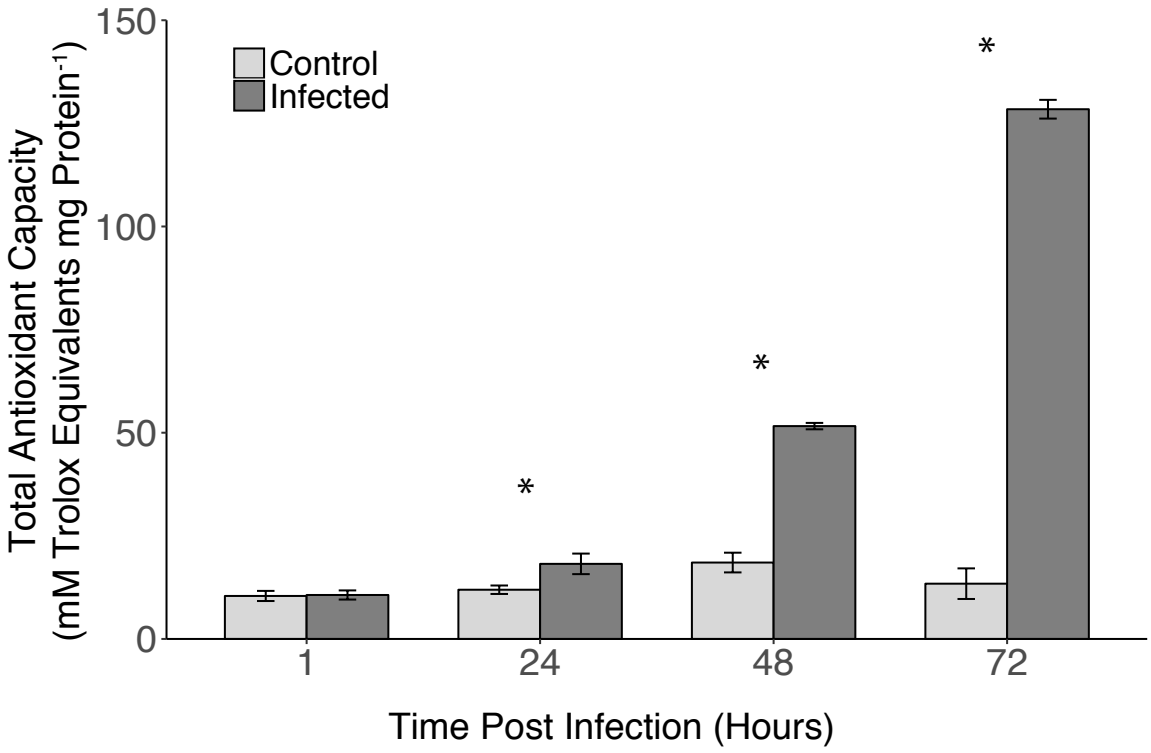

Figure 2.6 Protein-normalized, cellular antioxidant capacity of lysates from *E. huxleyi* CCMP1516 cultures undergoing infection with EhV201 (dark gray bars) and uninfected control cultures (light gray bars). Values represent the mean of $n = 5$ (+/− se) pooled from biological duplicates from one experiment. Statistically significance between control and infected cultures was determined used a Student's *t*-test (*$p < 0.05$)

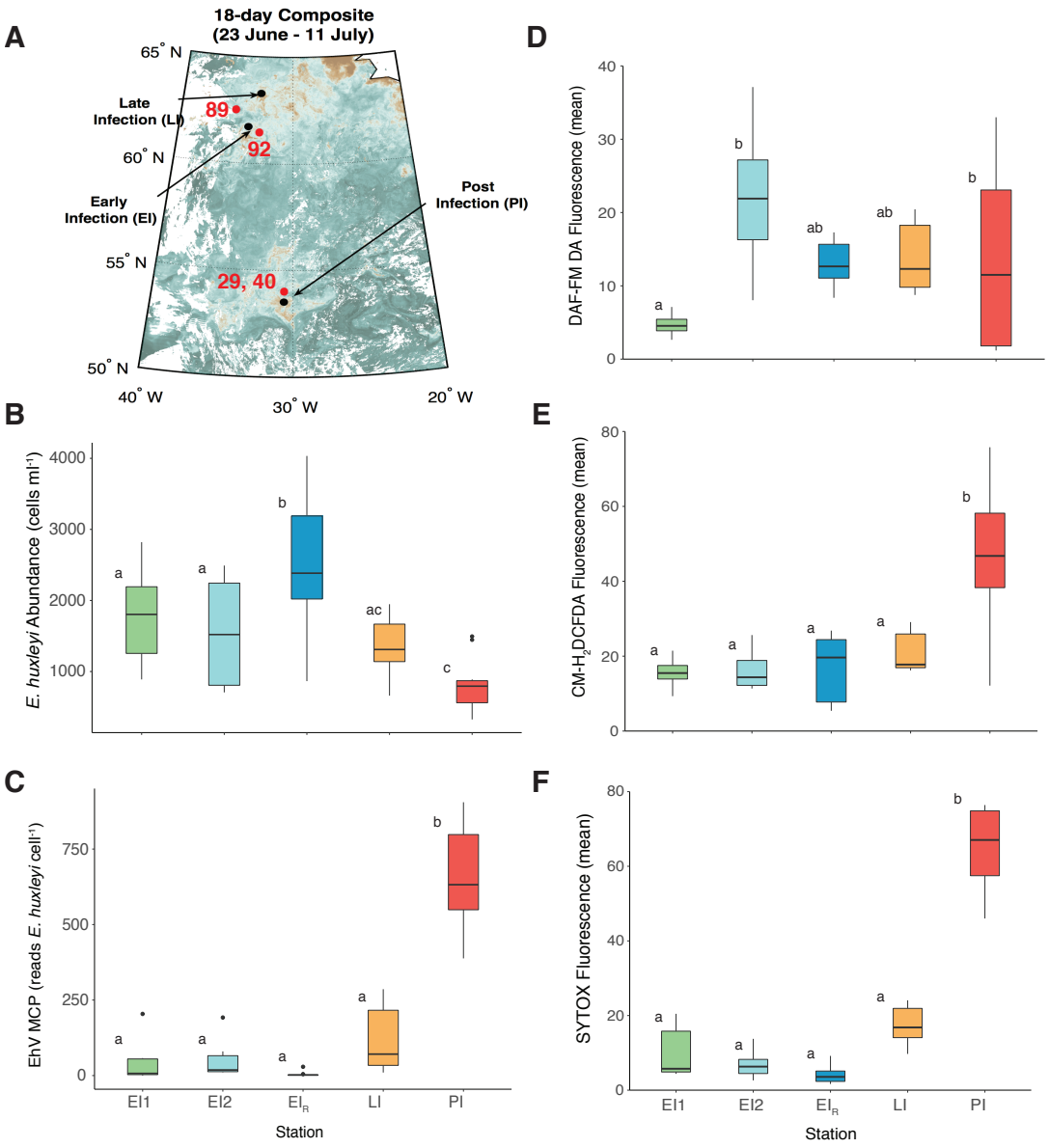

Figure 2.7 Assessment of diagnostic stains for natural *E. huxleyi* populations in the North Atlantic. **a** Locations of distinct water masses sampled on the NA-VICE cruise along a 2000 nautical mile transect in the North Atlantic. Early, late, and post infection populations were previously characterized using lipid- and gene-based biomarkers [12]. Red numbers 29, 40, 89, and 92 represent CTD casts for which additional analyses are performed in this study. **b**, **c** Box-and-whisker plots showing the respective abundances of host *E. huxleyi* cells (cells ml^{-1}) and replicating EhVs (MCP gene copies *E. huxleyi* $cell^{-1}$) for the different sampled populations at three depths where *E. huxleyi* were present in highest abundance. **d**–**f** Box-and-whisker plots

showing corresponding DAF-FM DA, CM-H_2DCFDA, and SYTOX Green fluorescence for these populations. Data are an average of two replicates per depth sampled. Data in (**a**, **b**, **c**, and **f**) were published by Laber et al. [12]. For all box plots, upper and lower bounds of the box represent the 25% and 75% quartiles around the median. Vertical lines extend to data points no greater than 1.5 times the inter-quartile range. Data points that extend beyond this range are represented by dots. Statistically significant differences were determined using one-way ANOVA with the Tukey HSD post hoc test (letters denote statistically different subgroups, $p < 0.05$)

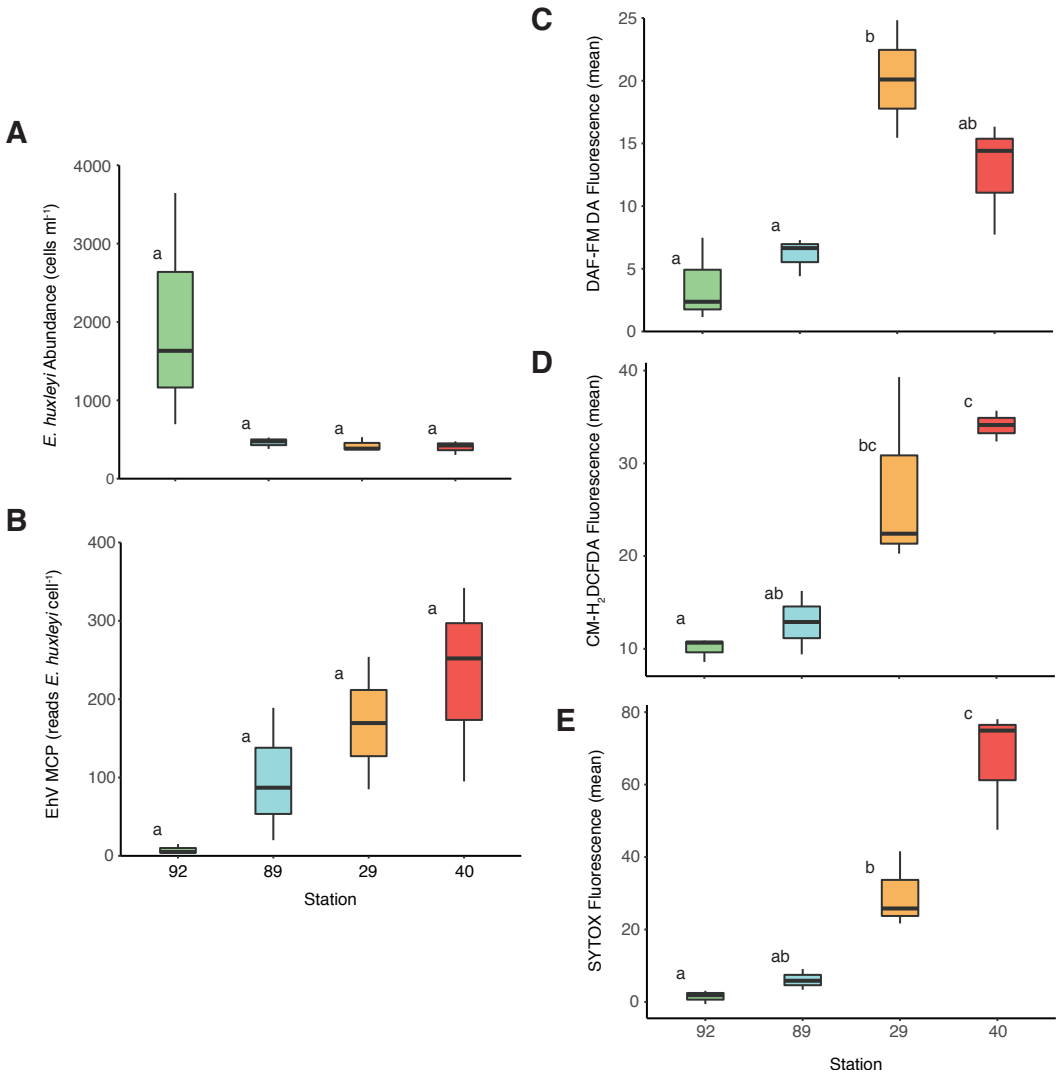

Figure 2.8 Gene- and fluorescence-based biomarkers for four additional CTD casts conducted during the NA-VICE cruise. **a**, **b** Box-and-whisker plots showing *E. huxleyi* cell abundance (cells ml^{-1}) and EhV-derived MCP gene copies *E. huxleyi* $cell^{-1}$ for these casts at three depths where *E. huxleyi* were present in highest abundance. **c**–**e** Box-and-whisker plots showing corresponding DAF-FM DA, CM-H_2DCFDA, and SYTOX Green fluorescence for these casts. Data are an average of two replicates per depth. For all box plots, upper and lower bounds of the box represent the 25% and 75% quartiles around the median. Vertical lines extend to data points no greater than 1.5 times the inter-quartile range. Statistically significant differences were determined using one-way ANOVA with the Tukey HSD post hoc test (letters denote statistically different subgroups, $p < 0.05$)

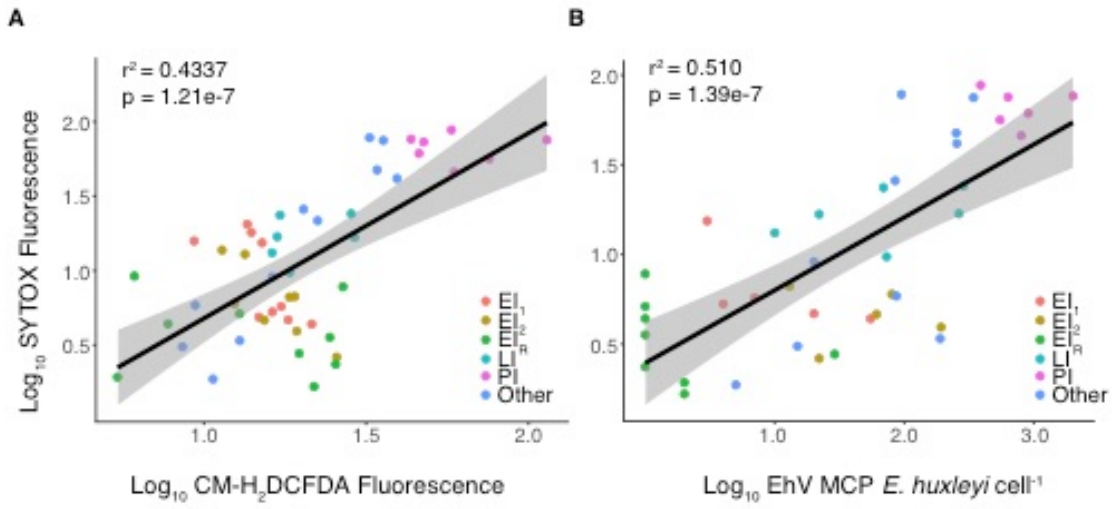

Figure 2.9 Linear regression analysis of various diagnostic parameters measured across the NA-VICE cruise. **a** Regression of log_{10}-transformed mean SYTOX fluorescence vs. log_{10}-transformed mean CM-H_2DCFDA fluorescence. **b** Regression of log_{10}-transformed EhV-derived MCP gene copy per *E. huxleyi* cell vs. log_{10}-transformed mean SYTOX fluorescence. Shading indicates 95% confidence interval for the regression line

2.10 SUPPLEMENTAL METHODS

2.10. 1 Culture conditions and viral infections

Emiliania huxleyi strain CCMP1516 was obtained from the Provasoli-Guillard National Center for Marine Algae and Microbiota and grown in batch culture in f/2 (minus Si) media at 18 ^{o}C on a 14:10 light:dark cycle at a light intensity of 250 µmol m^{-2} s^{-1}. Virus infections were done using strain EhV201 (obtained courtesy of W. Wilson, Marine Biological Association, Plymouth, UK) propagated in batch cultures of *E. huxleyi* CCMP1516. Viral lysates were passed through a 0.45 µm pore-size PVDF syringe filter to remove cell debris. For infection experiments, *E. huxleyi* were inoculated with EhV during mid-exponential growth (~5.0 x 10^5 cells mL^{-1}) at a virus to host ratio of 5:1. Uninfected *E. huxleyi* cultures served as controls.

2.10.2 Enumeration of cells and viruses

E. huxleyi cell abundances were quantified using either a BD InFlux Mariner 209S flow cytometer or a BD Accuri C6 flow cytometer, both equipped with a 488 nm laser. Cell abundances were determined based on the chlorophyll autofluorescence (E_x/E_m: 488 nm, 692 nm) vs. forward scatter (FSC) signature typical for *E. huxleyi*. Typical flow rates used with the BD InFlux ranged from 10 µL min^{-1} to 25 µL min^{-1}. The flow rate on the BD Accuri C6 was set to slow (14 µL min^{-1}). At least 1000 *E. huxleyi* cells were sampled per replicate for cell abundance determination, as well as for the fluorescence measurements described below.

Free viruses were quantified using a BD InFlux Mariner 209S flow cytometer according to (Brussaard et al. 2000). Samples were fixed with 0.5% glutaraldehyde

(Sigma-Aldrich, St. Louis, MO), flash frozen in liquid nitrogen, and stored at -80^{o}C. Samples were then thawed, diluted 1:50 with Tris-EDTA buffer containing SYBR Gold (Thermo Fisher, Waltham, MA) at a dilution of 1:20,000 of the commercial stock, and heated for 10 min at 80 ^{o}C. The EhV population was gated and enumerated based on the 520 nm fluorescence vs. side scatter (SSC) signature. Typical flow rates used for enumeration ranged from 10 μL min^{-1} to 25 μL min^{-1} and samples were collected from 15-30 s.

2.10.3 Intracellular NO detection

Semi-quantitative measurements of intracellular NO in *E. huxleyi* were made using the NO specific fluorescent probe DAF-FM Diacetate (DAF-FM DA; Thermo Fisher). DAF-FM DA passes through cell membranes, is cleaved by intracellular esterases to DAF-FM, and accumulates inside the cell. DAF-FM is non-fluorescent until it binds to NO or its oxidized products to form the fluorescent triazole product, DAF-FM-T (Kojima et al. 1999). Stocks of DAF-FM DA were made to 5 mM in DMSO (Sigma-Aldrich) and used at a final concentration of 5 μM. Stained samples were incubated in the dark at RT for 45 min. The mean fluorescence intensity per cell was then determined by flow cytometry (E_x/E_m: 488 nm, 520 nm). For each stained sample a corresponding unstained sample was run to account for background autofluorescence. Several controls were run to contextualize DAF-FM DA results and are described below.

2.10.4 Chemical identification of DAF-FM-T in cells

The presence of the fluorescent DAF-FM-T triazole product in cells treated with NO donors was chemically confirmed by using high performance liquid chromatography (HPLC) and ion-trap mass spectrometry (MS). Cultures of *E. huxleyi* CCMP1516 were treated with both S-nitroso-N-acetylpenicillamine (SNAP; Thermo Fisher) and sodium nitroprusside (SNP; Sigma-Aldrich) at 100 µM and 1 mM, respectively, and stained with 5 µM DAF-FM DA. After 1 h incubation, cells were pelleted by centrifugation (20,000g, 15 min, 4 ^{o}C), resuspended in MilliQ, and sonicated (3 X 30 sec on ice, power setting 1, Microson ultrasonic cell disrupter; Misonix, Farmingdale, NY) followed by flash freezing in liquid nitrogen. Lysed samples were then centrifuged again and the supernatant analyzed.

HPLC was performed using a Novapak C18 (4 µm, 3.9 x 150 mm; Waters) column with two eluents at a constant flow rate of 500 µL min^{-1}: A = water, B = 70:30 acetonitrile:isopropanol. Both eluents also contained 0.1% acetic acid and 1% 1M ammonium acetate. The eluent gradient was from 95% A to 30% A over 15 minutes with an equilibration period of 5 min at 95% A at the end of the run. A Thermo LCQ Fleet ion-trap mass spectrometer was used with a heated- electrospray source with the following settings: source temp 350ºC, capillary temp 250ºC, sheath and auxiliary gas flows 20 and 15 respectively (arbitrary units), source voltage 4.5kV. Source conditions were determined by tuning while infusing a solution of the DAF-FM and DAF-FM-T analytes. Positive ionization was used, though both analytes yielded suitable signals in both positive and negative ion modes. Under these conditions retention times of DAF-FM and DAF-FM-T were 16.4 and 11.9 minutes respectively. Molecular ions were observed as expected at 413 m/z for DAF-FM and 424m/z for DAF-FM-T. The mass spectrometer

was operated in full scan mode from 100-1500m/z, though extracted ion chromatograms were used for quantitation. A DAF-FM-T standard was generated in vitro by exposing 50 μM DAF-FM (Thermo Fisher) to an excess (>50 mM) of the NO donor sodium nitroprusside (SNP). Quantitation of DAF-FM-T in cell extracts was achieved by external calibration with DAF-FM-T standard solutions between 0.2 to 8 μM (10 μL injections) and a linear response was observed for DAF-FM-T between 2 and 80 pmol on column. The limit of detection, as defined by a 3:1 signal to noise ratio, was determined to be 2 pmol on column. Identification of DAF-FM and DAF-FM-T was confirmed by MS^2 spectra of the 413 m/z and 424 m/z molecular ions, which showed diagnostic neutral loss of CO_2 (44 m/z) as previously characterized (Cortese-Krott et al. 2012).

2.10.5 Intracellular esterase activity

Intracellular esterase activity was measured in infected and uninfected cells using a general esterase fluorogenic substrate. To generate cell lysates, *E. huxleyi* biomass was harvested by filtering 50-125 ml of cell culture onto 1.2 μm pore-size Isopore filters (RTTP; EMD Millipore) under low vacuum (<20 kPa). Filters were immediately flash frozen in liquid nitrogen and stored at -80^{o}C until analysis. Biomass was resuspended in PBS (5 mM potassium phosphate, pH 7.4, containing 0.9% sodium chloride) and lysed by sonication (3 X 30 sec on ice, power setting 1; Microson ultrasonic cell disrupter) followed by flash freezing in liquid nitrogen. Lysates were centrifuged (20,000g, 15 min, 4^{o}C) and the supernatant was retained. Protein in lysates was quantified with the DC protein assay kit, following the manufacturer's instructions (Bio-Rad, Hercules, CA),

using standards of bovine serum albumin (Thermo Fisher) diluted in PBS. Absorbance at 750 nm was read using a SpectraMax M3 microplate reader (Molecular Devices).

Intracellular esterase activity was measured by incubating cell lysates containing a total of 2 µg of protein with 25 µM 4-Methylumbelliferyl butyrate (Sigma-Aldrich). Fluorescence (E_x/E_m: 365 nm, 440 nm) was measured every 2 min for 1 h using a SpectraMax M3 microplate reader. Esterase activity was expressed as the rate of change in fluorescence (RFU) per µg protein. Fresh standards of MUF (Sigma-Aldrich) were run daily to ensure the linear relationship between free MUF and 440 nm fluorescence between a concentration of 25 µM and 0.025 µM.

2.10.6 Intracellular ROS and cell death analysis

Cellular ROS production was assessed using the fluorescent probe CM-H_2DCFDA (Thermo Fisher), which has a broad reactivity with a variety of radical and non-radical ROS. Stocks of CM-H_2DCFDA were made up to 1 mM in DMSO and used at a final concentration of 5 µM. Samples were incubated in the dark at RT for 60 min. The percentage of dead cells in cultures was determined using SYTOX Green (Thermo Fisher). SYTOX Green (5 mM stock solution in DMSO) was used at a final concentration of 1 µM. Samples were incubated in the dark at RT for 10-15 min. Stained samples (E_x/E_m: 488 nm, 520 nm), along with an unstained control, were analyzed by flow cytometry.

2.10.7 Extracellular NO measurements

In situ, cell-derived NO produced during infection and present in the surrounding media was monitored using liposome-encapsulated spin trap (LEST) and electron paramagnetic resonance (EPR) spectroscopy, as previously described (Hirsh et al. 2016). In brief, liposomes were prepared from a 9:1 molar ratio of the phospholipids 1-palmitoyl-2-oleoyl-sn-glycero-3-phosphocholine and 1,2-dipalmitoyl-*sn*-glycero-3-phospho-(1′-*rac*-glycerol), POPC and DPPG respectively, in chloroform (Avanti Polar Lipids, Alabaster, AL). A lipid film was formed by rotary evaporation and dried overnight under vacuum. The lipid film was suspended in buffer containing 10 mM of the spin trap N-methyl-D-glucamine dithiocarbamate (MGD) and 2mM ammonium iron(II) sulfate in a ratio of 1 mL buffer to 100 mg lipid mixture. The resulting multilamellar vescivles (MLVs) were freeze-thawed (x 5 cycles) in liquid nitrogen and stored in liquid nitrogen. Prior to use, the MLVs were suspended in HEPES buffer (20 mM, 140 mM NaCl, pH 7.4) and filtered through a PD-10 desalting column (GE Life Sciences, Chicago, IL) to remove extra-liposomal MGD and iron, yielding LEST.

LEST (25 μL) was incubated in 10 ml of triplicate infected and uninfected cultures adjusted to equal cell densities with f/2 (minus Si) media for 3 h in the dark at RT. LEST incubated in f/2 (minus Si) served as a negative control; LEST incubated in the presence of 200 μM of the NO donor NOC-9 (Sigma-Aldrich) served as a positive control. After incubation, LEST was pelleted by centrifugation (20,000g, 30 min, 4 ^{o}C). The supernatant was removed such that 30 μL of LEST pellet and buffer remained. The pellet and buffer were homogenized, flash frozen in liquid nitrogen, and stored at -80 ^{o}C until analysis. For EPR analysis, frozen LEST was thawed and drawn up into microcapillary tubes. EPR spectra were collected and the signal from spin-trapped NO

quantified as described previously (Hirsh et al. 2016). In brief, continuous-wave EPR spectra were collected at X-band, 9.8 GHz, with a Bruker EMXPlus EPR spectrometer with the standard high sensitivity X-band resonator. $MGD_2Fe(II)$-NO was quantified by comparing spectra peak areas or peak-to-trough heights to a standard generated from the stable nitroxide radical TEMPOL (Sigma-Aldrich) of a known concentration.

To test whether incubation with LEST had cytotoxic effects on cells, a suite of physiological measurements were taken before and after cells were incubated at RT in the dark for 3 h and compared to a control culture which had no LEST addition. These measurements included intracellular NO, intracellular ROS, % dead cells, cell abundance as well as the photochemical quantum yield of photosystem II (F_v/F_m) and functional cross-section of photosystem II (sigma). Photosynthetic parameters were measured using a custom-built fast Fluorescence Induction and Relaxation System (Gorbunov & Falkowski 2005).

2.10.8 NO donor, NO scavenger, and hydrogen peroxide treatments

To further investigate the cellular role of NO during infection, the following experiments were conducted: (1) *E. huxleyi* infection in the presence of an NO scavenger, (2) monitoring physiology of *E. huxleyi* pre-treated with various concentrations of an NO donor and subsequently challenged with hydrogen peroxide (H_2O_2), and (3) determination of the total antioxidant capacity of *E. huxleyi* cell lysates both treated with an NO donor and undergoing infection. The NO donor used was S-nitroso-N-acetylpenicillamine (SNAP) and treatments were done at concentrations empirically determined to be non-lethal (less than 250 μM; data not shown) for at least 16 h prior to

H2O2 treatment or biomass harvest. Given SNAP has a donor half-life of ~6 h, this time period represents >2 half-lives. The NO scavenger used was carboxy-PTIO potassium salt (c-PTIO; Thermo Fisher) and was applied to cells at the time of infection (T_0) at a range of concentrations (250 μM – 1 mM dissolved in MilliQ). Treatments with H_2O_2 (30% w/w; Sigma-Aldrich) were performed between 10 – 100 μM**.** Cell abundance, percent dead cells, intracellular NO and ROS, and the photochemical quantum yield of photosystem II (F_v/F_m) were monitored for these experiments. Photosynthetic parameters were measured using a custom-built fast Fluorescence Induction and Relaxation System (Gorbunov & Falkowski 2005).

2.10.9 Total antioxidant capacity

E. huxleyi lysates were generated and protein concentration was determined as described previously. The total enzymatic and non-enzymatic antioxidant capacity (TAC) of the extracts was determined using the Antioxidant Assay Kit (Cayman Chemical, Ann Arbor, MI), which measures the capacity of cell extracts to prevent the oxidation of ABTS (2,2'-azino-di-[3-ethylbenzthiazoline sulphonate) in the presence of H_2O_2 compared to a standard of the vitamin E analog Trolox (6-hydroxy-2,5,7,8-tetramethylchroman-2-carboxylic acid). The assay and standard curve were run according to the manufacturer's instructions. Absorbance at 750 nm was measured using a SpectraMax M3 microplate reader. TAC is expressed as the concentration (mM) of antioxidants in equivalents of Trolox normalized to the total protein concentration of the sample.

2.10.10 Fieldwork

Intracellular NO, ROS, and cell death were assessed for open ocean, EhV-infected *E. huxleyi* populations in the Northeast Atlantic during the *North Atlantic Virus Infection of Coccolithophores Expedition* (http://www.bco-dmo.org/project/2136) aboard the *R/V Knorr*. The NA-VICE traversed a 2000 nautical mile transect from the Azores to Iceland and identified *E. huxleyi* blooms at different stages of bloom formation and viral infection (Lehahn et al. 2014, Laber et al. 2018, Sheyn et al. 2018). Individual CTD casts were characterized and grouped into "early infection (EI)," "early infection revisited (EI_R)," "late infection (LI)," or "post infection (PI)," using a combination of MODIS/AQUA satellite imagery, a suite of diagnostic lipid- and gene-based molecular biomarkers, analytical flow cytometry, *in situ* optical sensors, and sediment traps (Laber et al. 2018).

Here, we further divided the "early infection" population into "early infection 1" and "early infection 2" in order to provide higher temporal sampling resolution for these parameters given the greater number of samples available at this site for analysis. CTD cast designations were thus as follows: EI_1 (casts 50, 52, 56, 57, 63; 30 June – 3 July), EI_2 (casts 68, 70, 72, 76; 4 July – 5 July), EI_R (casts 81, 84, 92, 93, 97; 7 July – 10 July), LI (casts 77 and 79; 6 July), and PI (casts 20, 25, 27, 33; 23 June 23 – 27 June). We also present data from three additional CTD casts not analyzed in the aforementioned study (Laber et al. 2018), along with an individual CTD cast (cast 92) from EI_R to illustrate a comparative signal for an early infected population. They include 29 (June 26), 40 (June 28), 89 (July 8).

Water was collected at six depths—extending from the subsurface, through the mixed layer encompassing the chlorophyll maximum, and down to 150 m—using Niskin

bottles mounted on a 24-position rosette equipped with a Seabird SBE conductivity-temperature-depth (CTD) profiler. Sub-samples were stained with DAF-FM Diacetate, CM-H_2DCFDA, and SYTOX Green (5 μM) as described above. Stained samples, along with an unstained control, were run on a Guava flow cytometer (EMD Millipore, Burlington, MA) in duplicate. We present data from 3 depths per cast corresponding to the depth at which *E. huxleyi* cell abundance was highest, along with one sampling depth above and one sampling depth below the *E. huxleyi* maximum, in box-and-whisker plots. These depths generally ranged from 8 – 40 m and are listed in Table S2.

2.10.11 Data analysis and statistics

Flow cytometry data collected for laboratory experiments were analyzed using FlowJo (v. 10.2). Statistics (counts and mean fluorescence) were based on at least 1000 *E. huxleyi* events. Mean fluorescence per cell for DAF-FM Diacetate and CM-H_2DCFDA stained samples are reported as the difference between the mean fluorescence per cell of the stained sample and an unstained sample. Percent SYTOX Green positive cells are reported as the percent of the total *E. huxleyi* population that has elevated 520 nm fluorescence relative to an unstained control.

Flow cytometry data for fieldwork were analyzed using GuavaSoft InCyte (v. 2.2.2). *E. huxleyi* was distinguished by pre-gating all events by chlorophyll and gating the *E. huxleyi* population off side-scatter and forward scatter signatures corresponding to a reference culture. Statistics (counts and mean fluorescence) were based on at least 50 *E. huxleyi* events, with most samples encompassing 100-400 events, and averaged between two replicates per depth.

Statistically significant differences between infected and uninfected cultures for the parameters measured in this study were determined with Student's t-tests ($p<0.05$). To test differences between multiple means, a one-way ANOVA with a Tukey HSD post-hoc test was used. Error bars on all graphs are $\pm$ standard error of the mean (se). Linear regression analysis was used to explore relationships between various parameters in the NA-VICE dataset. All statistical tests were performed in R and plots generated using the ggplot2 package.

2.11 SUPPLEMENTAL TABLES & FIGURES

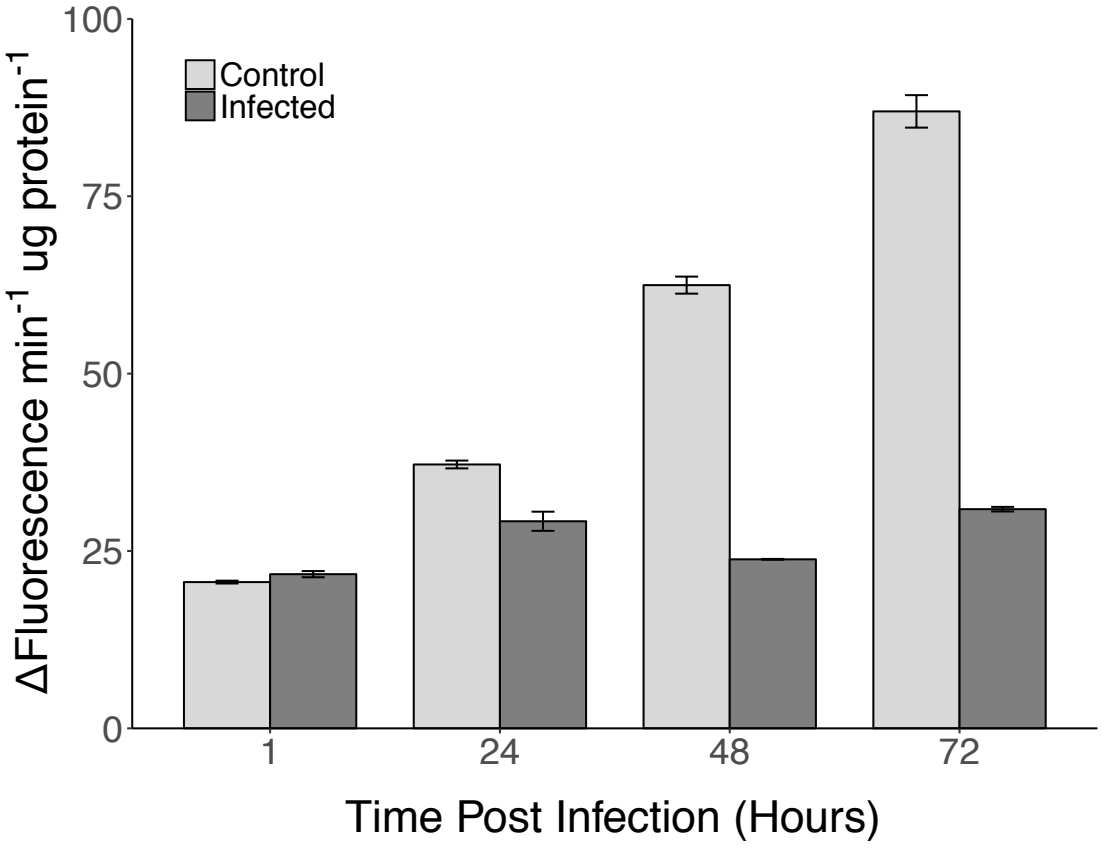

Figure S2.1 Intracellular esterase activity of *E. huxleyi* CCMP1516 in EhV201 infected (dark grey bars) and control (light grey bars) over 72 h based on MUF-butyrate cleavage. Activity is expressed as the mean change in MUF fluorescence per min per µg protein (n=3, ± se).

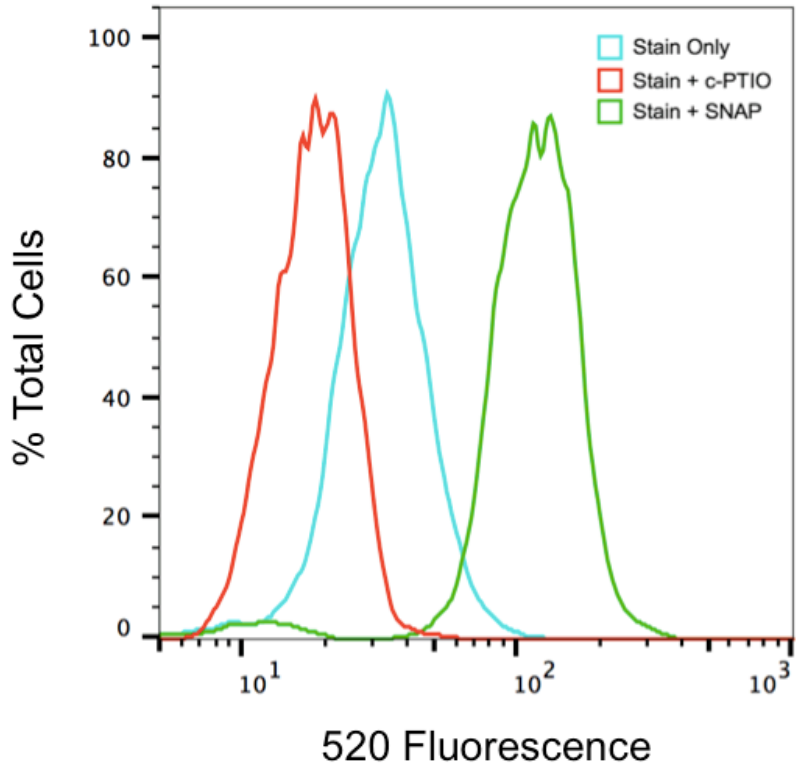

Figure S2.2 Histogram overlay of the 520 nm fluorescence of *E. huxleyi* CCMP1516 cultures stained with DAF-FM DA and either treated with the NO donor SNAP (250 µM, green), the NO scavenger c-PTIO (1 mM, red), or untreated (blue). Treatment with SNAP enhances DAF-FM DA fluorescence and c-PTIO diminished DAF-FM DA fluorescence.

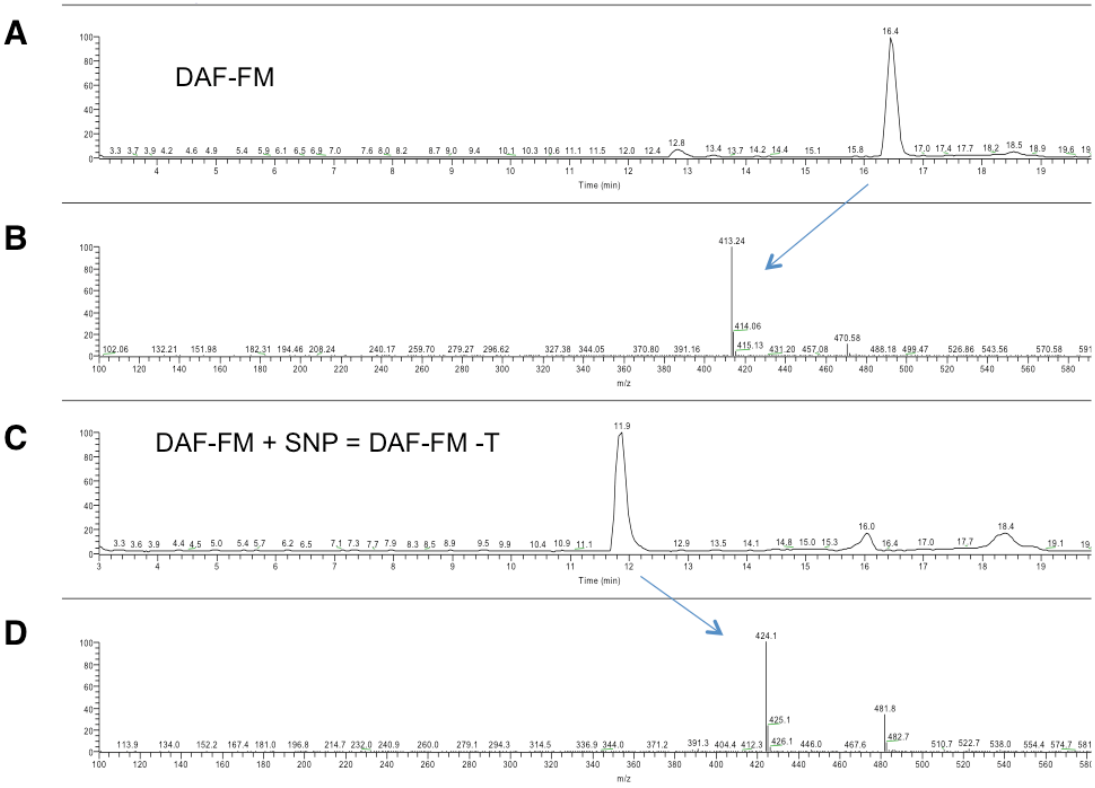

Figure S2.3 Full scan HPLC chromatograms showing peaks for DAF-FM (A) and DAF-FM-T (C), the product formed upon treatment of DAF-FM with the NO donor sodium nitroprusside (SNP). Mass spectra of DAF-FM peak (B) and DAF-FM-T peaks (D) showing their diagnostic molecular ions.

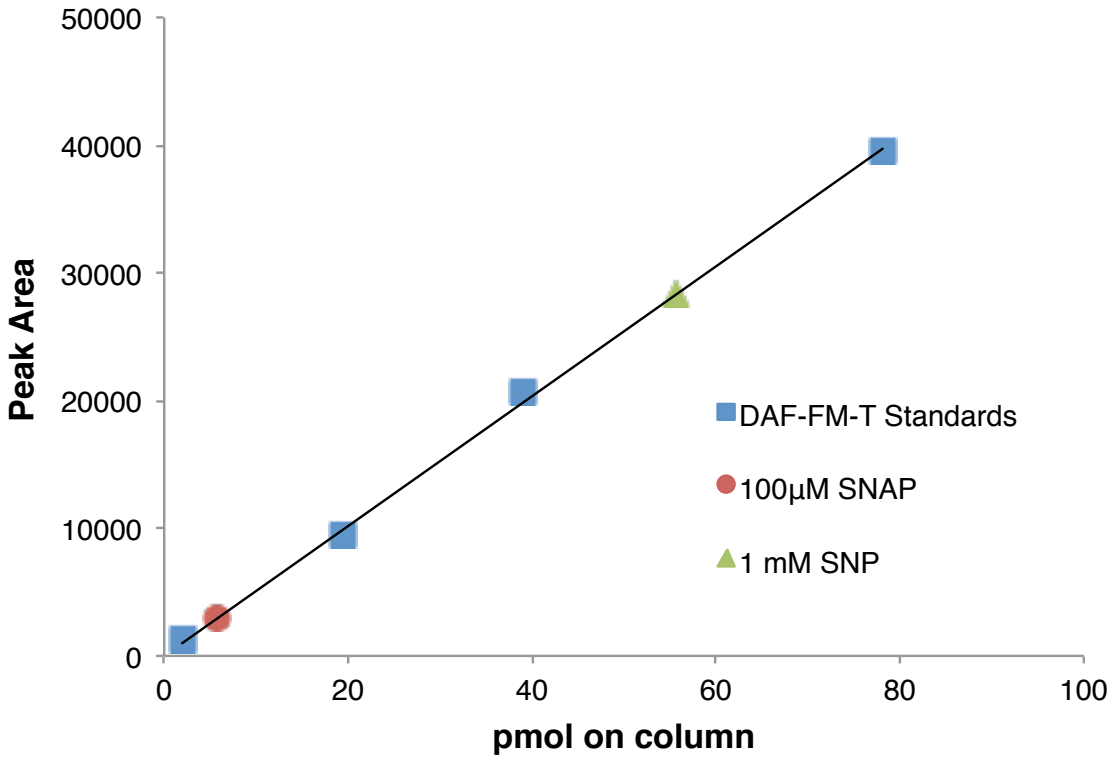

Figure S2.4 Calibration curve of serial dilutions of DAF-FM-T standard (blue squares) detected and quantified by HPLC MS/MS overlayed by DAF-FM-T detected and quantified in *E. huxleyi* CCMP1516 cells treated with 100 µM of the NO donor SNAP (red circle) and 1 mM of the NO donor SNP (green triangle) for 1 h. Note that a 100 µM addition of SNAP to cells, a relatively high exogenous dose, lies close to the detection limit of DAF-FM-T.

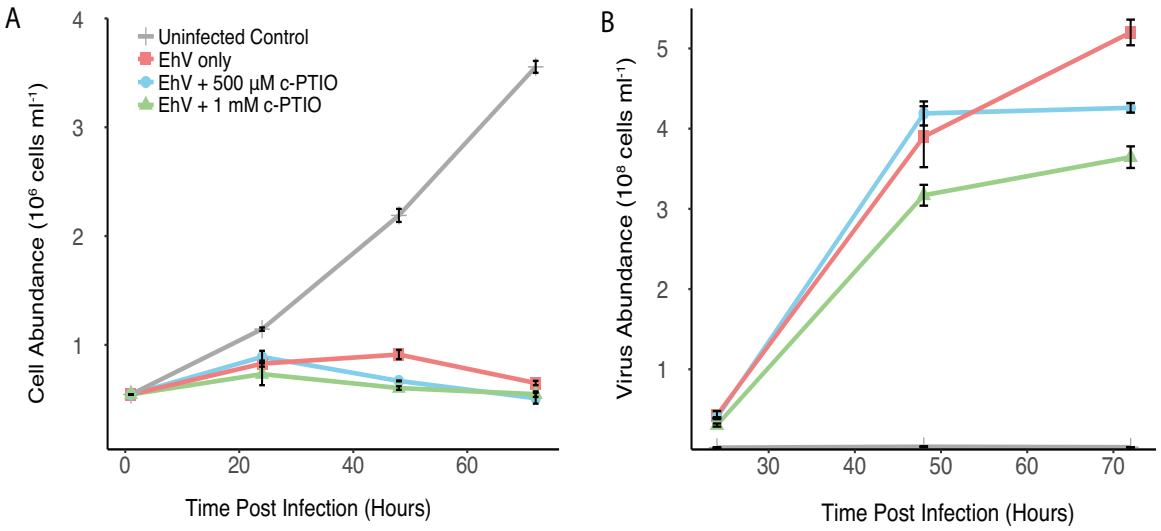

Figure S2.5 Infection dynamics of *E. huxleyi* CCMP1516 cultures treated with various concentrations of the NO scavenger, c-PTIO. (A) Cell and (B) viral abundance of infected *E. huxleyi* cultures and an uninfected, non c-PTIO treated control (n=2, ± se). Data are a representative subset of two separate experiments.

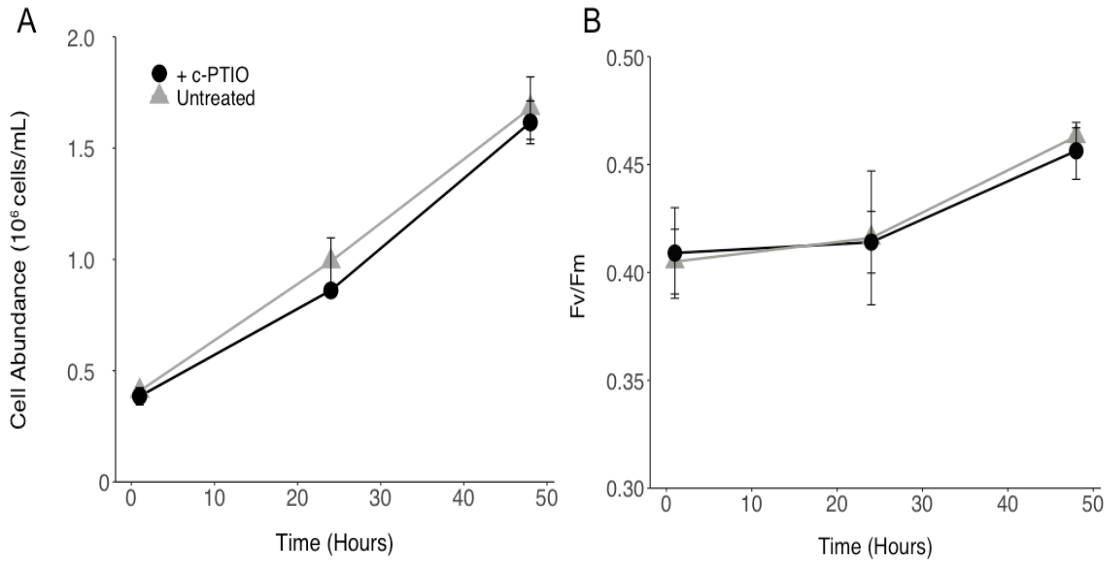

Figure S2.6 (A) Cell abundances and (B) F_v/F_m values of uninfected *E. huxleyi* CCMP1516 cultures treated with c-PTIO (black, circles) or untreated (grey, triangles). Values are the mean of n=2 for untreated cultures and n=3 for c-PTIO treated cultures pooled from 2 replicates of 500 µM treatment and 1 replicate of a 1 mM treatment (± se).

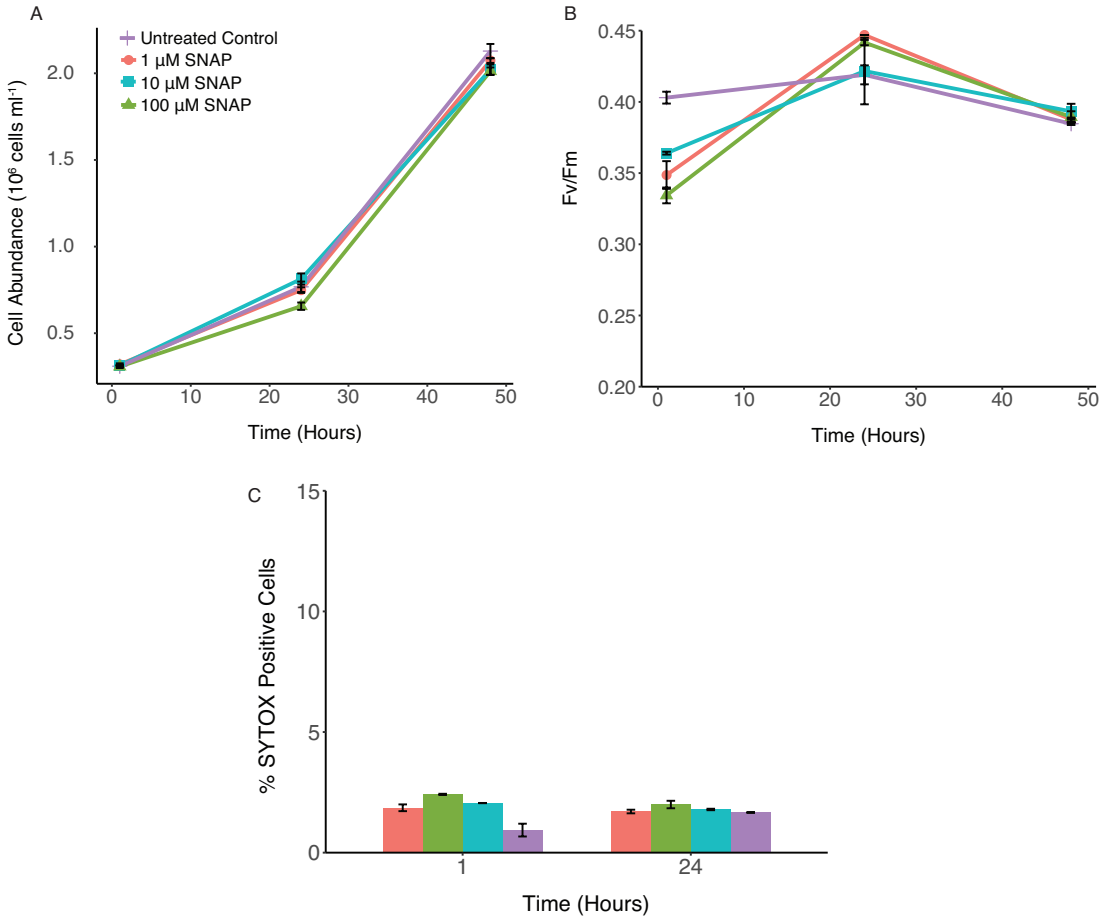

Figure S2.7 Determination of non-lethal doses of the NO donor, S-nitroso-N-acetylpenicillamine (SNAP), for exponentially growing *E. huxleyi* CCMP1516. (A) Cell abundance, (B) Fv/Fm, and (c) % SYTOX positive cells over 24 - 48 hours in cultures treated with 0, 1, 10, and 100 µM SNAP (n=3, $\pm$ se).

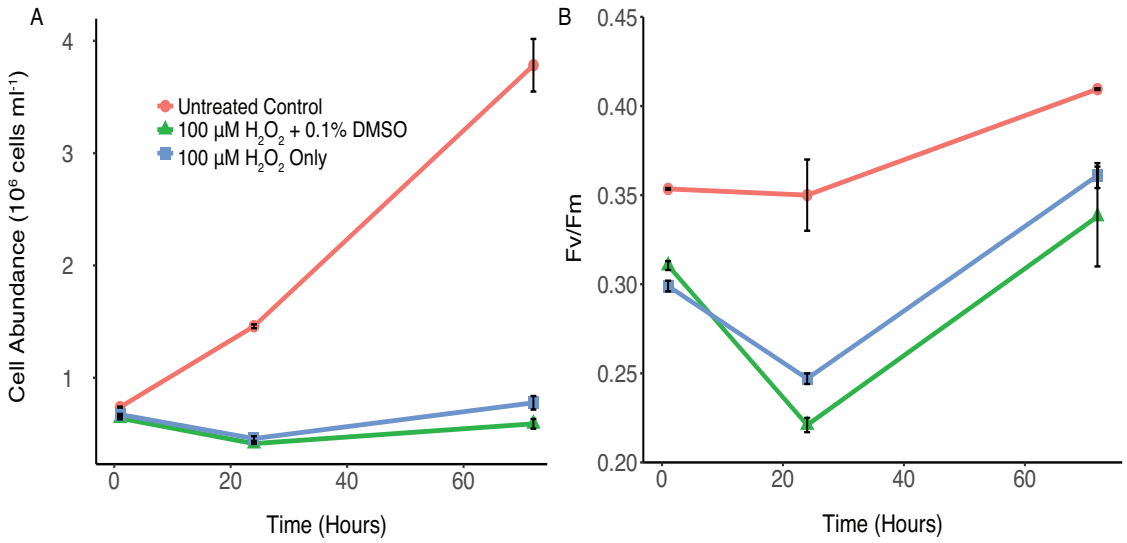

Figure S2.8 DMSO only control of SNAP/H_2O_2 experiments. (A) Cell abundances and (B) F_v/F_m of *E. huxleyi* CCMP1516 challenged with 100 µM H_2O_2, with and without pre-treatment with 0.1% DMSO, along with an untreated control (n=2, ± se). Data are a representative subset of two separate experiments.

Table S2.1 Comparison of various physiological parameters of *E. huxleyi* CCMP1516 cultures incubated in the presence or absence of 25 µL of LEST for 3 h (n=1).

	No LEST	**With 25uL LEST**
Photophysiology		
F_v/F_m	0.331	0.326
Sigma	354.4	354.5
Flow Cytometry		
NO Production (Mean DAF-FM DA Fluorescence)	4.9	2.31
Oxidative Stress (Mean CM-H_2DCFDA Fluorescence)	0.91	0.39
% Cells SYTOX Positive	9.6%	7.3%
Cell Abundance	$1.47x10^6$ cells/mL	$1.40x10^6$ cells/mL

Table S2.2 Water depths sampled during NA-VICE that were used for the analyses presented in Figures 7 and Figure 8. Depths chosen at each station for detailed analysis correspond to the depth within the mixed layer that had the highest *E. huxleyi* cell abundance, along with one sampling depth immediately above and immediately below the E. huxleyi maximum. In cases where the highest *E. huxleyi* abundance was the first subsurface sample, the depths chosen were the subsurface and the next two depths sampled.

Cast #	Depths sampled (m)
20	8, 12, 16
25	8, 15, 25
27	5, 15, 26
29	5, 18, 28
33	5, 14, 21
40	11, 25, 34
50	9, 17, 25
52	4, 11, 21
56	8, 20, 31
57	11, 20, 30
63	17, 24, 31
68	10, 21, 30
70	9, 15, 22
72	20, 30, 40
76	6, 16, 20
77	8, 14, 20
79	7, 10, 20
81	5, 12, 20
84	7, 17, 24
89	7, 16, 25
92	14, 24, 34
93	9, 18, 25
97	8, 14, 22

2.12 SUPPLEMENTAL REFERENCES

Gorbunov MY, Falkowski PG. Fluorescence Induction and Relaxation (FIRe) Technique and instrumentation for monitoring photosynthetic processes and primary production in aquatic ecosystems. In: Van der Est A, Bruce D, eds. Photosynthesis: Fundamental Aspects to Global Perspectives. 2. Montreal: Alliance Communications Group; 2005. p. 1029-31.

CHAPTER 3: Strain Variability in Nitric Oxide Production, Reactive Oxygen Stress, and Antioxidant Capacity in *Emiliania huxleyi*

3.1 ABSTRACT

Nitric oxide (NO) is a membrane permeable, gaseous free radical that is known to have an impressive list of physiological functions across all domains of life. It has been previously demonstrated that NO is a critical molecule involved in the lytic viral infection of the coccolithophore *Emiliania huxleyi.* While it was suggested the NO has an antioxidant function during infection, it is still unclear what the relationships are between NO production, oxidative stress, antioxidant capacity, and viral susceptibility and whether this may play some role in the resistant cell's mechanism of resistance. We aim to address these open questions by surveying these traits in various strains of *E. huxleyi* that range in their sensitivity to infection by *coccolithoviruses*. Here we show that two virus-resistant strains (CCMP373 and CCMP379) produce less NO (measured intra- and extra-cellulary) than two virus sensitive strains (CCMP374 and CCMP1516). In addition, the resistant strains have higher basal ROS production and cell death. Surprisingly, however, it was the resistant strains that displayed higher antioxidant capacity, indicated by physiology experiments with hydrogen peroxide (H_2O_2), direct assay of cell lysate's ability to detoxify H_2O_2, and a bioinformatics analysis of differences in basal antioxidant gene expression between strain 379 (resistant) and 374 (sensitive). We discuss the importance of quantifying possible intracellular NO reservoirs, such as proteins and small molecular weight thiols like glutathione, to fully contextualize NO production measurements, and interpret the possible implications for "cost-of-resistance" in 379 and 373.

3.2 INTRODUCTION

Viruses are the most abundant biological entities in the ocean with typical densities of 10^7 ml^{-1} leading to an estimated 10^{23} viral infections s^{-1} (Suttle 2007). Although there is likely a virus for every type of marine organism (Munn 2006), the vast majority of viruses in the ocean are those that infect the most abundant host organisms: marine microbes. The spatial and temporal distributions of marine viruses closely trace bacterial abundance and chlorophyll-a concentration (a phytoplankton biomass proxy), signifying a close relationship between viruses and microbes. For example, viruses are particularly enriched in the upper sunlit ocean and productive coastal systems (Cochlan et al. 1993), as well as during the end of algal blooms (Bratbak et al. 1990, Bratbak et al. 1993, Yager et al. 2001, Laber et al. 2018).

Viral lysis of phytoplankton cells is believed to process about 25% of photosynthetically fixed organic carbon, diverting it away from vertical sinking flux and higher trophic levels and through the microbial loop (Wilhelm & Suttle 1999). However, it is becoming increasingly acknowledged that the overall impact of viral lysis on biogeochemical cycling is species-specific (Evans & Wilson 2008). For example, evidence suggests that viral infection of the bloom-forming, cosmopolitan coccolithophore *Emiliania huxleyi* by coccolithoviruses (known as EhVs) may actually enhance vertical flux of carbon (Laber et al. 2018, Sheyn et al. 2018) as a result of aggregation via increased production of transparent exopolymeric particles (TEP) (Vardi et al. 2012, Laber et al. 2018) and enhanced zooplankton grazing on virus-infected cells (Evans & Wilson 2008, Frada et al. 2014). In addition, viral infection plays a major role in structuring microbial communities in the ocean by both directly facilitating horizontal

genetic exchange between hosts (Jiang & Paul 1998), as well as indirectly by enhancing diversity via the removal dominant genotypes (Thingstad & Lignell 1997, Van Hannen et al. 1999).

E. huxleyi and their viruses have emerged in recent decades as one of the most actively studied host-virus systems for marine eukaryotic algae (Bidle & Vardi 2011). This is in part due to the fact the *E. huxleyi* is an environmentally important cocolithophore species that forms large annual blooms in the North Atlantic (Holligan et al. 1993, Brown & Yoder 1994, Tyrrell & Merico 2004) and are major contributors to the production and export of calcium carbonate in the ocean. It is also due to the existence of molecular tools to interrogate subcellular mechanisms of infection, the size of EhVs (~200nm) being amenable to established methods in phytoplankton and virology research such as flow cytometry, and the availability of numerous *E. huxleyi* host strains and EhV isolates in culture that display varying degrees of resistance to infection (Schroeder et al. 2002), infection dynamics (Nissimov et al. 2016), and levels of calcification (Johns et al. 2018). The existence of these isolated host and virus strains allows for questions regarding the mechanisms of viral infectivity and resistance, population-level impacts of viral infection, and potential influences of a changing climate to be addressed systematically.

It has been clearly and consistently demonstrated that viral infection in *E. huxleyi* involves substantial changes to the cell's redox environment via the production of reactive oxygen species (ROS)- potentially toxic radical and non-radical oxygen intermediates such as $HO^{\cdot}$, H_2O_2, and O_2^{-} - (Evans et al. 2006, Vardi et al. 2012, Sheyn et al. 2016), specifically H_2O_2 (Sheyn et al. 2016), and dimethyl sulfide DMS (Evans et al.

2007), a potential antioxidant (Sunda et al. 2002). It is believed that it is this late-stage (72 hr and beyond) burst of ROS that induces the cell's programmed cell death (PCD) machinery by activating metacaspase expression and caspase-like activity (Bidle et al. 2007, Vardi et al. 2009, Vardi et al. 2012). Recently, a critical role for the gaseous, nitrogen-based free radical nitric oxide (NO) has also been demonstrated (Schieler et al. 2019). Unlike ROS production, however, intracellular NO levels increase by 24 hr post infection. ,Although the role of NO production during infection is still unclear, Schieler et al. (2019) suggested that it might provide an antioxidant function during early infection, allowing viral replication to occur in a redox favorable environment and/or inhibiting early-onset PCD. This was based on observations that NO scavenging decreases viral burst size and that cells pre-treated with an NO donor display enhanced survival when subsequently challenged with toxic levels of H_2O_2. Indeed, there has been previously published evidence that changes to a cell's antioxidant system occur well before any evidence of ROS accumulation emerges during lytic infection (Sheyn et al. 2016).

Nitric oxide is an enigmatic molecule. It is a small, diatomic free radical that readily diffuses across cell membranes and reacts with a variety of cellular targets (see Chapter 1). It has been implicated in various, sometimes opposing, biological processes in plants, animals, and algae (Moncada 1999, Besson-Bard et al. 2008, Kumar et al. 2015). It is clear, however, that NO displays significant cross-talk with ROS to elicit distinct cellular responses to abiotic and biotic stressors (Zhao et al. 2007). For example, the soybean hypersensitive cell-death response triggered by pathogen invasion requires cooperation between NO and H_2O_2 (Delledonne et al. 2001). This NO/ROS cross-talk can take form as direct radical-radical reactions (e.g. the reaction of NO and O_2- to form

$ONOO^-$) or by NO-mediated regulation of pro- and anti-oxidant pathways through protein post-translational modifications (Begara-Morales et al. 2016). The intricacies of this NO/ROS cross-talk are both poorly constrained and seemingly species-specific. For example, NO-mediated nitrosylation of the critical antioxidant enzyme ascorbate peroxidase (APX) enhances its H_2O_2 scavenging activity in *Arabidopsis thaliana* (Yang et al. 2015), but decreases its activity in tobacco (*Nicotiana tabacum*) to induce an NO/H_2O_2 controlled PCD (de Pinto et al. 2013). It is thus clear from the current literature that, while being a useful guide, the manner in which NO functions in the physiology of *Emiliania huxleyi* cannot be extrapolated from other model photosynthetic organisms.

The goal of this study is to better understand the function and relationship of nitric oxide production, reactive oxygen production/redox chemistry, and antioxidant capacity in the ecophysiology and viral infection of *Emiliania huxleyi* by surveying these traits in four *E. huxleyi* strains that differ in their susceptibility to viral infection. Here, we show that two virus-resistant strains of *E. huxleyi* produce significantly less nitric oxide than two virus-sensitive strains, demonstrating a previously unappreciated existence of intra-species variability in this important signaling molecule. Strain CCMP379, which has been previously shown to be "hyper-resistant" to infection (Bidle & Kwityn 2012), also produces the lowest NO of all four strains surveyed. We conversely show that the lowest NO producing strains also have the highest levels of basal oxidative stress. We show evidence that the two resistant strains have an enhanced basal antioxidant capacity, with CCMP379 also having the highest capability for dealing with exogenous H_2O_2 stress. These inherent antioxidant differences are inferred from both laboratory experiments and by a comparison of the gene expression profiles of one EhV-sensitive (CCMP374) and

one EhV-resistant (CCMP379) strain during normal, exponential growth. We conclude with a discussion of the implications of these results for uncovering potential "costs-of-resistance" in *E. huxleyi*.

3.3 MATERIALS & METHODS

3.3.1 Culture conditions and biomass harvesting

Emiliania huxleyi strains CCMP1516, CCMP374, CCMP373, and CCMP379 were obtained from the Provasoli-Guillard National Center for Marine Algae and Microbiota and grown in batch culture in f/2 (minus Si) media at 18 °C on a 14:10 light:dark cycle at a light intensity of 250 μmol $m^{-2}s^{-1}$. *E. huxleyi* strains CCMP1516 and CCMP374 have been empirically determined to be susceptible to viral infection by various isolated strains of coccolithoviruses (EhVs) and are hereafter referred to as 1516^S and 374^S. Likewise, strains CCMP373 and CCMP379 have been determined to be resistant to infection by all EhV strains tested and are hereafter referred to as 373^R and 379^R (Schroeder et al. 2002, Bidle & Kwityn 2012).

Unless otherwise noted, biomass for analyses discussed here was obtained by filtering exponential phase (~$5.0x10^5$ – $1.0x10^6$ cells ml^{-1}) cultures through 1.2 μm polycarbonate Isopore filters (RTTP; EMD Millipore Burlington, MA) under low vacuum (<20 kPa). Filters were immediately flash frozen in liquid nitrogen and stored at -80°C until further analysis.

3.3.2 Cell enumeration and growth rate calculation

E. huxleyi cell abundance was quantified using either a BD InFlux Mariner 209S flow cytometer or a BD Accuri C6 flow cytometer, both equipped with a 488 nm laser, based on the chlorophyll autofluorescence (E_x/E_m: 488 nm, 692 nm) vs. forward scatter (FSC). Typical flow rates used with the BD InFlux ranged from 10 µL min^{-1} to 25 µL min^{-1}. The flow rate on the BD Accuri C6 was set to slow (14 µL min^{-1}). At least 1000 *E. huxleyi* cells were sampled per replicate for cell abundance determination, as well as for the fluorescence measurements described below. Specific growth rate, µ (d^{-1}), during exponential growth was calculated using the equation:

$$\mu = \ln (C_2 - C_1) / \ln (t_2 - t_1) \quad (1)$$

Where C_2 and C_1 are the cell concentrations (cells ml^{-1}) at time point 2 (t_2) and time point 1 (t_1), in days, respectively. The impact of H_2O_2 treatments on growth rates were quantified as ΔGrowth and were calculated using the equation:

$$\Delta\text{Growth} = \mu T - \mu C \quad (2)$$

Where µT is the specific growth rate at a particular treatment and µC is the specific growth rate of an untreated control.

3.3.3 Assessment of intracellular NO, intracellular ROS, and cell death

Semi-quantitative measurements of intracellular NO were made using the NO specific fluorescent probe DAF-FM Diacetate (DAF-FM DA; Thermo Fisher, Waltham, MA). Stocks of DAF-FM DA were made to 5 mM in DMSO (Sigma-Aldrich, St. Louis, MO) and used at a final concentration of 5 µM. Stained samples were incubated in the dark at RT for 45 min. Mean fluorescence intensity per cell and percent of culture positively stained was determined by flow cytometry (E_x/E_m:

488 nm, 520 nm) using either a BD InFlux Mariner 209S flow cytometer or a BD Accuri C6 flow cytometer. An unstained sample was run to account for background autofluorescence. Positive controls to ensure efficient dye loading were performed by treating DAF-FM DA stained samples with 100-250 μM of the NO donor s-nitroso-N-acetylpenicillamine (SNAP; Thermo Fisher).

Cellular ROS production was assessed using the fluorescent probe CM-H_2DCFDA (Thermo Fisher), which has a broad reactivity with a variety of ROS. Stocks of CM-H_2DCFDA were made up to 1 mM in DMSO and used at a final concentration of 5 μM. Samples were incubated in the dark at RT for 60 min. The percentage of dead cells in cultures was determined using SYTOX Green (Thermo Fisher). SYTOX Green (5 mM stock solution in DMSO) was used at a final concentration of 1 μM and incubated in the dark at RT for 10–15 min. Stained samples (E_x/E_m: 488 nm, 520 nm), along with an unstained control, were analyzed by flow cytometry using either a BD InFlux Mariner 209S flow cytometer or a BD Accuri C6 flow cytometer.

3.3.4 Extracellular NO measurements

In situ, cell-derived NO produced by exponentially growing 1516^S, 374^S, and 379^R and present in the surrounding media was monitored using liposome-encapsulated spin trap (LEST) and electron paramagnetic resonance (EPR) spectroscopy, as previously described (Hirsh et al. 2016, Schieler et al. 2019). In brief, liposomes were prepared from a 9:1 molar ratio of the phospholipids: 1-palmitoyl-2-oleoyl-sn-glycero-3-phosphocholine and 1,2-dipalmitoyl-*sn*-glycero-3-phospho-(1′-*rac*-glycerol), POPC and DPPG

respectively, in chloroform (Avanti Polar Lipids, Alabaster, AL). A lipid film was formed by rotary evaporation and dried overnight under vacuum. The lipid film was suspended in buffer containing 10 mM of the spin trap N-methyl-D-glucamine dithiocarbamate (MGD) and 2mM ammonium iron(II) sulfate in a ratio of 1 mL buffer to 100 mg lipid mixture. The resulting multilamellar vesicles (MLVs) were freeze-thawed (x 5 cycles) in liquid nitrogen and stored in liquid nitrogen. Prior to use, the MLVs were suspended in HEPES buffer (20 mM, 140 mM NaCl, pH 7.4) and filtered through a PD-10 desalting column (GE Life Sciences, Chicago, IL) to remove extra-liposomal MGD and iron, yielding LEST.

LEST (25 μL) was incubated in 10 ml of each culture in triplicate adjusted to equal cell densities with f/2 (minus Si) media for 3 h in the dark at RT. LEST incubated in f/2 (minus Si) served as a negative control; LEST incubated in the presence of 200 μM of the NO donor NOC-9 (Sigma-Aldrich) served as a positive control. After incubation, LEST was pelleted by centrifugation (20,000 x g, 30 min, 4 ^{o}C). The supernatant was removed such that 30 μL of LEST pellet and buffer remained. The pellet and buffer were homogenized, flash frozen in liquid nitrogen, and stored at -80 ^{o}C until analysis. For EPR analysis, frozen LEST was thawed and drawn up into microcapillary tubes.

EPR spectra were collected and the signal from spin-trapped NO quantified as described previously (Hirsh et al. 2016). In brief, continuous-wave EPR spectra were collected at X-band, 9.8 GHz, with a Bruker EMXPlus EPR spectrometer with the standard high sensitivity X-band resonator. $MGD_2Fe(II)$-NO was quantified by comparing spectra peak areas or peak-to-trough heights to a standard generated from the stable nitroxide radical TEMPOL (Sigma-Aldrich) of a known concentration.

3.3.5 Hydrogen peroxide treatments and antioxidant capacity assessment

Basal antioxidant capacity of exponentially growing *E. huxleyi* 1516^{S}, 374^{S}, and 379^{R}, and 373^{R} were assessed in two ways: by monitoring cellular physiological response to exogenous H_2O_2 additions and by assaying cell lysates directly for their capacity to detoxify H_2O_2. H_2O_2 additions were performed by diluting a 30% w/w stock of H_2O_2 (Sigma-Aldrich) to a moderate (50 μM) and high (125 μM) concentration. Cell abundance, specific growth rates, percent dead cells, intracellular NO and ROS, and the photochemical quantum yield of photosystem II (F_v/F_m) were monitored at 1, 24, and 48 hr post addition as described above. Three independent experiments were performed, with two experiments in duplicate and one experiment without technical replication. One experiment included in this analysis only has 1 and 24 hr time points due to instrument failure at the 48 hr time point.

The total enzymatic and non-enzymatic antioxidant capacity (TAC) of the extracts of these strains was determined using the Antioxidant Assay Kit (Cayman Chemical, Ann Arbor, MI), which measures the capacity of cell extracts to prevent the oxidation of ABTS (2,2'-azino-di-[3-ethylbenzthiazoline sulphonate) in the presence of H_2O_2 compared to a standard of the vitamin E analog Trolox (6-hydroxy-2,5,7,8-tetramethylchroman-2-carboxylic acid). The assay and standard curve were run according to the manufacturer's instructions. Absorbance at 750 nm was measured using a SpectraMax M3 microplate reader (Molecular Devices, San Jose, CA). TAC is expressed as the concentration (mM) of antioxidants in equivalents of Trolox normalized to the total cells expected on the filter by multiplying the cell concentration of the culture by the

volume filtered. Five independent biomass samples were assessed and each sample was run in triplicate for technical replication.

3.3.6 *E. huxleyi* transcriptome analysis

Transcriptome sequencing of 379^R and 374^S *E. huxleyi* stains was done as part of the Marine Microbial Eukaryote Transcriptome Sequencing Project (MMETSP; Keeling et al. 2014). Large batch cultures of 379^R and 374^S were grown in typical growth conditions (see above) in triplicate and RNA was collected at two time points (2 hr and 24 hr) by filtering biomass onto a 0.8 μm polycarbonate filter under low vacuum (< 3 psi). Biomass was immediately scraped off filter, resuspended in 1 mL f/2-Si media, and centrifuged for 5 min. Supernatant was removed and cell pellets were flash frozen in liquid N. RNA was from each triplicate was pooled into one sample. RNA sequencing and assembly methods can be found in Keeling et al. (2014).

The assemblies (379^R and 374^S for both time points) were downloaded from the iMicrobe website (https://www.imicrobe.us). Gene expression was compared for oxidative stress-related genes between *E. huxleyi* 379^R and 374^S at each time point of growth. We first constructed one reference transcriptome that represented a combination of all assemblies with redundant sequences removed using CD-HIT (Li & Godzik 2006) with a sequence identity threshold of 85%. The resulting combined assembly consisted of 28,261 contigs and was used as a reference transcriptome assembly for downstream analysis.

Using CLC genomic workbench, the four transcriptomes were trimmed (discarding adapter sequences and low-quality base pairs) and mapped to the non-

redundant combined reference transcriptome assembly. An expression value in the form of Reads Per Kilobase of transcript, per Million mapped reads (RPKM) was calculated for all contigs and all samples, fold-changes were calculated as the ratio of the RPKM values between 2 samples. To identify contigs in the *E. huxleyi* non-redundant combined reference transcriptome assembly that might take part in ROS and antioxidant metabolism we used 144 *Arabidopsis thaliana* proteins with verified antioxidant functions (Mittler et al. 2004, Sheyn et al. 2016) to query the transcriptome assembly with tBLASTn. The analysis presented here is of the 2 hr time point only.

3.3.7 Virus Infections

The dynamics of NO production in strains 373^{R} and 379^{R} in response to viral infection were monitored to determine whether active changes in NO signaling are involved in the resistance response. Virus strain EhV201 (obtained courtesy of W. Wilson, Marine Biological Association, Plymouth, UK) was propagated in batch cultures of *E. huxleyi* CCMP1516. Viral lysates were passed through a 0.45 µm pore-size PVDF syringe filter to remove cell debris. For infection experiments, *E. huxleyi* strains 373^{R} and 379^{R}, along with 1516^{S} as a positive control, was inoculated with EhV201 during mid-exponential growth (~5.0×10^{5} cells ml^{-1}) at a virus-to-host ratio of 5:1. Uninfected *E. huxleyi* cultures of these strains served as controls.

In a separate experiment, the impact of exogenous NO on viral production dynamics in 373^{R} and 379^{R} inoculated with EhV201 was determined by pre-treating exponentially growing cultures with the NO donor SNAP at final concentrations of 100 µM and 250 µM. Viral abundance was determined according to (Brussaard et al.

2000). In summary, samples were fixed with 0.5% glutaraldehyde (Sigma-Aldrich, St. Louis, MO), flash frozen in liquid nitrogen, and stored at -80^{o}C. Samples were then thawed, diluted 1:50 with Tris-EDTA buffer containing SYBR Gold (Thermo Fisher, Waltham, MA) at a dilution of 1:20,000 of the commercial stock, and heated for 10 min at 80 ^{o}C. The EhV population was gated and enumerated based on the 520 nm fluorescence vs. side scatter (SSC) signature. Typical flow rates used for enumeration ranged from 10 μL min^{-1} to 25 μL min^{-1} and samples were collected from 15-30 s.

3.3.8 Data analysis and statistics

Flow cytometry data were analyzed using either FlowJo (v. 10.2) or BD Accuri C6 software. Statistics (counts, mean fluorescence, and median fluorescence) were based on at least 1000 *E. huxleyi* events. In many cases, median fluorescence per cell is reported, rather than mean, to better characterize typical fluorescence values in samples that have small subsets of higher values. Mean and median fluorescence per cell for DAF-FM Diacetate and CM-H_2DCFDA stained samples are reported as the difference between the mean or median 520 nm fluorescence per cell of the stained sample and an unstained control. Percent SYTOX Green, CM-H_2DCFDA, and DAF-FM DA positive cells are reported as the percent of the total *E. huxleyi* population that has elevated 520 nm fluorescence relative to an unstained control.

Statistically significant differences between multiple means were determined using a one-way ANOVA with a Tukey HSD post hoc. Error bars on all graphs are ± standard error of the mean (se). All statistical tests were performed in R and plots

were generated using the ggplot2 package, except bivariate flow cytograms and histograms, which were generated using FlowJo (v. 10.2).

3.4 RESULTS

3.4.1 Strain variability in basal NO production

E. huxleyi strains 373^{R}, 379^{R}, 374^{S}, and 1516^{S} exhibited vastly different intracellular NO production dynamics during exponential growth. Based on median per cell DAF-FM DA fluorescence, 374^{S} consistently produced the most NO of the four strains, followed by 1516^{S}, 373^{R}, and 379^{R}; 379^{R} produced the least amount of NO per cell (Fig. 3.1 & Fig. 3.3a). Only ~65% and ~10% (median value of n=5 across 2 independent staining experiments) of the total population are positively stained with DAF-FM in 373^{R} and 379^{R} cultures, respectively (Fig. 3.1, Fig. 3.3b), while nearly ~100% of cells stain positively with DAF-FM in exponential phase 374^{S} and 1516^{S} (Fig 3.1, Fig. 3.3b).

The possibility that inefficient dye loading in 373^{R} and 379^{R} resulted in these observations was addressed by treating these cultures with the NO donor SNAP, and monitoring fluorescence response. Treatment of 379^{R} with SNAP lead to dose-dependent increases in mean per cell DAF-FM fluorescence and percent stained, suggesting that DAF-FM DA is indeed successfully loaded into these cells (Fig. 3.2). A treatment of 500 μM SNAP leads to a nearly 100% of cells staining positively with DAF-FM DA. Similar results occur when 373^{R} is treated with SNAP (data not shown).

Extracellular NO production, assessed with a liposome-encapsulated spin trap for EPR spectroscopy, displayed similar patterns to intracellular NO production. Both 374^{S}

and 1516^S displayed higher extracellular NO concentrations in the media than 379^R (Fig. 3.4). MGD2Fe(II)NO concentrations in cultures of 374^S, 1516^S, and 379^R were 4.3 pmol $cell^{-1}$ hr^{-1}, 3.5 pmol $cell^{-1}$ hr^{-1}, and 0.95 pmol $cell^{-1}$ hr^{-1} respectively. One-way ANOVA revealed lack of a robust statistical significance in the differences in this data ($p= 0.054$) that may be due to the small sample size (n=3) of this analysis.

3.4.2 Strain variability in basal oxidative stress, cell death, and growth dynamics

E. huxleyi strains 373^R, 379^R, 374^S, and 1516^S also exhibited differences in basal ROS production and percentage of dead cells in exponentially growing cultures (Fig. 3.3 c,d). The two resistant strains, 373^R and 379^R, showed higher basal ROS stress in exponential growth than the two sensitive strains with a median value of 18% and 3% of the population staining positively with CM-H_2DCFDA, respectively (Figure 3.3c). The two sensitive strains consistently displayed nearly 0% of the population staining positively with CM-H_2DCFDA, indicating the lack of ROS stress in these cultures during normal, exponential growth. Similar trends were seen in the percent of cells in the culture that are dead or dying, as indicated by SYTOX Green (Figure 3.3d). 373^R and 379^R cultures had a median cell death of 13.7% and 10%, respectively. Cell death was comparatively minimal in the two sensitive strains, with 3% and 2% SYTOX positive cells in 1516^S and 374^S, respectively.

Basal growth rates in the four strains varied greatly between experiments. One-way ANOVA revealed lack of statistical differences in growth rate ($p=0.144$) across all data, although in several experiments the two sensitive strains displayed higher growth rates (Fig. 3.5a). Strains 374^S and 1516^S, however, consistently reach higher maximum

cell densities in stationary phase then 373^R and 379^R (Fig. 3.5b), suggesting the possibility of a difference in the carrying capacity and/or "cost-of-resistance" in these strains.

3.4.3 Strain variability in response to hydrogen peroxide

Given the observation that NO has an antioxidant function in *E. huxleyi* (Schieler et al. 2019), we hypothesized that the sensitive, high NO-producing strains would be less sensitive to H_2O_2 stress. Across three independent experiments, strain 379^R experienced the smallest ΔGrowth over 48 hr after treatment with the moderate H_2O_2 treatment (50 μM), followed by 373^R, 1516^S, and 374^S (Fig. 3.6a). In some experiments, strain 379^R even experienced slightly positive ΔGrowth in the presence of moderate levels of H_2O_2 (Fig. S3.1). At the high H_2O_2 treatment (125 μM), 373^R experienced the smallest ΔGrowth over 48 hr, followed by 1516^S, 379^R, and 374^S (Fig. 3.6b). There was considerable variability in how each strain's growth dynamics responded to challenge with H_2O_2 (Figure S.3.1) from experiment to experiment. However, the general trend was that the two resistant *E. huxleyi* strains were more likely to respond more favorably than the two sensitive strains.

Cell lysates of exponentially growing 373^R, 379^R, 374^S, and 1516^S were directly assayed for their capacity to inhibit H_2O_2-mediated oxidation of ABTS, what is considered the total antioxidant capacity (TAC) of the lysate. Across five sampling days from three independent experiments, the per-cell enzymatic and non-enzymatic TAC was generally highest for strain 379^R and 373^R, followed by 374^S and 1516^S (Fig 3.7). Strain 373^R exhibited the highest per cell TAC in one experiment (Sampling #1). When TAC

was normalized to protein concentration of the lysate instead (Figure S3.2a), overall differences between strains become less robust, likely due to higher per cell protein concentrations in the resistant strains observed in across experiments (Fig S3.2b).

3.4.4 Antioxidant gene expression in 374^S and 379^R

374^S and 379^R displayed markedly different antioxidant gene expression profiles during basal exponential growth. A total of 159 genes with a putative antioxidant function were identified in the 374^S and 379^R shared transcriptome by homology to *Arabidopsis* antioxidant-related genes (see Supplementary Table 1 for full and detailed list). These 159 genes were grouped into 17 unique gene categories. By far the most widespread gene type represented in the dataset was thioredoxin, with 89 of the 159 expressed genes having sequence homology to various types of *Arabidopsis* thioredoxins (Fig. 3.8). Of the genes that were more strongly expressed in either 379^R or 374^S, the majority of them were a type of thioredoxin. Overall, 379^R had a greater diversity of antioxidant genes more strongly expressed than 374^S (Fig 3.8).

Of the total 159 shared expressed antioxidant genes, 72% (114 genes) were more strongly expressed in 379^R compared to 374^S (Fig. 3.9a,b), which points to a general enhancement of basal antioxidant activity in 379^R. Of the 17 unique categories, most were more strongly expressed in 379^R (Fig.3.9a). For example, of the 89 described and expressed thioredoxins, 62 (70%) were more strongly expressed in 379^R compared to 374^4 (Fig. 3.9a). In addition, there were four thioredoxins that were expressed in 379^R, but not 374_S (Table S3.1). Notably, 374^S had elevated expression of two described manganese superoxide dismutase (MnSOD) genes (Fig. 3.9a,b). In addition, there was no

measured expression of blue-copper binding protein in 379^R (Table S3.1). These observations suggest that the enrichment of antioxidant activity in 379^R is not uniform among all the components of the cellular antioxidant machinery.

To account for magnitude of upregulation, total reads per kilobase of transcript, per million mapped reads (RPKM) for all antioxidant genes identified were considered (Fig 3.9b). 379^R had a total 1.5 fold increase in expression over 374^S across all genes (Fig. 3.9b). In addition, of the top ten most represented gene categories, seven were more strongly expressed in 379^R (thioredoxins, protein disulfide isomerases, glutathione reductases, 5'andylylphosphosulfate reductase, glutaredoxins, NADPH-dependent thioredoxin reductase C, and dehydroascrobate reductase), while the remaining three (glutathione peroxidase, manganese superoxide dismutase, and ascorbate peroxidase). were more strongly expressed in 374^S.

3.4.5 Virus Infections

Infection of 379^R by EhV201 lead to no observable differences in intracellular NO production between infected cultures and uninfected controls over the course of 48 hr, while host cells continued to grow during this same timeframe (Fig. S3.3). Infection of 373^R by EhV201, however, led to a noticeable decrease in intracellular NO production in infected cells relative to uninfected controls over the course of 48 hr, while host cells also continued to grow over this same timeframe (Fig S3.4). At 1 and 48 hours post infection (hpi), DAF-FM DA fluorescence was nearly two-fold higher in uninfected 373^R relative to EhV201-infected cells. This 373^R infection experiment only monitored one replicate of each treatment, thus bears repeating.

Additionally, pre-treatment of 373^{R} and 379^{R} with two different concentrations of SNAP that have been empirically determined to both stimulate intracellular NO concentrates and be non-lethal to cells (Chapter 2) failed to render these strains sensitive to viral infection. At 48 hpi there was no observable viral production in SNAP pre-treated 373^{R} or 379^{R}, while there was considerable production in a 1516^{S} positive control (Fig S3.5).

3.5 DISCUSSION

A unique aspect of the *Emiliania huxleyi* model system is the existence of a wide diversity of strains in culture that vary significantly in physiological traits that are tied to key ecologically relevant environmental processes. One such process is viral infection; *E. huxleyi* bloom termination by lytic viral infection has been shown to impact carbon export (Laber et al. 2018), grazing dynamics (Evans & Wilson 2008, Frada et al. 2014), and leads to the production of several volatile compounds like DMS, ROS, and NO (Evans et al. 2006, Evans et al. 2007, Sheyn et al. 2016, Schieler et al. 2019). Various strains of *E. huxleyi* vary in their susceptibility to viral infection, with CCMP373 and CCMP379 displaying resistance to all tested viral isolates (Schroeder et al. 2002, Bidle & Kwityn 2012). In fact, CCMP379 experiences elevated growth when infected with EhV1, leading to its designation as a "hyper-resistant" strain (Bidle & Kwityn 2012). These strains can help answer critical questions about various aspects of cell physiology as it relates to costs and benefits of viral infection in this cosmopolitan species including mechanisms and "costs" of viral resistance, population-wide impacts of viral infection, and influence of environmental change on the infection dynamic.

The production of free radicals and other reactive species have been shown to be critical during lytic infection. These include NO (Schieler et al. 2019) and ROS, specifically H_2O_2 (Evans et al. 2006, Sheyn et al. 2016). Exactly how these molecules interact to regulate viral infection is still unknown. Schieler et al. (2019) suggested that NO production during early- to mid-infection may have an antioxidant function, keeping cellular oxidative stress (ROS) low to allow new virions to properly replicate and assemble. Here we address whether basal NO, oxidative stress, and antioxidant capacity are characteristic of resistant phenotypes, with an aim of better understanding their role in facilitating infection in susceptible strains. We surveyed these traits and their relationships in four *E. huxleyi* strains the range in their susceptibility to infection (i.e. $374^S > 1516^S > 373^R > 379^R$).

Previous work has already demonstrated that the four strains investigated in this study exhibit fundamental physiological and ecological differences that may have important ecosystem-wide implications. For example, resistant strains 373^R and 379^R were previously shown to have significantly lower basal levels of caspase activity and metacaspase esxpression and that these traits were correlated to infectivity across a gradient of susceptibility (Bidle & Kwityn 2012). While the roles of metacaspases in phytoplankton are not well known, caspase activity (and expression of putative metacaspase genes) has been shown to be required for successful viral infection (Bidle et al. 2007) and is linked to various stress pathways in phytoplankton (Bidle & Bender 2008). Bidle & Kwityn (2012) shed light on a possible mechanism of resistance in which basal caspase activity (and metaspcase expression) may have a role in predisposing cells to viral infection.

In addition, there are clear strain-specific grazing dynamics of *E. huxleyi* cells by the dinoflagellate *Oxyrrhis marina* (Harvey et al. 2015). For example, *O. marina* had enhanced ingestion efficiency (percentage of encountered cells that were ultimately ingested) when grazing upon the two resistant strains 373^{R} and 379^{R} relative to the sensitive strain studied, 374^{S}, across a range of prey (*E. huxleyi*) concentrations. No mechanism to explain these strain-to-strain differences in ingestion efficiency was proposed. However, these observations suggest that intra-species variability in presently unknown physiological characteristics have ecosystem wide consequences.

We show here that these four strains differ across a range of NO production, oxidative stress, and antioxidant activity. Exponentially growing 373^{R} and 379^{R} consistently exhibited lower intracellular NO then 1516^{S} and 374^{S}. These intracellular NO signatures very clearly followed the established resistance gradient (Bidle & Kwityn 2012), with the highest NO production seen in the most susceptible strain (374^{S}) and the lowest NO production observed in the hyper-resistant strain (379^{R}). Intracellular patterns in NO production are reflected in both the median per cell DAF-FM DA fluorescence as well as the percent of the population that are DAF-FM positive, although there is some variability across independent experiments in absolute values. Interestingly, resistant strains display significant subpopulations that do not produce detectable NO. Only ~10% of 379^{R} cultures display detectable levels of intracellular NO (median across experiments presented here). This phenotype was notably not observed in the sensitive strains tested here. Extracellular NO concentrations present in the media of these cultures followed their typical intracellular NO levels. 374^{S} displayed the highest extracellular NO per cell,

followed by 1516^{S}. Strain 379^{R} had the lowest extracellular NO per cell, with two of the three replicates below level of detection.

It has been previously reported that phytoplankton species do vary greatly in their capacity for NO production. For example, there is genus-level variability in basal NO production within *Chlorella sp.* (Estevez & Puntarulo 2005), among various species responsible for harmful algal blooms (Kim et al. 2008), and among *Symbiodinium* types in response to heat stress (Hawkins & Davy 2012). However, to our knowledge, these results are the first time significant intra-species differences in this key signaling molecule have been demonstrated both intra- and extra-cellularly. This has implications for predicting the ability of particular phytoplankton populations to be sources of NO in the environment. For example, blooms of *E. huxleyi* may produce more or less NO, depending on the ecotypes present within the bloom or whether the bloom is experiencing pressure from the presence of viruses.

In agreement with the putative antioxidant function of NO production in *E. huxleyi* during viral infection (Schieler et al. 2019) and other phytoplankton species in response to various abiotic stressors (Mallick et al. 2002, Singh et al. 2004, Li et al. 2013), the strains in this study with lowest intrinsic NO production also exhibited highest levels of basal intracellular ROS and cell death. The two resistant strains both had a subset of cells within the population that stain positive with the broad-target ROS fluorescent stain, CM-H_2DCFDA. The two sensitive strains, on the other hand, typically display nearly 0% positive for ROS throughout through out various stages of growth. The percent of cells within cultures that are dead or dying, indicated by positive SYTOX Green staining, closely match what was observed for ROS production. Namely, 373^{R} and

379^R had elevated cell death when compared to 374^S and 1516^S. This is in agreement with previously published correlations between intracellular ROS levels and cell death in both lab cultures and field populations (Vardi et al. 2012, Schieler et al. 2019) of *E. huxleyi*.

Considering our hypothesis that NO production in *E. huxleyi* is linked to antioxidant capacity, we were surprised to uncover that resistant strains 373^R and 379^R, with consistently the lowest intra- and extra-cellular NO levels (and highest oxidative stress), actually displayed the highest basal antioxidant capacities. Across at least three independent experiments, growth rates of 373^R and 379^R were impacted least by treatment with moderate levels (50 μM) of H_2O_2. However, when treated with high levels (125 μM) of H_2O_2, the growth rate impact on 379^R more reflected a sensitive phenotype, with 373^R displaying the smallest impact on growth rate of the four strains. In agreement with our H_2O_2 treatment experiments, cellular lysates of resistant strains had a higher ability to detoxify H_2O_2 then the two sensitive strains, which we express as the total enzymatic and non-enzymatic antioxidant capacity (TAC). In fact, hyper-resistant strain 379^R, which had the lowest NO production of the four strains, also had the highest per cell TAC. There was significant inter-experimental variability in all physiological traits discussed above, however, indicating the plasticity of NO production, reactive oxygen stress, and antioxidant activity over time.

One possible explanation for these results is that antioxidant capacity during basal growing conditions in cells is controlled at the level of gene expression, rather than modulated by NO production. Indeed, comparative expression profiles of putative antioxidant genes in 374^S and 379^R, two strains that represent the extremes of the viral susceptibility gradient, revealed that 379^R has elevated expression of antioxidant genes.

72% of all the described antioxidant genes were more strongly expressed in 379^R, with the total fold increase of the described antioxidant genes in 379^R relative to 374^S was 1.5. Many of the genes upregulated in 379^R are involved the recycling of glutathione (GSH) and ascorbate (glutathione reductases and dehydroascorbate reductases), small molecular-weight antioxidants used to detoxify H_2O_2. In addition, four thioredoxin genes were expressed in 379^R that were not expressed in 374^S. 379^R did not, however, display elevated expression across all antioxidant gene types identified. For example there was a 4.8 fold increase in two putative manganese superoxide dismutase genes in 374^S over 379^R. This suggests that the enhancement of antioxidant activity may not be uniform among all the components of cellular antioxidant machinery in 379^R. Additionally, it is unknown whether 1516^S and 373^R follow these trends, as there are no transcriptomes currently for these species.

An alternative explanation of these findings is that antioxidant activity is controlled at the level of NO production, but the NO produced by the resistant strains is bound up in intracellular reservoirs and is not free to react with DAF-FM or to escape the cell for extracellular detection. Indeed, if this is the case, the major route of control would be through post-translational modifications of antioxidant enzymes (Begara-Morales et al. 2016). This would have the overall impact of sequestering free NO into proteins. In addition to proteins, there are other molecular sinks of NO in the cell. For example, glutathione is a ubiquitous, efficient, and stable cellular sink of NO in the form of s-nitrosoglutathione (GSNO) (Corpas et al. 2013). GSNO (and other nitrosothiols) has been shown to execute NO-mediated effects by directly nitrosylating target molecules through trans-nitrsoylation (Zaffagnini et al. 2016) and by the controlled release NO via activity

of several enzymes including GSNO reductases and thioredoxins (Nikitovic & Holmgren 1996, Feechan et al. 2005). Indeed, strain 379^{R} displays enhanced expression of genes known to be involved in glutathione recycling (glutathione reductase) and s-nitrosylation (such as protein disulfide isomerases and thioredoxins). It is thus conceivable that resistant strains 379^{R} and 373^{R}, which have a diminished free intracellular NO, may actually have higher overall NO production, but a tighter cycling of NO between various sinks and sources within the cell. Future work should address this possibility by quantifying cellular s-nitrosothiol content in these strains, alongside detection of free NO with methods used in this study.

Lastly, it is of broad interest to the field to determine what the costs and mechanisms of resistance are in this cosmopolitan coccolithophore species. As susceptibility to viral lysis has no obvious benefit to an *E. huxleyi* cell within a population or the population as a whole, the trade-offs to being resistant to infection have interesting implications for evolution and diversity of seemingly monoclonal bloom and the ongoing "chemical arms race" that dictates the outcomes of viral infection at sea (Bidle & Vardi 2011). Our work suggests that resistant strains may invest more heavily in maintaining their antioxidant machinery then sensitive strains. This is probably best illustrated by the enrichment of antioxidant gene expression in strain 379^{R} relative to 374^{S} compared to their transcriptomes as a whole.

It remains unclear whether enhanced antioxidant activity and/or diminished NO production in these strains affords them their resistance or whether these traits are a byproduct of some other resistance mechanism. Indeed, treatment of the resistant strains with exogenous NO failed to render them sensitive to infection, indicating that their NO

production dynamics do not de facto control their resistance. In addition inoculation of 379^R with viruses does not lead to any changes in intracellular NO production, indicating that it is not an active player in resistance. Interestingly, 373^R did display decreased NO production when challenged with EhV201, suggesting there may be inherent differences in the resistance mechanisms of 373^R and 379^R. However, each of these experiments was performed once and thus bears replication.

It is also unknown what cost being virus-resistant has on the cell metabolically. Here it is shown that at least one possible cost of the resistant phenotype is related to greater investment in antioxidants in these strains. Prior work has demonstrated that elevated antioxidant capacity in other algae, namely *Chlamydomonas reinhardtii* and *Peridinium gatunense*, does indeed elicit metabolic costs in the form of hyper-sensitivity to subsequent oxidative stress, stimulated in part by the accumulation of certain byproducts of antioxidant activity (Murik & Kaplan 2009, Murik et al. 2014). The results presented here hint that resistant *E. huxleyi* strains may also have metabolic trade-offs. While resistant strains had diminished growth rates in only some experiments, these strains routinely reached significantly lower maximum densities in stationary phase and also consistently had higher per cell protein content then the sensitive strains (Fig. S3.2B), indicating greater resource requirements in 379^R and 373^R.

3.6 CONCLUSION

In this study, we describe unique phenotypes of two virus-resistant (373^R and 379^R) and two virus-susceptible (1516^S and 374^S) strains of *E. huxleyi* in terms of basal nitric oxide production, reactive oxygen production, and antioxidant capacity- three traits

that been previously shown to be important for and influenced by viral infection. In general, resistant strains displayed lower basal NO production than sensitive strains, with the gradient in basal NO content following an established gradient in viral susceptibility (namely $374^S > 1516^S > 373^R > 379^R$). In addition, resistant strains had higher basal ROS production and cell death, indicating that these strains experience higher levels of oxidative stress then their sensitive counterparts.

Resistant strains displayed significantly higher basal antioxidant capacity, indicated by growth rate responses to H_2O_2 treatments, ability of cell extracts to directly detoxify H_2O_2, and comparison of expression profiles of putative antioxidant genes. Because it has been shown that NO bound in intracellular nitrosothiols, such as GSNO, is bioactive and physiologically relevant, it is important to quantify this NO pool in order to get a clearer understanding of the variability of basal NO production in these strains and its relationship to antioxidant activity.

It is indeterminable from the data presented what the costs of resistance are in 373^R and 379^R; resistant strains did display a diminished carrying capacity, although potential differences in specific growth rates between the strains were more ambiguous. Indeed, despite enhanced antioxidant capacity, the resistant strains were under higher oxidative stress during basal growth, indicating that production of ROS still outpaced their detoxification by antioxidants. Because our results show that 373^R and 379^R place a heavy metabolic investment in antioxidant activity, and that significant rewiring of host pro- and anti-oxidant pathways occurs during infection, this represents an intriguing area to further explore mechanisms of viral resistance in *E. huxleyi*.

3.7 ACKNOWLEDGEMENTS

Bioinformatics analysis, creation of the shared transcriptome of 373^{R} and 374^{S}, and tBLASTn of known *Arabidopsis thaliana* antioxidant genes against the transcriptome were performed by Udi ZelZion (Genome Cooperative, School of Environmental and Biological Science, Rutgers University). Donald J. Hirsh led the experimental design of extracellular NO measurements (Chemistry Department, The College of New Jersey). Megha V. Soni (Department of Marine & Coastal Sciences, Rutgers University) performed and analyzed physiology experiments and TAC assays.

3.8 REFERENCES

Begara-Morales JC, Sanchez-Calvo B, Chaki M, Valderrama R, Mata-Perez C, Padilla MN, Corpas FJ, Barroso JB (2016) Antioxidant Systems are Regulated by Nitric Oxide-Mediated Post-translational Modifications (NO-PTMs). Frontiers in plant science 7:152

Besson-Bard A, Pugin A, Wendehenne D (2008) New insights into nitric oxide signaling in plants. Annual review of plant biology 59:21-39

Bidle KD, Bender SJ (2008) Iron starvation and culture age activate metacaspases and programmed cell death in the marine diatom *Thalassiosira pseudonana*. Eukaryotic cell 7:223-236

Bidle KD, Haramaty L, Barcelos ERJ, Falkowski P (2007) Viral activation and recruitment of metacaspases in the unicellular coccolithophore, *Emiliania huxleyi*. Proceedings of the National Academy of Sciences of the United States of America 104:6049-6054

Bidle KD, Kwityn CJ (2012) Assessing the Role of Caspase Activity and Metacaspase Expression on Viral Susceptibility of the Coccolithophore, *Emiliania huxleyi* (Haptophyta). J Phycol 48:1079-1089

Bidle KD, Vardi A (2011) A chemical arms race at sea mediates algal host-virus interactions. Current opinion in microbiology 14:449-457

Bratbak G, Egge JK, Heldal M (1993) Viral mortality of the marine alga *Emiliania huxleyi* (Haptophyceae) and termination of algal blooms. Marine Ecology Progress Series 93:39-58

Bratbak G, Heldal M, Norland S, Thingstad TF (1990) Viruses as partners in spring bloom micorbial trophodynamics. Applied and environmental microbiology 56:1400-1405

Brown CW, Yoder JA (1994) Coccolithophorid blooms in the global ocean. Journal of Geophysical Research 99:7467-7482

Brussaard CPD, Marie D, Bratbak G (2000) Flow cytometric detection of viruses. Journal of Virological Methods 85:175-182

Cochlan WP, Wikner J, Steward GF, Smith DC, Azam F (1993) Spatial distribution of viruses, bacteria, and chlorophyll a in neritic, oceanic, and estuarine environments. Marine Ecology Progress Series 92:77-87

Corpas FJ, Alche JD, Barroso JB (2013) Current overview of S-nitrosoglutathione (GSNO) in higher plants. Frontiers in plant science 4:126

de Pinto MC, Locato V, Sgobba A, Romero-Puertas Mdel C, Gadaleta C, Delledonne M, De Gara L (2013) S-nitrosylation of ascorbate peroxidase is part of programmed cell death signaling in tobacco Bright Yellow-2 cells. Plant physiology 163:1766-1775

Delledonne M, Zeier J, Marocco A, Lamb C (2001) Signal interactions between nitric oxide and reactive oxygen intermediates in the plant hypersensitive disease resistance response. Proceedings of the National Academy of Sciences of the United States of America 98:13454-13459

Estevez MS, Puntarulo S (2005) Nitric oxide generation upon growth of Antarctic *Chlorella* sp. cells. Physiologia Plantarum 125:192-201

Evans C, Kadner SV, Darroch LJ, Wilson WH, Liss PS, Malin G (2007) The relative significance of viral lysis and microzooplankton grazing as pathways of dimethylsulfoniopropionate (DMSP) cleavage: An *Emiliania huxleyi* culture study Limnology and Oceanography 52:1036-1045

Evans C, Malin G, Mills GP, Wilson WH (2006) Viral Infection of *Emiliania Huxleyi* (Prymnesiophyceae) Leads to Elevated Production of Reactive Oxygen Species. Journal of Phycology 42:1040-1047

Evans C, Wilson WH (2008) Preferential grazing of *Oxyrrhis marina* on virus-infected *Emiliania huxleyi* Limnology and Oceanography 53:2035-2040

Feechan A, Kwon E, Yun BW, Wang Y, Pallas JA, Loake GJ (2005) A central role for S-nitrosothiols in plant disease resistance. Proceedings of the National Academy of Sciences of the United States of America 102:8054-8059

Frada MJ, Schatz D, Farstey V, Ossolinski JE, Sabanay H, Ben-Dor S, Koren I, Vardi A (2014) Zooplankton may serve as transmission vectors for viruses infecting algal blooms in the ocean. Current biology : CB 24:2592-2597

Harvey EL, Bidle KD, Johnson MD (2015) Consequences of strain variability and calcification in *Emiliania huxleyi* on microzooplankton grazing. Journal of Plankton Research:fbv081

Hawkins TD, Davy SK (2012) Nitric oxide production and tolerance differ among *Symbiodinium* types exposed to heat stress. Plant & cell physiology 53:1889-1898

Hirsh DJ, Schieler BM, Fomchenko KM, Jordan ET, Bidle KD (2016) A liposome-encapsulated spin trap for the detection of nitric oxide. Free radical biology & medicine 96:199-210

Holligan PM, Fernández E, Aiken J, Balch WM, Boyd P, Burkill PH, Finch M, Groom SB, Malin G, Muller K, Purdie DA, Robinson C, Trees CC, Turner SM, van der Wal P (1993) A biogemical study of the coccolithophore, *Emiliania huxleyi,* in the North Atlantic Global Biogeochemical Cycles 7:879-900

Jiang SC, Paul JH (1998) Gene transfer by transduction in the marine environment. Applied and environmental microbiology 64:2780-2787

Johns CT, Grubb AR, Nissimov JI, Natale F, Knapp V, Mui A, Fredricks HF, Van Mooy BAS, Bidle KD (2018) The mutual interplay between clacification and coccolithovirus infection. Environmental microbiology

Kim D, Kang YS, Lee Y, Yamaguchi K, Matsuoka K, Lee KW, Choi KS, Oda T (2008) Detection of nitric oxide (NO) in marine phytoplankters. Journal of bioscience and bioengineering 105:414-417

Kumar A, Castellano I, Patti FP, Palumbo A, Buia MC (2015) Nitric oxide in marine photosynthetic organisms. Nitric oxide : biology and chemistry 47:34-39

Laber CP, Hunter JE, Carvalho F, Collins JR, Hunter EJ, Schieler BM, Boss E, More K, Frada M, Thamatrakoln K, Brown CM, Haramaty L, Ossolinski J, Fredricks H, Nissimov JI, Vandzura R, Sheyn U, Lehahn Y, Chant RJ, Martins AM, Coolen MJL, Vardi A, DiTullio GR, Van Mooy BAS, Bidle KD (2018) *Coccolithovirus* facilitation of carbon export in the North Atlantic. Nature microbiology 3:537-547

Li P, Liu CY, Liu H, Zhang Q, Wang L (2013) Protective function of nitric oxide on marine phytoplankton under abiotic stresses. Nitric oxide : biology and chemistry 33:88-96

Li W, Godzik A (2006) Cd-hit: a fast program for clustering and comparing large sets of protein or nucleotide sequences. Bioinformatics 22:1658-1659

Mallick N, Mohn FH, Soeder CJ, Grobbelaar JU (2002) Ameliorative role of ntiric oxide on H2O2 toxicity to a chlorophycean alga *Scenedesmus obliquus*.

Mittler R, Vanderauwera S, Gollery M, Van Breusegem F (2004) Reactive oxygen gene network of plants. Trends in plant science 9:490-498

Moncada S (1999) Nitric oxide: discovery and impact on clinical medicine. Journal of the Royal Society of Medicine 92:164-169

Munn CB (2006) Viruses as pathogens of marine organisms-- from bacteria to whales. J Mar Biol Ass UK 86:453-467

Murik O, Elboher A, Kaplan A (2014) Dehydroascorbate: a possible surveillance molecule of oxidative stress and programmed cell death in the green alga *Chlamydomonas reinhardtii*. The New phytologist 202:471-484

Murik O, Kaplan A (2009) Paradoxically, prior acquisition of antioxidant activity enhances oxidative stress-induced cell death. Environmental microbiology 11:2301-2309

Nikitovic D, Holmgren A (1996) S-nitrosoglutathione is cleaved by the thioredoxin system with liberation of glutathione and redox regulating nitric oxide. Journal of Biological Chemistry 271:19180-18185

Nissimov JI, Napier JA, Allen MJ, Kimmance SA (2016) Intragenus competition between *coccolithoviruses*: an insight on how a select few can come to dominate many. Environmental microbiology 18:133-145

Schieler BM, Soni MV, Brown CM, Coolen MJL, Fredricks H, Van Mooy BAS, Hirsh DJ, Bidle KD (2019) Nitric oxide production and antioxidant function during viral infection of the coccolithophore *Emiliania huxleyi*. The ISME journal

Schroeder DC, Oke J, Malin G, Wilson WH (2002) Coccolithovirus (Phycodnaviridae): characterisation of a new large dsDNA algal virus that infects *Emiliana huxleyi*. Archives of virology 147:1685-1698

Sheyn U, Rosenwasser S, Ben-Dor S, Porat Z, Vardi A (2016) Modulation of host ROS metabolism is essential for viral infection of a bloom-forming coccolithophore in the ocean. The ISME journal 10:1742-1754

Sheyn U, Rosenwasser S, Lehahn Y, Barak-Gavish N, Rotkopf R, Bidle KD, Koren I, Schatz D, Vardi A (2018) Expression profiling of host and virus during a coccolithophore bloom provides insights into the role of viral infection in promoting carbon export. The ISME journal 12:704-713

Singh A, Sharma L, Mallick N (2004) Antioxidative role of nitric oxide on copper toxicity to a chlorophycean alga, *Chlorella*. Ecotoxicology and environmental safety 59:223-227

Sunda W, Kieber DJ, Kiene RP, Huntsman S (2002) An antioxidant function for DMSP and DMS in marine algae. Nature 418:31-320

Suttle CA (2007) Marine viruses--major players in the global ecosystem. Nature reviews Microbiology 5:801-812

Thingstad TF, Lignell R (1997) Theoretical models for the control of bacterial growth rate, abundance, diversity, and carbon demand. Aquatic Microbial Ecology 13:19-27

Tyrrell T, Merico A (2004) *Emiliania huxleyi*: bloom observations and the conditions that induce them. In: Thierstein HR, Young JR (eds) Coccolithophores: From Molecular Processes to Global Impact. Springer, Germany

Van Hannen EJ, Zward G, Van Agterveld MP, Gons HJ, Ebert J, Laanbroek HJ (1999) Changes in bacterial and eukaryotic community structure after mass lysis of filamentous cyanobacteria associated with viruses. Applied and environmental microbiology 65:795-801

Vardi A, Haramaty L, Van Mooy BAS, Fredricks HF, Kimmance SA, Larsen A, Bidle KD (2012) Host-virus dynamics and subcellular controls of cell fate in a natural coccolithophore population. Proceedings of the National Academy of Sciences of the United States of America 109:19327-19332

Vardi A, Van Mooy BA, Fredricks HF, Popendorf KJ, Ossolinski JE, Haramaty L, Bidle KD (2009) Viral glycosphingolipids induce lytic infection and cell death in marine phytoplankton. Science 326:861-865

Wilhelm SW, Suttle CA (1999) Viruses and nutrient cycles in the sea. BioScience 49:781-788

Yager PL, Connelly TL, Mortazavi B, Wommack KE, Bano N, Bauer JE, Opsahl S, Hollibaugh JT (2001) Dynamic bacterial and viral response to an algal bloom at subzero temperatures. Limnology and Oceanography 46:790-801

Yang H, Mu J, Chen L, Feng J, Hu J, Li L, Zhou JM, Zuo J (2015) S-nitrosylation positively regulates ascorbate peroxidase activity during plant stress responses. Plant physiology 167:1604-1615

Zaffagnini M, De Mia M, Morisse S, Di Giacinto N, Marchand CH, Maes A, Lemaire SD, Trost P (2016) Protein S-nitrosylation in photosynthetic organisms: A comprehensive overview with future perspectives. Biochimica et biophysica acta 1864:952-966

Zhao J, Fujita K, Sakai K (2007) Reactive oxygen species, nitric oxide, and their interactions play different roles in *Cupressus lusitanica* cell death and phytoalexin biosynthesis. The New phytologist 175:215-229

3.9 FIGURES & TABLES

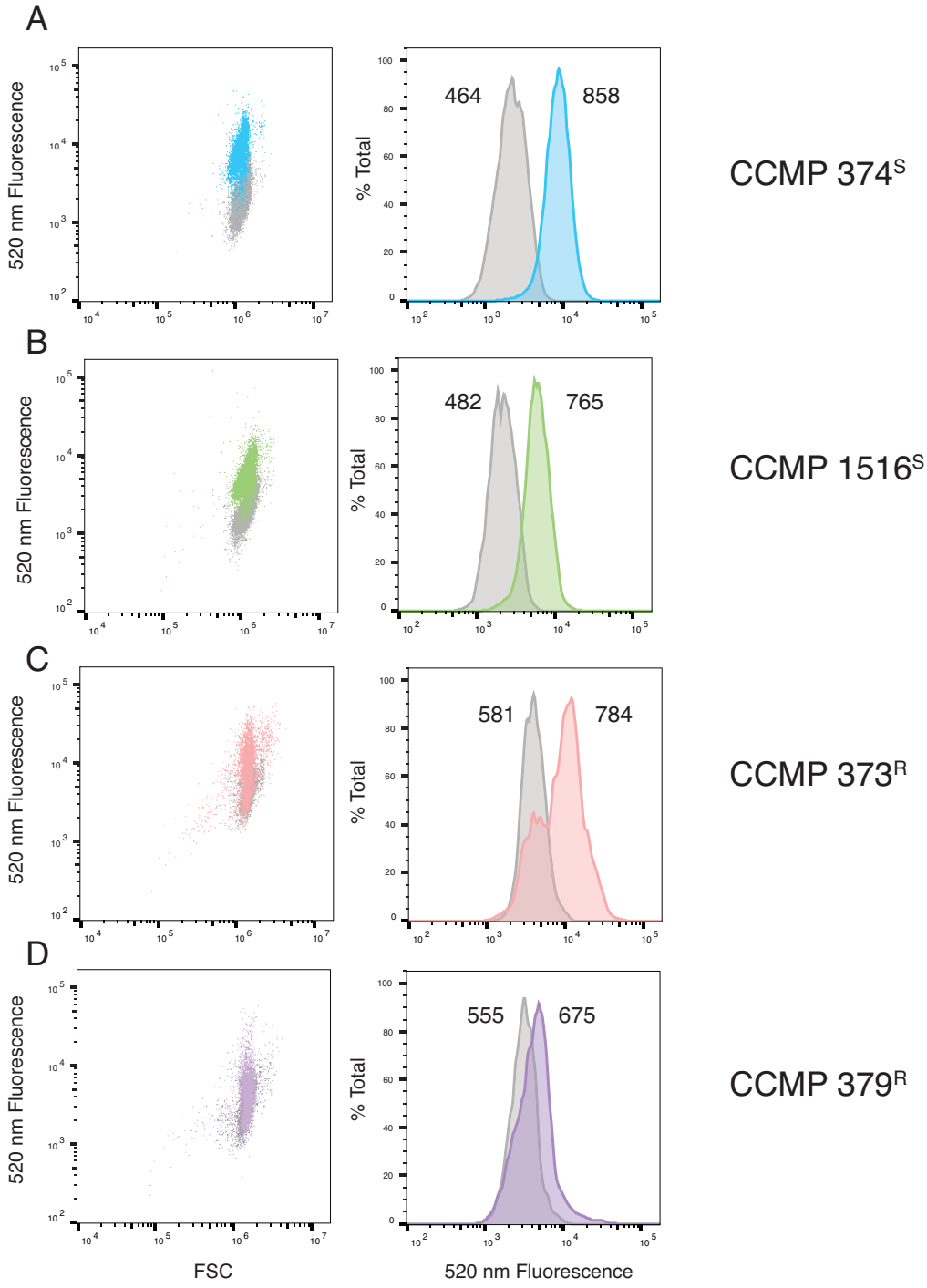

Figure 3.1 Representative flow cytograms and histograms of typical exponential phase CCMP374^{S} (A), CCMP1516^{S} (B), CCMP373^{R} (C), and CCMP379^{R} (D) stained with DAF-FM DA (colors) overlayed by an unstained control (grey). Median 520 fluorescence value for each unstained and stained sample for each culture are indicated in right panels.

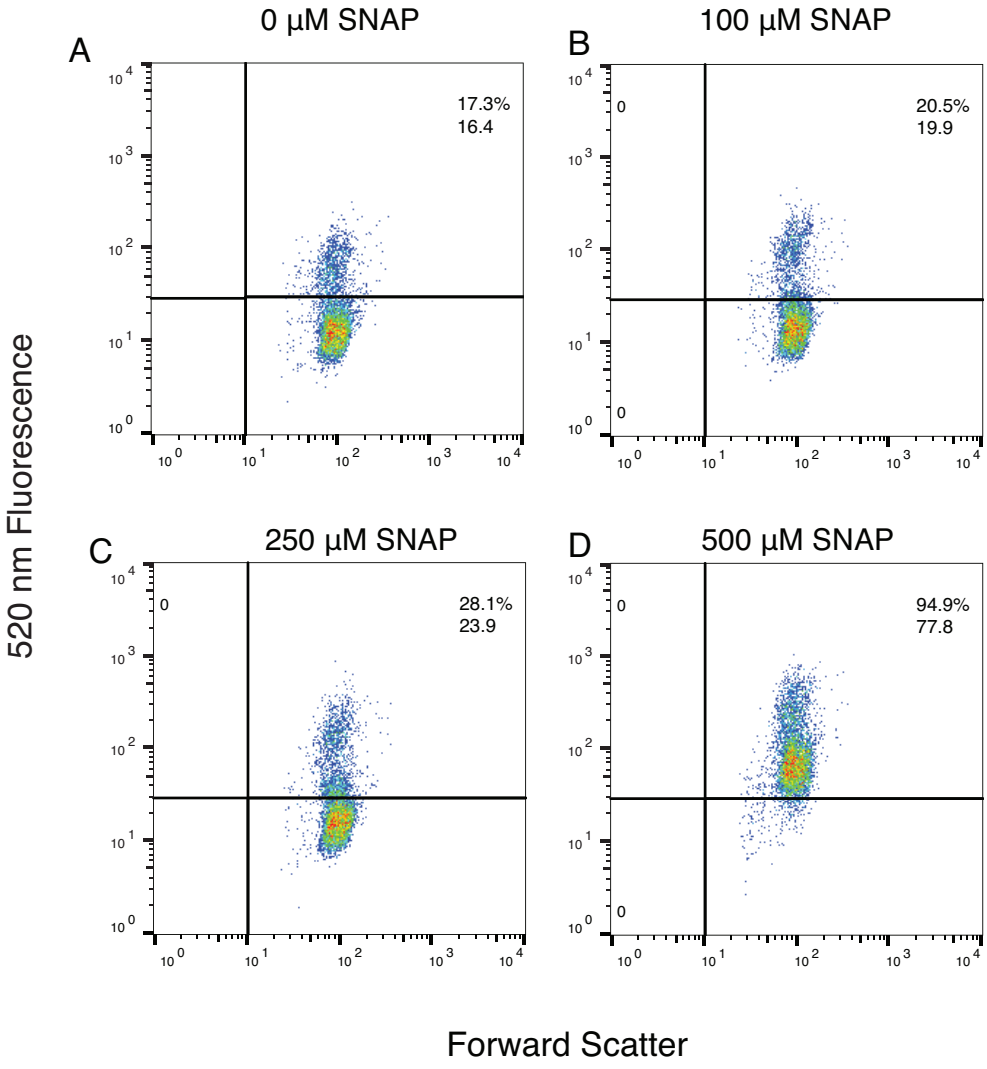

Figure 3.2 Determination of efficient DAF-FM DA dye loading in resistant *E. huxleyi* strains by treating DAF-FM DA stained CCMP379^{R} cultures with 0 µM (A), 100 µM (B), 250 µM (C), and 500 µM (D) of the NO donor s-nitroso-n-acetylpenicillamine (SNAP). Plots are representative bivariate flow cytograms of 520 nm fluorescence vs. forward scatter (perpendicular) from a one experiment. Each plot includes the % of cells positively stained compared to an unstained control (top number; quadrant gate) and the mean (geometric) 520 nm fluorescence of the entire population (bottom number).

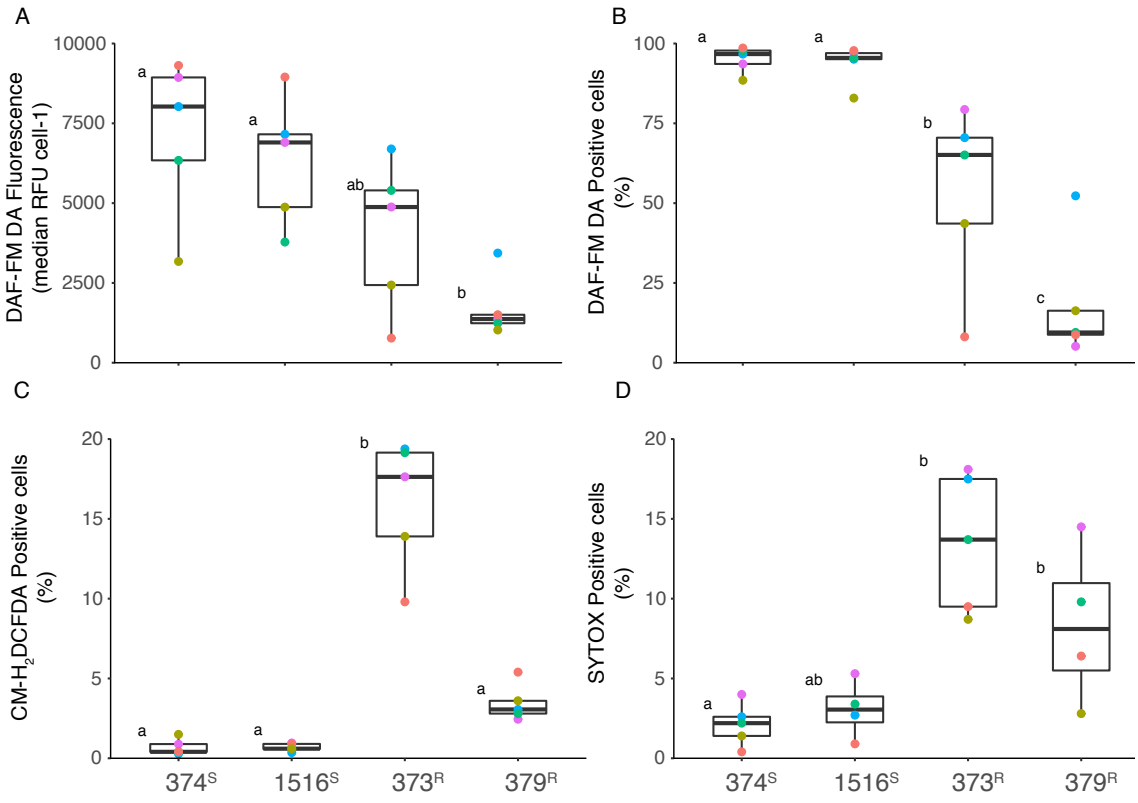

Figure 3.3 Basal NO production, reactive oxygen (ROS) stress, and cell death in typical cultures of exponential phase CCMP374^{S}, CCMP1516^{S}, CCMP373^{R}, and CCMP379^{R}. NO production, assessed with DAF-FM DA, is represented as median 520 nm fluorescence per cell (A) and percentage of cells that stain positive (B). ROS and cell death are represented as percentage of cells that stain positive for CM-H_2DCFDA (C) and SYTOX Green (D), respectively. Data are displayed as box-plots with the upper and lower bounds of the box representing the 25% and 75% quartiles around the median. Individual data points are overlayed to display intra- and inter-experimental variability and are colored by unique sampling day. Statistically significant differences between means were determined using one-way ANOVA with the Tukey HSD post hoc test (letters denote statistically different subgroups; $p < 0.05$; n=5 across two independent experiments).

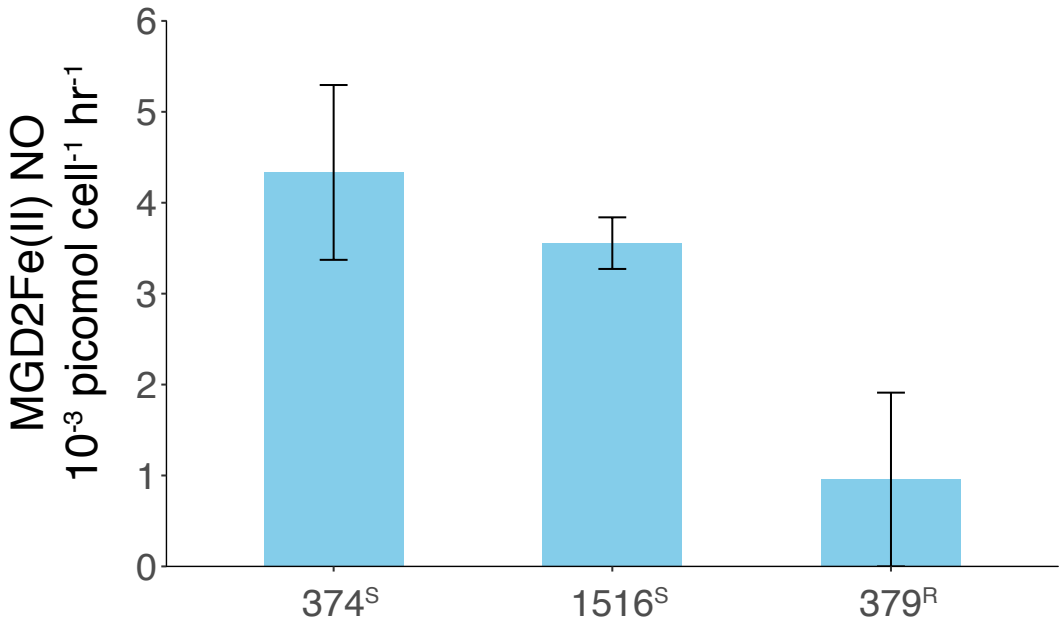

Figure 3.4 Concentration of extracellular NO in *E. huxleyi* CCMP374^{S}, CCMP1516^{S}, and CCMP379^{R}. Values represent the mean picomol of spin trap-bound NO cell^{-1} hr^{-1} detected with EPR spectroscopy over a 3 h incubation period (n = 3, ±se).

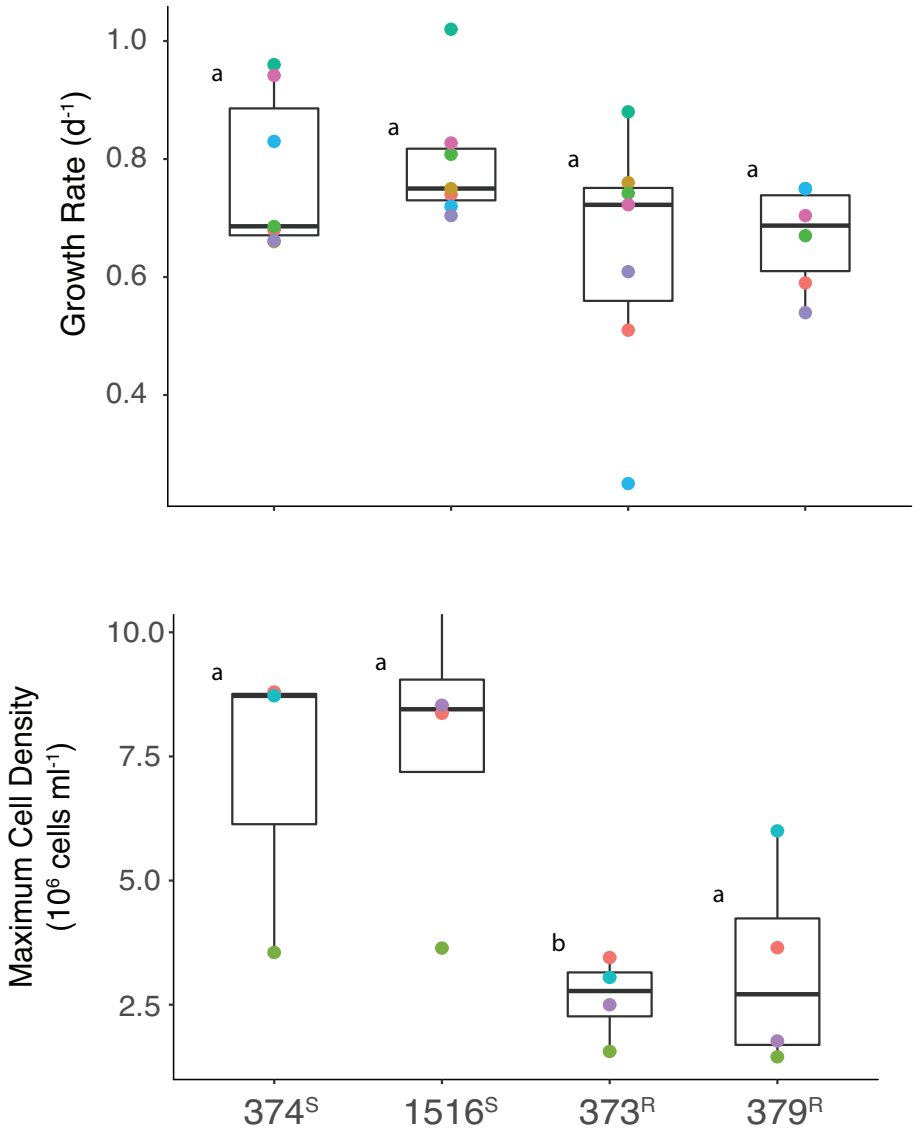

Figure 3.5 Basal growth dynamics of typical cultures of CCMP374^{S}, CCMP1516^{S}, CCMP373^{R}, and CCMP379^{R}. Specific growth rates during exponential growth (A) and maximum cell densities reached during stationary phase (B) are displayed as box-plots with the upper and lower bounds of the box representing the 25% and 75% quartiles around the median (n=7 and n=4 independent growth experiments for A and B, respectively). Individual data points are overlayed to display intra- and inter-experimental variability and are colored by unique sampling day. Statistically significant differences between means were determined using one-way ANOVA with the Tukey HSD post hoc test (letters denote statistically different subgroups; $p < 0.05$).

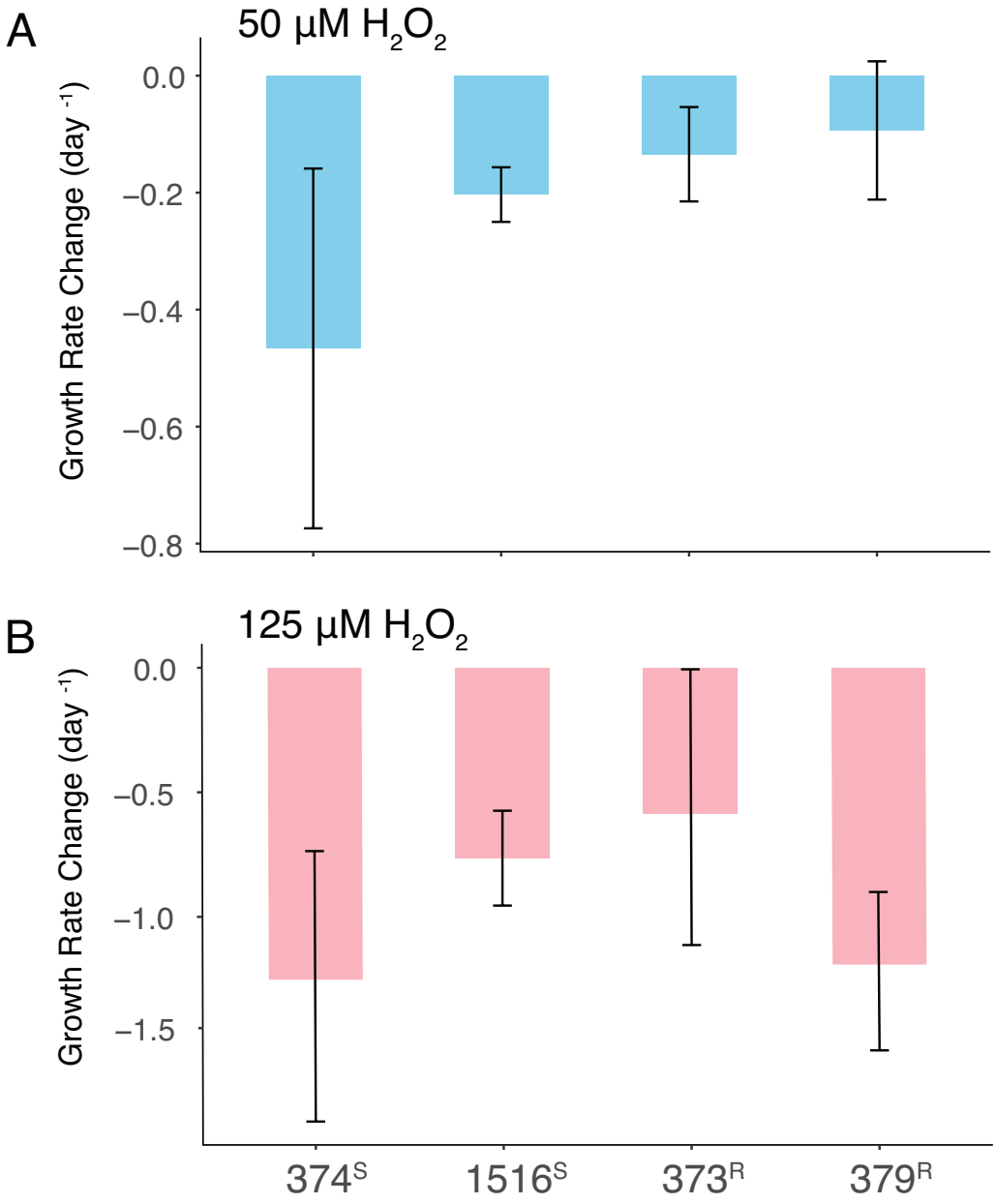

Figure 3.6 Impact of H_2O_2 on growth rate dyanmics of *E. huxleyi* strains CCMP374^S, CCMP1516^S, CCMP373^R, and CCMP379^R. Data represent mean change in growth rate (day^{-1}) of cultures treated with (A) 50 µM H_2O_2 and (B) 125 µM H_2O_2 relative to an untreated control culture across three independent experiments with technical duplication (±se).

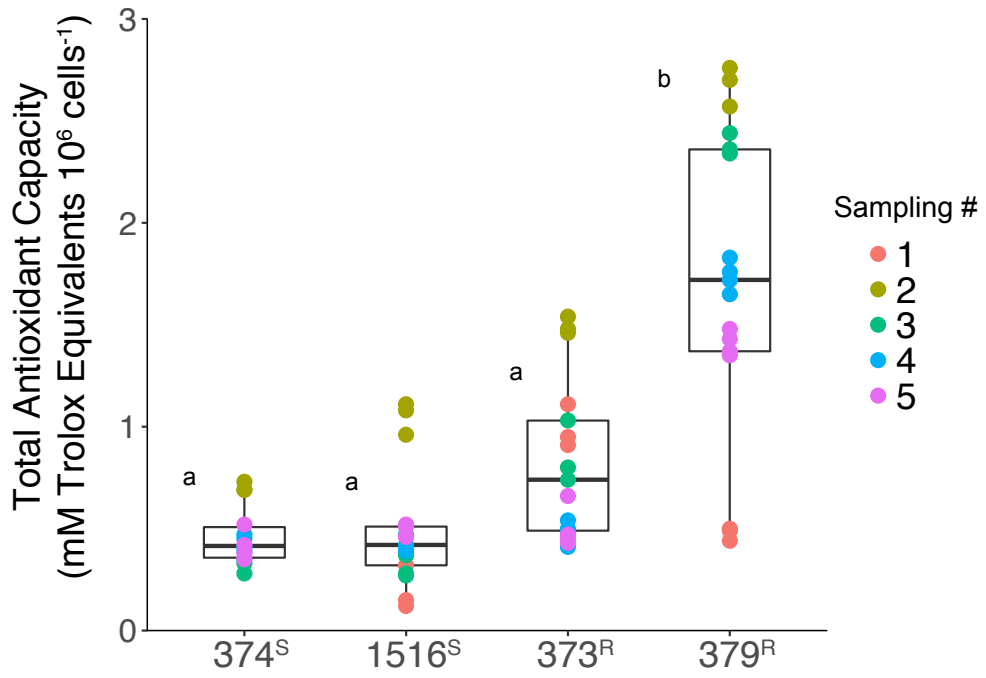

Figure 3.7 Total enzymatic and non-enzymatic antioxidant capacity (TAC) of *E. huxleyi* strains CCMP374^{S}, CCMP1516^{S}, CCMP373^{R}, and CCMP379^{R} normalized per 10^{6} cells in the lysate. Data are displayed as box-plots with the upper and lower bounds of the box representing the 25% and 75% quartiles around the median. Individual data points are overlayed to display intra- and inter-experimental variability. Statistically significant differences between means were determined using one-way ANOVA with the Tukey HSD post hoc test (letters denote statistically different subgroups; $p < 0.05$).

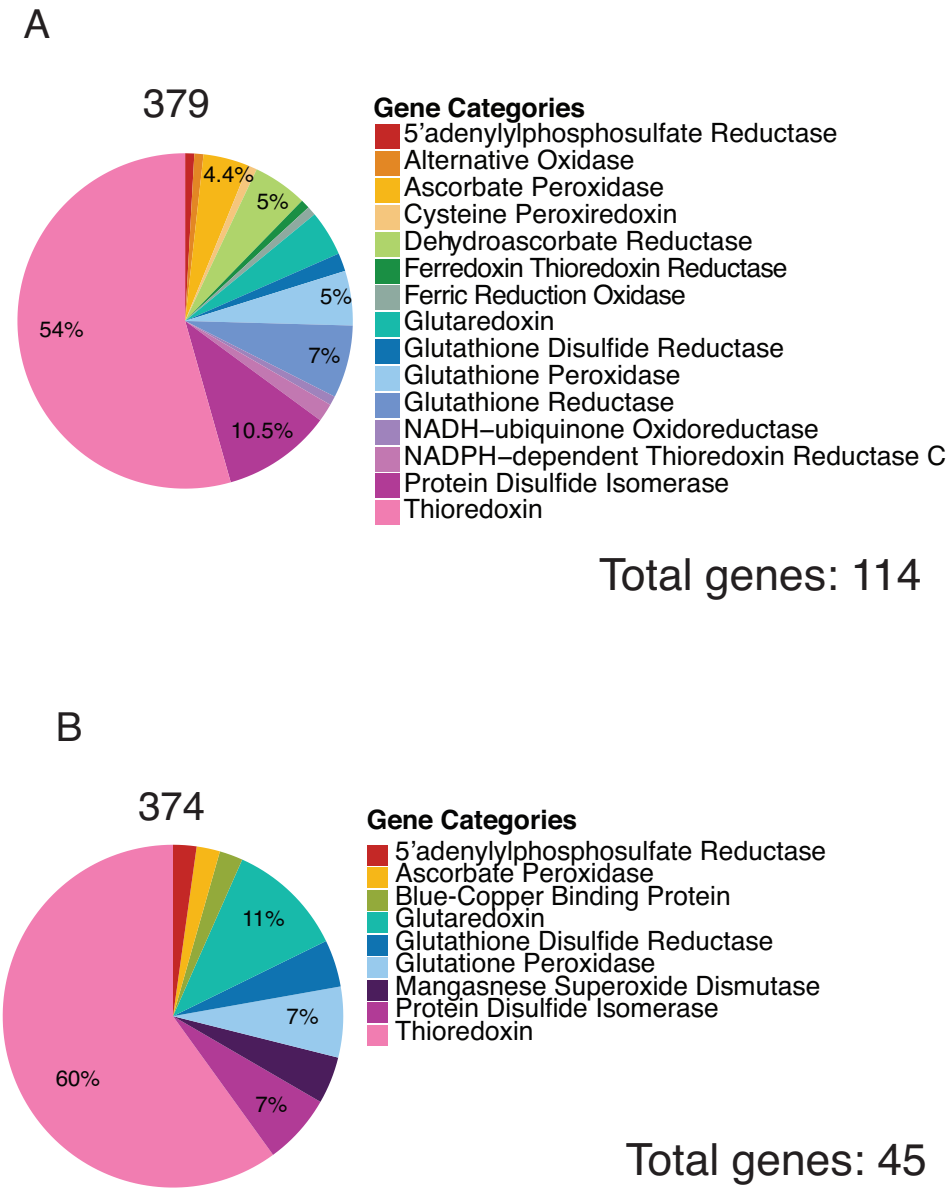

Figure 3.8 Comparative expression of putative antioxidant genes in exponentially growing CCMP374^{S} and CCMP379^{R} cells. Pie charts showing the diversity of putative antioxidant genes in a shared transcriptome (of 159 total genes) that are more strongly expressed in either (A) 379^{R} (114 genes) or (B) 374^{S} (45 genes).

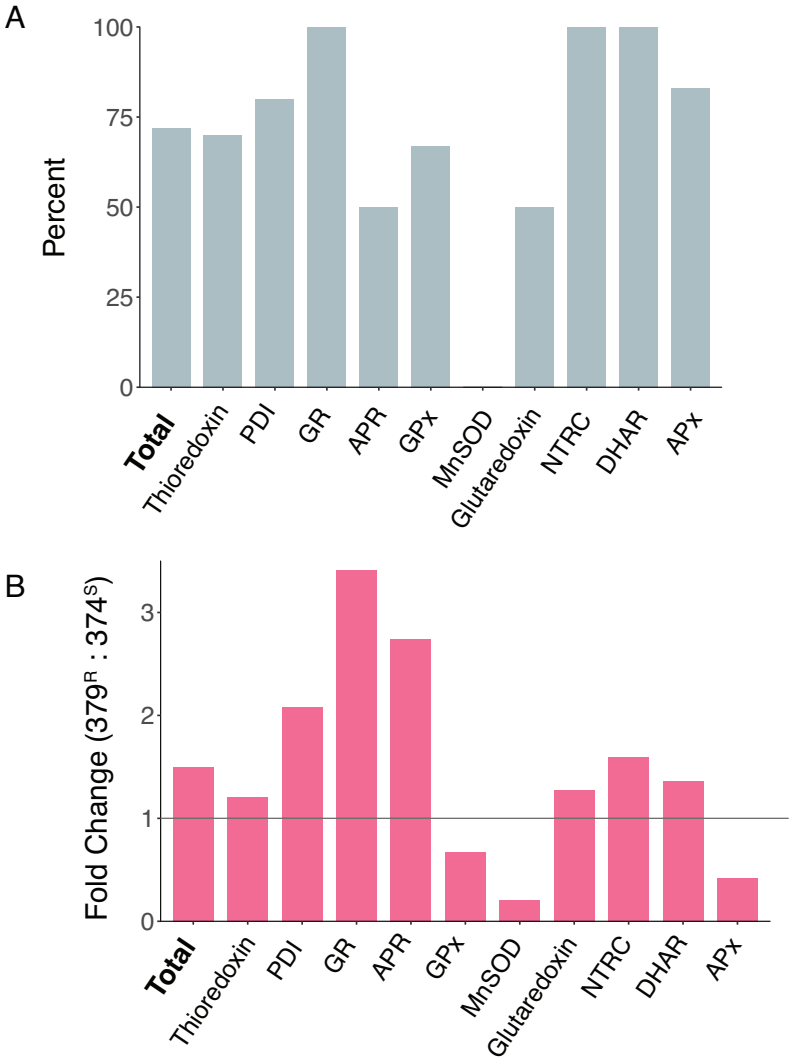

Figure 3.9 Differences in expression of putative antioxidant genes between 379^{R} and374^{S}. (A) Percent of total genes, along with percentage of genes within the top 10 gene categories represented in the shared transcriptome, that are more strongly expressed in 379^{R} then 374^{S} and (B) the fold change (379^{R} : 374^{S}) in RPKM of the same gene categories. Grey line is the 1:1 line above which genes are more strongly expressed in 379^{R}. (Abbreviations PDI, Protein Disulfide Isomerase; GR, Glutathione Reductase; APR, 5'Adenylylphosphosulfate Reductase; GPx, Glutathione Peroxidase; MnSOD, Manganese Superoxide Dismutase; NTRC, NADPH-dependent Thioredoxin Reductase C; DHAR, Dehydroascorbate Reductase; APx, Ascrobate Peroxidase).

3.10 SUPPLEMENTARY FIGURES & TABLES

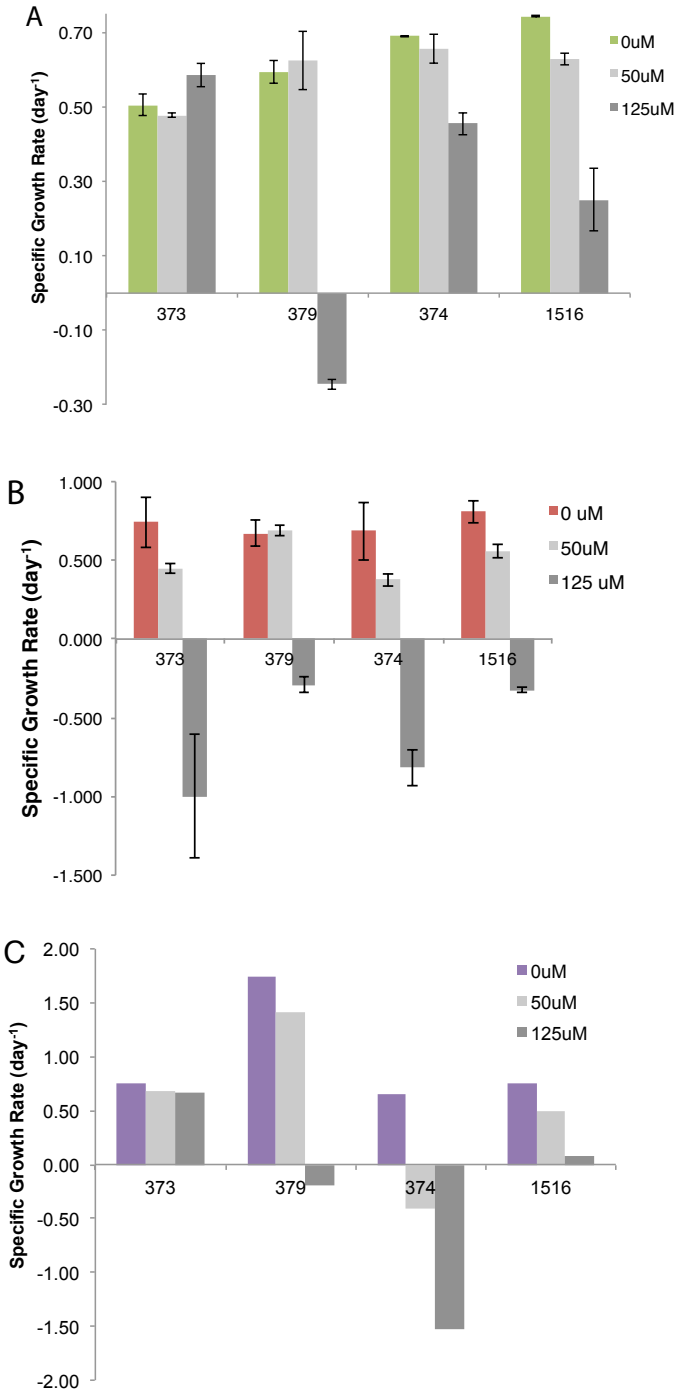

Fig S3.1 Inter-experimental variability in basal specific growth rates and growth rate changes in response to H_2O_2 treatments (50 μM and 125 μM). (A-C) represent mean specific growth rate for three independent experiments used to generate data in Fig. 3.6 (n=2; ±se).

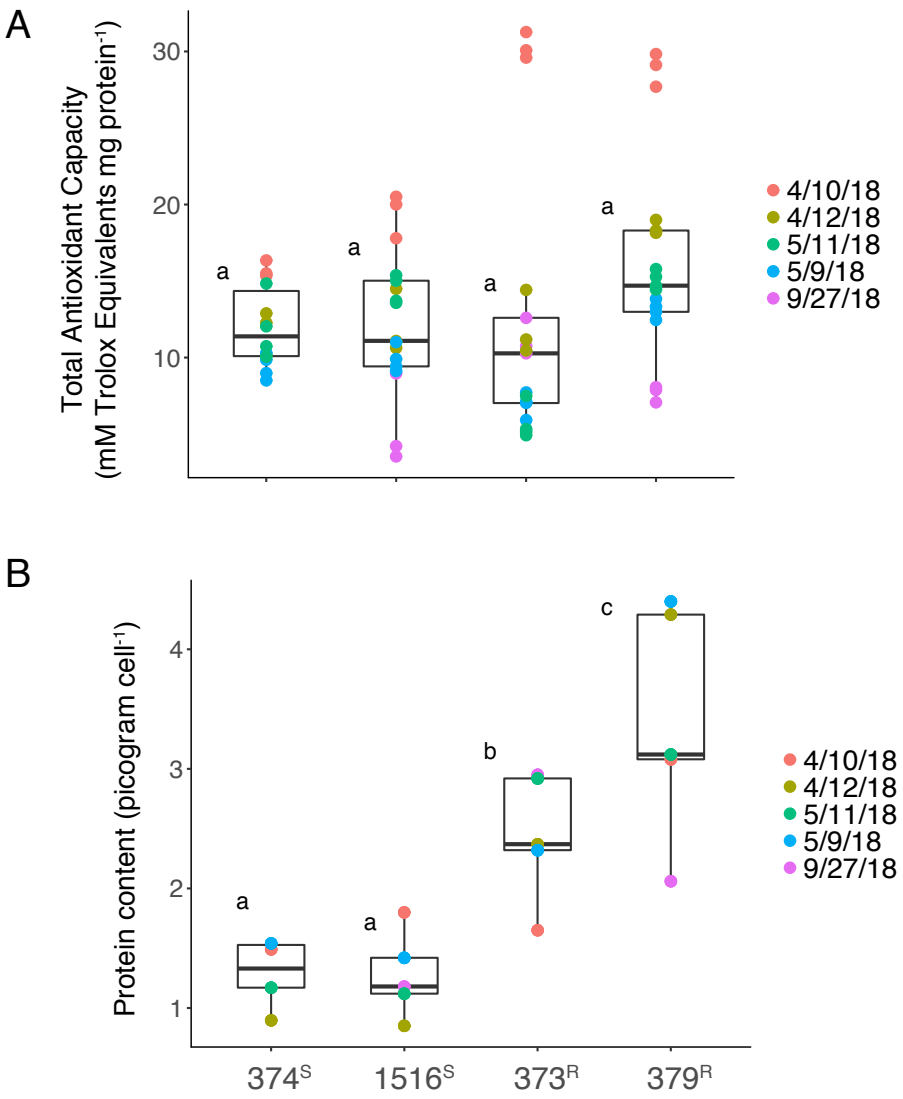

Fig S3.2 Total enzymatic and non-enzymatic antioxidant capacity (TAC) of *E. huxleyi* strains CCMP374^{S}, CCMP1516^{S}, CCMP373^{R}, and CCMP379^{R} normalized to total cellular protein content (A) and the total protein content (in pictograms cell^{-1}) of the strains for each TAC-assay experiment (B). Data are displayed as box-plots with the upper and lower bounds of the box representing the 25% and 75% quartiles around the median. Individual data points are overlayed to display intra- and inter-experimental variability. Statistically significant differences between means were determined using one-way ANOVA with the Tukey HSD post hoc test (letters denote statistically different subgroups; $p < 0.05$).

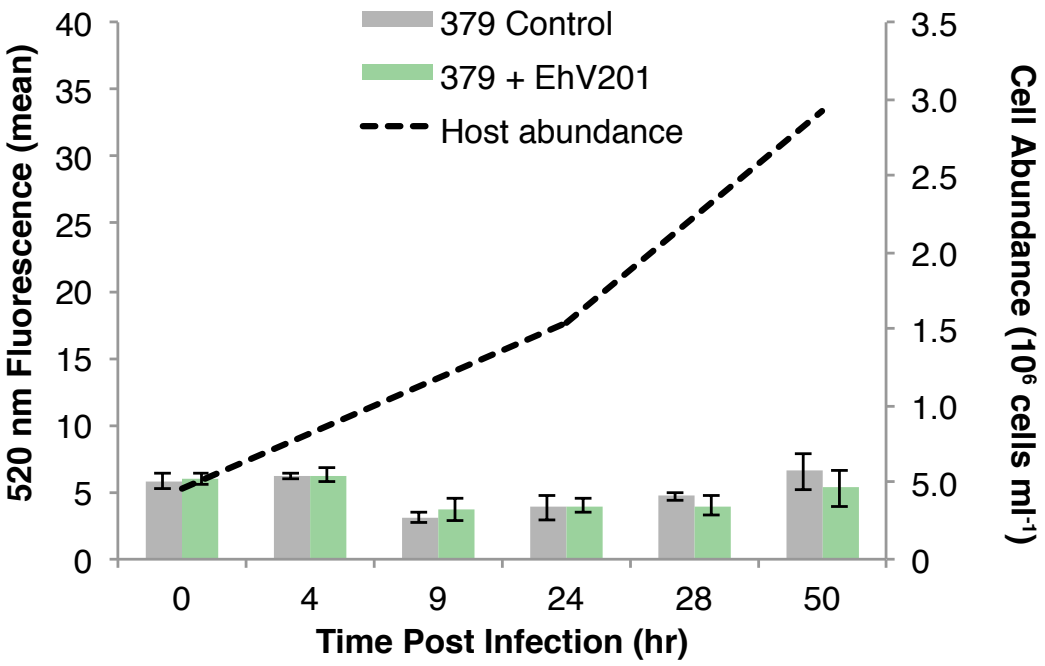

Figure S3.3 Intracellular NO production and cell abundance dynamics during infection of CCMP379^{R} with EhV201. Intracellular NO production is represented as the mean 520 nm fluorescence of DAF-FM DA stained uninfected (grey bars) and EhV201-infected (green bars) cultures (n=3, $\pm$ se) throughout the first 50 hr of infection. Cell abundances (10^6 cells ml^{-1}) are shown for one representative infected sample only for the same time frame.

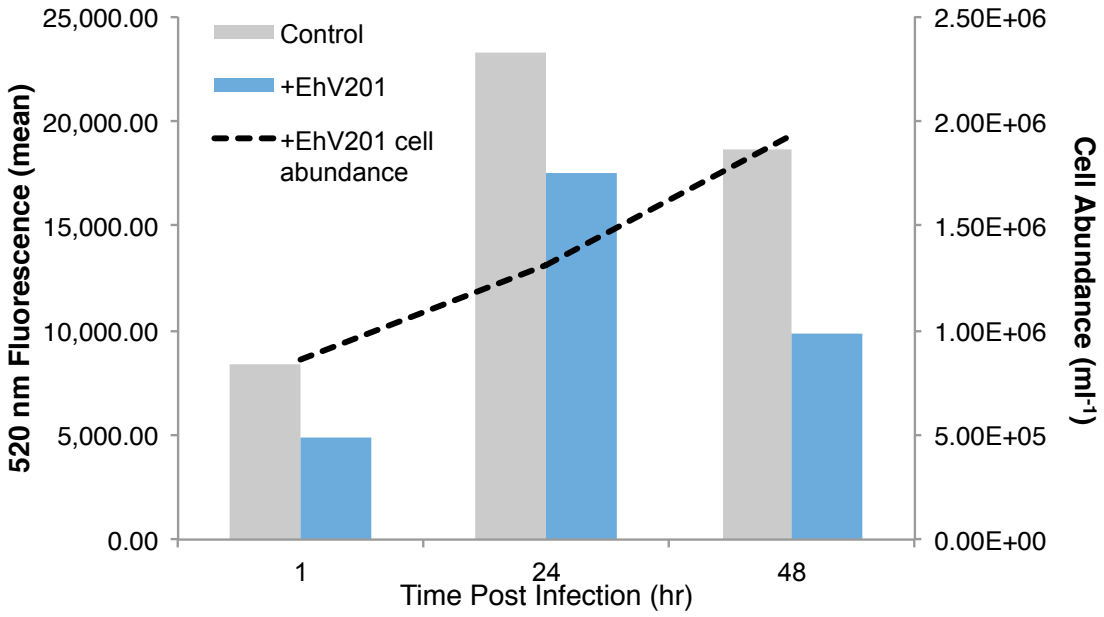

Figure S3.4 Intracellular NO production and cell abundance dynamics during infection of CCMP373^{R} with EhV201. Intracellular NO production is represented as the mean 520 nm fluorescence of DAF-FM DA stained uninfected (grey bars) and EhV201-infected (blue bars) cultures (n=1) throughout the first 48 hr of infection. Cell abundances (10^6 cells ml^{-1}; mean of n=2) are shown for the same timeframe.

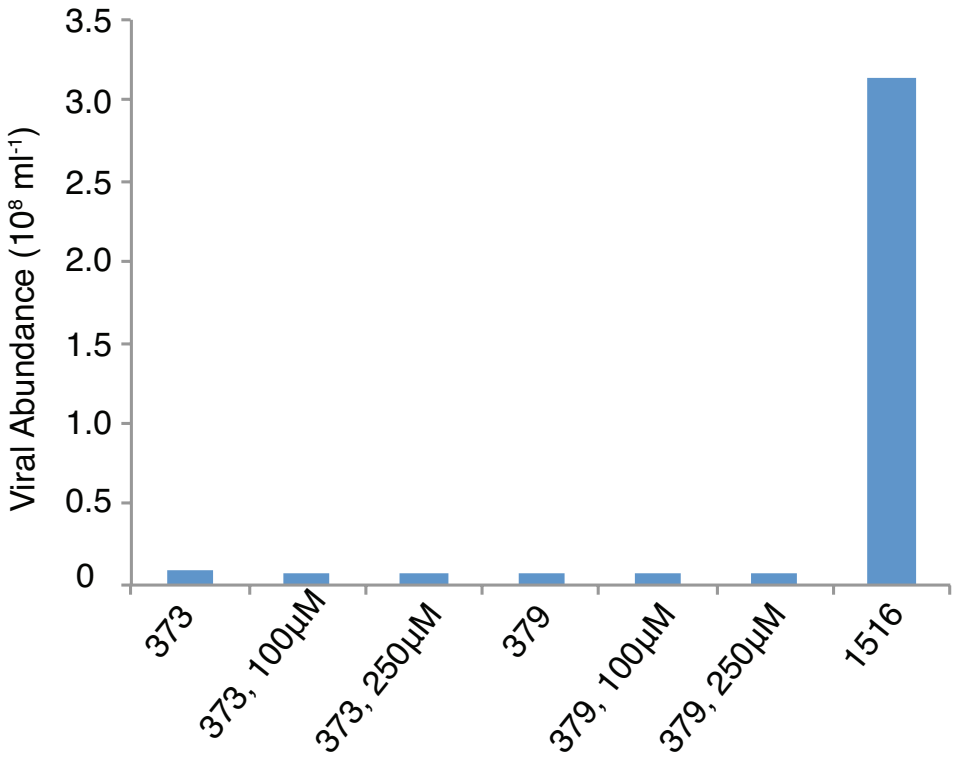

Figure S3.5 Viral abundance dynamics of CCMP373^{R} and CCMP379^{R} pre-treated with two concentrations of the NO donor SNAP prior to challenge with EhV201, with untreated and infected CCMP1516^{S} serving as a positive control. Viral abundance (10^{8} virions ml^{-1}) in cultures 48 hour post infection are a mean of n=2, except 1516^{S} (n=1).

Table S3.1 List of 159 putative antioxidant genes identified in a shared transcriptome of 374^S and 379^R by homology to known *Arabidopsis* genes. Table includes the ID of the transcript, reads per kilobase of transcript per million mapped reads (RPKM), fold change (FC) of 379^R expression over 374^S, and the *Arabidopsis* hit. RPKM values of 0.00001 are taken to represent no expression in the respective strain.

Feature ID	FC (379/374)	379 RPKM	374 RPKM	*Arabidopsis* hit
379-50677_1	6297186.749	62.97	0.00001	AT3G08710.1_thioredoxin_H-type_9
379-91994_1	2541177.236	25.41	0.00001	AT5G39950.1_thioredoxin_2
379-14986_1	1867111.779	18.67	0.00001	AT1G53300.1_tetratricopetide-repeat_thioredoxin-like_1
379-40319_1	217194.636	2.17	0.00001	AT1G03680.1_thioredoxin_M-type_1
379-12417_1	294.949	75.79	0.25696	AT2G42580.1_tetratricopetide-repeat_thioredoxin-like_3
379-95475_1	227.592	13.97	0.06137	AT1G19730.1_Thioredoxin_superfamily_protein
379-96713_1	48.717	21.79	0.44735	AT3G52960.1_Thioredoxin_superfamily_protein
379-96932_1	32.458	127.26	3.92084	AT4G03520.1_Thioredoxin_superfamily_protein
379-88094_1	28.951	37.86	1.30755	AT2G42580.1_tetratricopetide-repeat_thioredoxin-like_3
379-97167_1	28.556	54.25	1.89965	AT5G42980.1_thioredoxin_3
379-12498_1	26.125	34.01	1.30189	AT1G53300.1_tetratricopetide-repeat_thioredoxin-like_1
379-95883_1	25.493	23.45	0.91975	AT3G15360.1_thioredoxin_M-type_4
379-69059_1	20.528	37.27	1.81567	AT4G29670.2_atypical_CYS_HIS_rich_thioredoxin_2
379-95952_1	17.850	40.84	2.28814	AT1G53300.1_tetratricopetide-repeat_thioredoxin-like_1
379-51708_1	15.218	265.36	17.43659	AT3G26060.1_Thioredoxin_superfamily_protein
379-50406_1	12.323	34.67	2.81363	AT1G76760.1_thioredoxin_Y1
374-54014_1	11.156	7.07	0.63330	AT5G42980.1_thioredoxin_3
379-69532_1	10.657	29.50	2.76843	AT1G53300.1_tetratricopetide-repeat_thioredoxin-like_1
379-18032_1	7.619	21.77	2.85754	AT1G76760.1_thioredoxin_Y1

374-82276_1	6.871	46.44	6.75819	AT2G42580.1_tetratricopetide-repeat_thioredoxin-like_3
379-5739_1	5.578	1.75	0.31456	AT1G43560.1_thioredoxin_Y2
379-3504_1	5.474	63.94	11.68082	AT4G04950.1_thioredoxin_family_protein
379-32035_1	4.859	167.26	34.42115	AT1G53300.1_tetratricopetide-repeat_thioredoxin-like_1
379-43868_1	4.640	273.67	58.97773	AT4G29670.2_atypical_CYS_HIS_rich_thioredoxin_2
379-77366_1	4.184	5.53	1.32236	AT1G53300.1_tetratricopetide-repeat_thioredoxin-like_1
379-6336_1	3.941	66.12	16.77693	AT3G51030.1_thioredoxin_H-type_1
379-4337_1	3.793	4.29	1.13040	AT5G42980.1_thioredoxin_3
379-2034_1	3.660	27.07	7.39555	AT2G42580.1_tetratricopetide-repeat_thioredoxin-like_3
379-20774_1	3.347	3.09	0.92217	AT2G42580.1_tetratricopetide-repeat_thioredoxin-like_3
379-9061_1	3.207	10.52	3.27883	AT5G42980.1_thioredoxin_3
379-177_1	3.138	10.47	3.33738	AT5G42980.1_thioredoxin_3
379-6566_1	3.112	28.13	9.03899	AT2G42580.1_tetratricopetide-repeat_thioredoxin-like_3
379-32495_1	3.007	29.65	9.86225	AT1G43560.1_thioredoxin_Y2
379-10945_1	2.983	19.71	6.60637	AT3G52960.1_Thioredoxin_superfamily_protein
379-5718_1	2.892	21.05	7.27805	AT4G04950.1_thioredoxin_family_protein
379-10761_1	2.563	27.74	10.82352	AT1G50320.1_thioredoxin_X
379-95547_1	2.523	8.74	3.46302	AT1G19730.1_Thioredoxin_superfamily_protein
379-96604_1	2.489	5.21	2.09209	AT1G53300.1_tetratricopetide-repeat_thioredoxin-like_1
379-6906_1	2.380	9.27	3.89361	AT1G19730.1_Thioredoxin_superfamily_protein
379-7697_1	2.251	23.41	10.39803	AT2G42580.1_tetratricopetide-repeat_thioredoxin-like_3
379-4316_1	2.231	3.51	1.57494	AT1G76760.1_thioredoxin_Y1
374-12105_1	2.179	16.24	7.45089	AT1G53300.1_tetratricopetide-repeat_thioredoxin-like_1
379-17732_1	2.122	22.16	10.44074	AT3G51030.1_thioredoxin_H-type_1
379-41325_1	2.107	7.94	3.76951	AT1G53300.1_tetratricopetide-repeat_thioredoxin-like_1
379-73929_1	2.107	9.63	4.57076	AT1G50320.1_thioredoxin_X

374-81904_1	1.959	3.60	1.83962	AT3G15360.1_thioredoxin_M-type_4
379-18007_1	1.787	22.48	12.57935	AT4G29670.2_atypical_CYS_HIS_rich_thioredoxin_2
379-6204_1	1.693	7.65	4.51659	AT3G26060.1_Thioredoxin_superfamily_protein
379-95612_1	1.649	1.96	1.18963	AT1G53300.1_tetratricopetide-repeat_thioredoxin-like_1
379-74790_1	1.459	12.59	8.62788	AT2G42580.1_tetratricopetide-repeat_thioredoxin-like_3
379-32542_1	1.434	11.02	7.68401	AT4G29670.2_atypical_CYS_HIS_rich_thioredoxin_2
379-96135_1	1.402	25.56	18.23875	AT2G41680.1_NADPH-dependent_thioredoxin_reductase_C
379-41558_1	1.355	7.73	5.70459	AT4G37200.1_Thioredoxin_superfamily_protein
379-6060_1	1.349	8.30	6.15031	AT2G20270.1_Thioredoxin_superfamily_protein
379-60668_1	1.348	6.48	4.80582	AT1G19730.1_Thioredoxin_superfamily_protein
374-13748_1	1.333	66.02	49.52110	AT4G04950.1_thioredoxin_family_protein
374-81766_1	1.211	63.25	52.22890	AT2G42580.1_tetratricopetide-repeat_thioredoxin-like_3
379-7440_1	1.180	19.82	16.79622	AT1G19730.1_Thioredoxin_superfamily_protein
379-1601_1	1.116	22.83	20.46104	AT1G43560.1_thioredoxin_Y2
379-13044_1	1.083	13.61	12.56824	AT1G53300.1_tetratricopetide-repeat_thioredoxin-like_1
379-10958_1	1.064	21.19	19.90632	AT2G42580.1_tetratricopetide-repeat_thioredoxin-like_3
379-2156_1	1.041	16.65	15.98896	AT1G19730.1_Thioredoxin_superfamily_protein
374-68211_1	-1.126	55.39	62.39738	AT3G52960.1_Thioredoxin_superfamily_protein
379-663_1	-1.187	20.74	24.60998	AT3G15360.1_thioredoxin_M-type_4
379-19192_1	-1.245	18.04	22.46312	AT3G52960.1_Thioredoxin_superfamily_protein
379-96093_1	-1.400	11.26	15.76409	AT2G42580.1_tetratricopetide-repeat_thioredoxin-like_3
379-12723_1	-1.427	13.54	19.32932	AT4G29670.2_atypical_CYS_HIS_rich_thioredoxin_2
374-1414_1	-1.472	7.44	10.95077	AT1G43560.1_thioredoxin_Y2
374-5262_1	-1.536	37.27	57.23603	AT2G20270.1_Thioredoxin_superfamily_protein
374-65744_1	-1.690	12.22	20.65003	AT5G63030.1_Thioredoxin_superfamily_protein
374-83071_1	-1.728	103.54	178.88741	AT3G51030.1_thioredoxin_H-type_1

374-13790_1	-1.755	9.77	17.14844	AT1G76760.1_thioredoxin_Y1
374-83084_1	-2.140	1.58	3.38089	AT1G53300.1_tetratricopetide-repeat_thioredoxin-like_1
374-10687_1	-2.169	10.23	22.18633	AT2G42580.1_tetratricopetide-repeat_thioredoxin-like_3
374-3407_1	-2.406	66.55	160.10515	AT3G52960.1_Thioredoxin_superfamily_protein
379-14278_1	-2.540	48.27	122.58539	AT1G53300.1_tetratricopetide-repeat_thioredoxin-like_1
374-82072_1	-2.713	11.20	30.38541	AT3G06730.1_Thioredoxin_z
374-68793_1	-2.970	21.91	65.07887	AT1G60740.1_Thioredoxin_superfamily_protein
374-1091_1	-3.790	38.61	146.33476	AT3G51030.1_thioredoxin_H-type_1
374-6201_1	-4.780	1.78	8.49514	AT4G37200.1_Thioredoxin_superfamily_protein
374-13751_1	-5.117	9.77	50.01516	AT3G51030.1_thioredoxin_H-type_1
374-2445_1	-6.454	5.07	32.71388	AT1G19730.1_Thioredoxin_superfamily_protein
374-44782_1	-6.512	3.13	20.36586	AT2G42580.1_tetratricopetide-repeat_thioredoxin-like_3
374-82028_1	-7.171	0.04	0.28901	AT1G53300.1_tetratricopetide-repeat_thioredoxin-like_1
374-5142_1	-7.315	3.74	27.36341	AT2G42580.1_tetratricopetide-repeat_thioredoxin-like_3
379-97136_1	-7.625	7.46	56.88053	AT3G51030.1_thioredoxin_H-type_1
374-4127_1	-8.764	2.73	23.90494	AT1G53300.1_tetratricopetide-repeat_thioredoxin-like_1
374-5289_1	-15.890	1.00	15.81778	AT4G29670.2_atypical_CYS_HIS_rich_thioredoxin_2
374-3503_1	-75.703	6.43	486.51430	AT1G19730.1_Thioredoxin_superfamily_protein
379-7599_1	80.732	1124.81	13.93255	AT3G20560.1_PDI-like_5-3
374-7435_1	6.303	67.28	10.67283	AT3G20560.1_PDI-like_5-3
379-17394_1	4.365	39.16	8.97087	AT3G20560.1_PDI-like_5-3
379-6625_1	4.316	37.08	8.59106	AT3G20560.1_PDI-like_5-3
379-32565_1	4.003	19.08	4.76578	AT3G20560.1_PDI-like_5-3
379-10845_1	3.928	20.71	5.27285	AT3G20560.1_PDI-like_5-3
379-6548_1	3.858	31.68	8.21127	AT3G20560.1_PDI-like_5-3
379-11334_1	2.905	20.80	7.15761	AT3G20560.1_PDI-like_5-3

379-2668_1	2.610	72.66	27.84413	AT3G20560.1_PDI-like_5-3
379-1699_1	2.355	14.78	6.27626	AT3G20560.1_PDI-like_5-3
379-1740_1	2.223	25.65	11.53732	AT3G20560.1_PDI-like_5-3
379-8713_1	1.544	17.79	11.52297	AT3G20560.1_PDI-like_5-3
374-12270_1	-1.135	14.98	17.00967	AT3G20560.1_PDI-like_5-3
374-11795_1	-1.483	10.33	15.31486	AT3G20560.1_PDI-like_5-3
374-2077_1	-2.683	266.52	715.06664	AT3G20560.1_PDI-like_5-3
379-51868_1	3.664	30.06	8.20358	AT2G41680.1_NADPH-dependent_thioredoxin_reductase_C
374-4744_1	1.437	154.37	107.41048	AT2G41680.1_NADPH-dependent_thioredoxin_reductase_C
374-82631_1	2.185	22.65	10.36696	AT5G67590.1_NADH-ubiquinone_oxidoreductase-like_protein
374-5061_1	-2.355	66.97	157.69112	AT3G10920.1_manganese_superoxide_dismutase_1
374-10013_1	-22.284	9.44	210.46915	AT3G10920.1_manganese_superoxide_dismutase_1
379-19294_1	14.503	7.16	0.49356	AT3G54660.1_glutathione_reductase
379-14695_1	5.001	584.68	116.92186	AT3G54660.1_glutathione_reductase
374-5050_1	3.235	161.46	49.91709	AT3G54660.1_glutathione_reductase
379-1079_1	3.072	328.69	106.99946	AT3G54660.1_glutathione_reductase
379-3430_1	3.028	18.61	6.14425	AT3G54660.1_glutathione_reductase
379-68562_1	1.895	172.29	90.92719	AT3G54660.1_glutathione_reductase
379-97138_1	1.623	4.66	2.87126	AT3G54660.1_glutathione_reductase
379-82185_1	2.603	8.83	3.39121	AT3G54660.1_glutathione_reductase
379-211_1	16.735	12.03	0.71882	AT4G31870.1_glutathione_peroxidase_7
379-80656_1	3.347	7.87	2.35041	AT3G63080.1_glutathione_peroxidase_5
379-1918_1	2.543	18.95	7.45289	AT4G11600.1_glutathione_peroxidase_6
374-11891_1	-1.752	9.83	17.22087	AT4G11600.1_glutathione_peroxidase_6
374-30475_1	-2.157	30.63	66.07511	AT4G11600.1_glutathione_peroxidase_6
374-7911_1	-2.232	114.80	256.28283	AT1G63460.1_glutathione_peroxidase_8

379-96032_1	647658.702	6.48	0.00001	AT2G43350.1_glutathione_peroxidase_3
379-92614_1	3.730	20.92	5.60680	AT4G11600.1_glutathione_peroxidase_6
379-12416_1	2.770	22.55	8.14071	AT2G25080.1_glutathione_peroxidase_1
379-11234_1	7.265	19.84	2.73145	AT3G24170.1_glutathione-disulfide_reductase
379-12315_1	1.631	15.88	9.73864	AT3G24170.1_glutathione-disulfide_reductase
374-6364_1	-1.110	2.19	2.42961	AT3G24170.1_glutathione-disulfide_reductase
374-8542_1	-4.792	11.59	55.54162	AT3G24170.1_glutathione-disulfide_reductase
379-52086_1	9.328	65.38	7.00849	AT1G77370.1_Glutaredoxin_family_protein
379-6929_1	7.501	34.33	4.57599	AT5G40370.1_Glutaredoxin_family_protein
374-46962_1	3.264	38.37	11.75338	AT5G20500.1_Glutaredoxin_family_protein
379-11477_1	2.792	35.26	12.62952	AT4G28730.1_Glutaredoxin_family_protein
374-11092_1	1.252	29.97	23.94569	AT5G40370.1_Glutaredoxin_family_protein
374-48505_1	-1.345	1.48	1.98354	AT5G40370.1_Glutaredoxin_family_protein
379-15051_1	-3.457	2.58	8.92591	AT3G11920.1_glutaredoxin-like_protein
374-8803_1	-3.758	2.96	11.13595	AT3G11920.1_glutaredoxin-like_protein
374-17486_1	-5.109	4.03	20.59197	AT1G77370.1_Glutaredoxin_family_protein
374-60258_1	-9.113	1.21	11.01851	AT3G11920.1_glutaredoxin-like_protein
379-494_1	16.783	14.67	0.87416	AT5G49730.1_ferric_reduction_oxidase_6
379-2010_1	2.213	23.50	10.61893	AT2G04700.1_ferredoxin_thioredoxin_reductase_catalytic_beta_chain_family_protein
379-22847_1	2.715	11.15	4.10654	AT1G75270.1_dehydroascorbate_reductase_2
374-9688_1	2.423	16.71	6.89703	AT5G16710.1_dehydroascorbate_reductase_1
374-7981_1	1.196	27.95	23.36165	AT1G75270.1_dehydroascorbate_reductase_2
374-83335_1	1.136	8.84	7.78722	AT1G75270.1_dehydroascorbate_reductase_2
379-2899_1	1.066	15.06	14.13003	AT1G19570.1_dehydroascorbate_reductase
374-10251_1	1.032	9.77	9.47094	AT1G19570.1_dehydroascorbate_reductase
379-92101_1	2.763	25.93	9.38638	AT1G48130.1_1-cysteine_peroxiredoxin_1

374-49518_1	-79641.978	0.00	0.79642	AT5G20230.1_blue-copper-binding_protein
379-84532_1	2.028	3.04	1.49987	AT4G35000.1_ascorbate_peroxidase_3
379-7121_1	1.900	5.15	2.71249	AT4G35000.1_ascorbate_peroxidase_3
374-12877_1	1.810	8.81	4.86701	AT1G07890.1_ascorbate_peroxidase_1
374-10763_1	1.626	6.78	4.17172	AT1G07890.1_ascorbate_peroxidase_1
379-57071_1	1.093	13.59	12.43775	AT4G35970.1_ascorbate_peroxidase_5
374-5707_1	-14.469	5.21	75.42475	AT3G09640.1_ascorbate_peroxidase_2
379-9111_1	2.805	15.89	5.66506	AT4G22260.1_Alternative_oxidase_family_protein
379-14053_1	3.379	735.65	217.69974	AT1G62180.1_5'adenylylphosphosulfate_reductase_2
379-96165_1	-1.897	32.86	62.34005	AT1G62180.1_5'adenylylphosphosulfate_reductase_2

CHAPTER 4: Production Mechanisms and Post-translational Protein Modifications of Nitric Oxide in the Coccolithophore *Emiliania huxleyi* [*]

[*] Part of this chapter (sections 4.3.3, 4.4.1, and relevant discussion) have been published as: Hirsh, D.J., **Schieler, B.M.**, Fomchenko, K.M., Jordan, E.T., and K.D. Bidle (2016) A liposome-encapsulated spin trap for the detection of nitric oxide. *Free Radical Biology and Medicine* 96: 199-210. In some cases, these data have been re-analyzed here.

4.1 ABSTRACT

It has been demonstrated that the free radical nitric oxide (NO) plays important physiological roles in the coccolithophore *Emiliania huxleyi*, specifically during lytic viral infection, a process known to routinely terminate blooms in the North Atlantic. Here we aim to elucidate the relevant biosynthetic pathways of NO production in *E. huxleyi* and the possible protein targets of NO-mediated posttranslational modification (PTM), two important aspects needed to contextualize the roles of NO signaling in this species. Using a novel liposome-encapsulated spin trap enabled EPR method, we demonstrate that NR mediated, nitrite-dependent NO production, rather than nitric oxide synthase (NOS) activity, is present in cell lysates. In order for NR-mediated NO production to be physiologically important, intracellular nitrite concentrations must be high enough to remove substrate competitive exclusion by nitrate. We present preliminary data suggesting that intracellular nitrite concentrations may increase during viral infection, an observation that is consistent with previous demonstration of reduced photosynthetic activity. Lastly, we present the first evidence of protein tyrosine nitration in an algal species and demonstrate that it is associated with growth in replete conditions rather then the biotic stress of viral infection. *In silico* predictions of protein targets of tyrosine nitration and cysteine s-nitrosylation suggest that metacaspases and antioxidant proteins may be crucial targets of NO modulation. Therefore, it is important to specifically explore the roles of NO-mediated PTMs in altering their activity to better understand how NO functions during the life, and death, of *E. huxleyi.*

4.2 INTRODUCTION

Nitric oxide ($NO^{\cdot}$) is a gaseous free radical that has an impressive list of diverse biological functions in all domains of life (Moncada 1999, Besson-Bard et al. 2008, Gusarov et al. 2009, Martens-Habbena et al. 2015). Despite decades of research, there remains a number of outstanding questions regarding how it functions *in vivo*, even in mammalian systems where its biological relevance was first discovered. Even less is known about the ecophysiology of NO in marine phytoplankton (Kumar et al. 2015), the photosynthetic prokaryotic and eukaryotic microbes that are critical in shaping marine environments. There is a particular interest in understanding the role of NO in the life and death of phytoplankton due to the ability of NO to readily diffuse across cell membranes and potentially act as an "infochemical" in mixed microbial populations (Vardi et al. 2006, Bidle 2015), as well as to impact atmospheric and seawater chemistry (Ludwig et al. 2001, Olasehinde et al. 2010).

In order to be a considered a canonical "signaling molecule," nitric oxide must have (1) tightly controlled cellular production, (2) reversibility, and (3) specific targets within the cell that (4) elicit a defined response. All four features have been demonstrated in various systems to different extents. This chapter aims to address aspects (1) and (3) in the cosmopolitan coccolithophore *Emiliania huxleyi. E. huxleyi* is an abundant species known for forming large blooms in the North Atlantic (Holligan et al. 1993, Brown & Yoder 1994, Tyrrell & Merico 2004) that are routinely terminated by infection by viruses (Bratbak et al. 1993, Brussaard et al. 1996, Lehahn et al. 2014, Laber et al. 2018). NO production is poorly understood in this ecologically and environmentally important species, although we have previously demonstrated a role for intracellular NO during

early lytic viral infection in both the laboratory and field (Hirsh et al. 2016, Schieler et al. 2019). It is still unknown, however, by what mechanism(s) NO is produced and what the downstream targets of its production are.

The nitric oxide radical is known to be produced through a number of oxidative and reductive pathways, both enzymatically and non-enzymatically mediated (Frohlich & Durner 2011). The main enzymes responsible for NO production in animals are nitric oxide synthases (NOSs). NOSs (endothelial-, neuronal-, and inducible-) catalyze the five electron, NADPH- and oxygen-dependent oxidation of L-arginine to NO and L-citrulline (Knowles et al. 1989, Knowles & Moncada 1994). The active NOS enzyme is a homodimer with each monomer, linked by a zinc-thiolate cluster, comprising of an oxygenase domain (NOSoxy) and a reductase domain (NOSred), separated by calmodulin binding site and tightly binding the cofactors tetrahydrobiopterin, FAD, and FMN. Both eNOS and nNOS require the calcium-dependent binding of calmodulin to function, while iNOS has a permanently bound calmodulin and thus is calcium-independent (Alderton et al. 2001).

It remains unclear whether NOSs are relevant outside of mammalian systems, however. NOSs have been described in several prokaryote systems, although these bacterial NOSs (bNOSs) lack a site for calmodulin binding and only contain the NOSoxy domain. It is thought that other cellular reductases are utilized for NOS activity in these systems (Crane et al. 2010). In photosynthetic plants and protists, however, no true NOS gene has been identified, with the exception of *Ostreococcus tauri* (Foresi et al. 2010, Frohlich & Durner 2011, Correa-Aragunde et al. 2013). This is despite numerous reports of NOS-like activity in various plant (Corpas et al. 2009b) and algal (Kim et al. 2006,

Vardi et al. 2006, Vardi et al. 2008) species. In addition to NOS, another major route of NO production that is particularly relevant to photosynthetic organisms is the reduction of nitrite to NO via nitrate reductase (NR). Nitrite-dependent NO synthesis via NR activity has been extensively documented in various algal species such as the chlorophyte *Scenedesmus obliquus*, the freshwater model green alga *Chlamydomonas reinhardtii*, and Antarctic *Chlorella* (Mallick et al. 1999, Sakihama et al. 2002, Estevez & Puntarulo 2005). In total, at least seven putative pathways (both enzymatic and non-enzymatic) for NO production in photosynthetic organisms have been described (Mur et al. 2012). These include xanthine oxidoreductase and cytochrome c oxidase under anaerobic conditions, nitrite reductases, the non-enzymatic reduction of nitrite under acidic conditions, and oxidation of hydroxylamines (reviewed in Mur et al. 2012). Recently, another NO producing pathway was discovered in *Chalmydomonas reinhardtii* that does not require cellular nitrate to be relatively low- the reduction of nitrite via the amidoxime reducing complex (Chamizo-Ampudia et al. 2016). The NOS- and NR-mediated pathways, however, continue to receive most attention in the literature. No studies to date have examined which route(s) of NO production are relevant in *E. huxleyi.*

As enigmatic as its routes of production are the potential targets and molecular pathways of NO signaling in phytoplankton. Many studies implicate potential pathways in which NO may play a role by correlating its production to physiology or by monitoring cellular responses to the manipulation of intracellular NO levels with pharmacological NO donors and scavengers. Through these types of studies NO in phytoplankton has been shown to be involved in viral infection (Schieler et al. 2019), response to toxic aldehydes (Vardi et al. 2006, Vardi et al. 2008, Gallina et al. 2014), symbiosis (Perez & Weis 2006),

antioxidant activity (Mallick et al. 2002, Singh et al. 2004), biofilm formation and zoospore settlement (Thompson et al. 2008, Thompson et al. 2009), and possibly cell-to-cell communication (Vardi et al. 2006). Few studies, however, have attempted to determine the actual molecular targets of NO *in vivo* to directly link its production to pathways in phytoplankton, despite the existence of molecular and computational tools available to do so.

NO can react with a number of macromolecules *in vivo* including proteins, nucleic acids, lipids, metal complexes, and vitamins (Corpas et al. 2013). The biomolecules that have garnered most attention with respect to manipulation by NO, however, have been proteins, specifically the NO-mediated nitration of tyrosine residues and the s-nitrosylation of both cysteine residues and metal cofactors. These types of additions are called posttranslational modifications (PTMs) and have an important role in regulating protein function through changes that alter protein conformation, subcellular localization, stability, or chemistry. Tyrosine nitration involves the addition of a nitro (-NO_2) group to one of two ortho-carbons to form 3-nitrotyrosine, which changes the pKa such that at physiological pH the residue becomes negatively charged (Turko & Murad 2002). The current paradigm is that, although low levels do occur during physiological conditions, extensive tyrosine nitration is a marker of nitrosative and oxidative stress (Corpas et al. 2013). Indeed, the main pathway of nitration is through formation of the strong oxidant peroxynitrite (ONOO-) by the quick and irreversible reaction of NO with superoxide.

S-nitrosylation is the addition of a nitroso (-NO) group to a sulfhydryl (-SH) forming an s-nitrosothiol (-SNO) via several different pathways. For example, in the

presence of strong oxidants, thiols can form a thiyl radical and react directly with NO to form s-nitrosothiols. Additionally, when concentrations of NO are high enough in an oxic environment, NO and O_2 can react to form NO_2 and subsequent reactions with NO can lead to formation of dinitrogen trioxide (N_2O_3). Dinitrogen trioxide can then react with thiolates to form s-nitrosothiols, including nitrosocysteine. Lastly, it is known that protein cysteines can become s-nitrsolyated via a trans-nitrosylation reaction in which an NO group from one nitrosothiol, like s-nitrosoglutathione (GSNO), is transferred to cysteine residues (Zaffagnini et al. 2016).

Antioxidant proteins, proteins that are responsible for the detoxification of reactive oxygen species (ROS) inside the cell, and metacaspases, proteins that are linked to the PCD-catalyzing caspase activity, have emerged as two important classes of proteins that are critically regulated by NO-mediated posttranslational modification. For example, the *Arabidsopsis* metcaspase-9 zymogen is kept inactivated by s-nitrosylation at its active site (Belenghi et al. 2007). In addition, a wide variety of antioxidant proteins have been experimentally demonstrated to be modulated by NO in higher plants, including ascorbate peroxidase (APX), glutathione reductase (GR), and dehydroascorbate reductase (DHAR) (Begara-Morales et al. 2016).

Interestingly, how NO PTMs alter protein activity seems to vary from species to species and between the two types of NO-mediated PTMs. For example, s-nitrosylation of APX enhances its activity in *Arabidopsis thaliana* (Yang et al. 2015), but decreases its activity in tobacco plant (de Pinto et al. 2013). Additionally, pea plant APX experiences dual regulation by NO; S-nitrosylation of APX during salt stress increases its activity while peroxynitrite-mediated tyrosine nitration decreases activity (Begara-Morales et al.

2014). These examples clearly illustrate that investigations of how NO modulates protein activity and antioxidant pathways cannot be extrapolated from other model organisms. Because both antioxidants (Sheyn et al. 2016) and metacaspases (Bidle et al. 2007) have been shown to be critical to viral infection in *E. huxleyi*, along with NO production (Schieler et al. 2019), we specifically focus on their potential regulation by NO-mediated PTMs here.

In this study, we aim to shed light on the mechanisms of production as well as potential proteins posttranslationally modified by NO in *Emiliania huxleyi*. Using a novel electron paramagnetic resonance (EPR) spectroscopy method, we show that NO production in *E. huxleyi* mainly occurs through a nitrite-dependent pathway and that NOS activity, at least in the conditions tested here, is not detectable in this species. In order to examine the potential proteins involved in NO signaling we utilize both an *in silico* approach, leveraging published predictive models, and biochemical approaches to begin to characterize NO-mediated posttranslational protein modifications in the *E. huxleyi* proteome.

4.3 MATERIALS & METHODS

4.3.1 Culture conditions, viral infection, and biomass harvesting

Emiliania huxleyi strain CCMP1516 was obtained from the Provasoli-Guillard National Center for Marine Algae and Microbiota and grown in batch culture in f/2 (minus Si) media at 18 °C on a 14:10 light:dark cycle at a light intensity of 250 µmol $m^{-2}s^{-1}$. Virus strain EhV201 (obtained courtesy of W. Wilson, Marine Biological Association, Plymouth, UK) was propagated in batch cultures of *E.*

huxleyi CCMP1516. Viral lysates were passed through a 0.45 μm pore-size PVDF syringe filter to remove cell debris. For infection experiments, *E. huxleyi* was inoculated with EhV during mid-exponential growth (~5.0×10^5 cells ml^{-1}) at a virus-to-host ratio of 5:1. Uninfected *E. huxleyi* cultures served as controls.

Biomass for analyses discussed here was obtained by filtering exponential phase (~$5.0x10^5 – 1.0x10^6$ cells ml^{-1}) or virus-infected cultures through 1.2 μm polycarbonate Isopore filters (RTTP; EMD Millipore Burlington, MA) under low vacuum (<20 kPa). Filters were either immediately flash frozen in liquid nitrogen or resuspended in 0.22 μm filtered seawater and pelleted by centrifugation (16,000 x g, 5 min, RT). Filters and cell pelletes were stored at -80^{o}C until further analysis.

4.3.2 Protein quantification

Protein in cell lysates used for the analyses described below was quantified using the DC protein assay kit, following the manufacturer's instructions (Bio-Rad, Hercules, CA), using standards of bovine serum albumin (Thermo Fisher, Waltham, MA) diluted in either NO Assay Buffer (described below) or LDS buffer (140 mM Tris base, 10 5mM Tris HCl, 0.5 mM EDTA, 2% lithium dodecyl sulfate, 10% glycerol). Absorbance at 750nm was read using a SpectraMax M3 microplate reader (Molecular Devices, San Jose, CA).

4.3.3 Nitrite- vs. arginine-dependent NO production assay

The capacity for nitrite- vs. arginine-dependent NO production in *Emiliania huxleyi* cells lysates was determined using electron paramagnetic resonance (EPR)

spectroscopy with a liposome-encapsulated spin trap (Schieler et al., 2019; Hirsh et al., 2016; Chapter 3). *E. huxleyi* cell pellets were thawed and resuspended in NO assay buffer (20 mM HEPES, 140 mM NaCl, pH 7.4) and lysed with light sonication (3 rounds of 30 s sonication on ice, power setting 1) using a Microson ultrasonic cell disrupter (Misonix, Farmingdale, NY). Lysates were pelleted (20,000 x g, 30 min, 4^{o}C) and the supernatant and pelleted fractions were retained to interrogate the soluble and membrane bound proteins, respectively.

The *E. huxleyi* lysate fractions were incubated with either nitrate reductase (NR) substrates (1 mM $NaNO_2$, 1 mM NADH, 10 units ml^{-1} SOD and catalase) or inducible nitric oxide synthase (iNOS) substrates (1 mM L-arginine, 1 mM NADPH, 1.8 μM BH_4, 1.8 μM DTT, 1mM $MgCl_2$, 100 μM calmodulin, 1mM $CaCl_2$, 10 units ml^{-1} SOD and catalase) and 25 μL LEST (see supplementary information) for 3 h in the dark at RT. Both aliquots of proteins that were boiled and NO Assay buffer with substrates only were assayed to control for background, abiotic NO production. After incubation, LEST was harvested by centrifugation (20,000 x g, 30 min, 4^{o}C), resuspended to 50 μL with NO Assay buffer, and drawn up into glass microcapillary tubes that were sealed at the distal end with critoseal.

EPR spectra were collected and the signal from spin-trapped NO quantified as described previously (Hirsh et al. 2016). In brief, continuous-wave EPR spectra were collected at X-band, 9.8 GHz, with a Bruker EMXPlus EPR spectrometer with the standard high sensitivity X-band resonator. $MGD_2Fe(II)$-NO was quantified by comparing spectra peak areas or peak-to-trough heights to a standard generated from the stable nitroxide radical TEMPOL (Sigma-Aldrich) of a known concentration.

4.3.4 Nitrite quantification

Nitrite was quantified in cell lysates of *E. huxleyi* CCMP1516 undergoing viral infection and uninfected controls, along with exponential phase cultures that were treated with the NO donor s-nitroso-n-acetylpenicillamine (SNAP; Thermo Fisher), using the Griess reagent kit, according to the manufacturer's instructions (Thermo Fisher). Lysates were generated in PBS buffer (5 mM potassium phosphate, 0.9% NaCl, pH 7.4) using a Microson ultrasonic cell disrupter (3 X 30 sec on ice, power setting 1; Misonix). Absorbance at 548 nm of the lysates was measured using a SpectraMax M3 microplate reader (Molecular Devices). Then, Griess reagent (a 1:1 mixture of 0.1% N-(1-naphthyl)ethylenediamine dihydrochloride and 1% sulfanilic acid) was added to the wells and absorbance at 548 nm was recorded again after 30 min incubation at RT. ΔAbsorbance of the samples was taken as the difference between absorbance of sample with Griess reagent and sample without. ΔAbsorbance of the samples was compared to ΔAbsorbance of fresh standards of sodium nitrite (0-100 μM) diluted in DI water to quantify total nitrite in the sample.

4.3.5 *In silico* nitrated and s-nitrosylated protein predictions

The *E. huxleyi* proteome (proteome ID UP000013827) was obtained from UniProt (The UniProt Consortium; http://uniprot.org). The proteome was run through the GPS-SNO algorithm (v. 1.0) using a threshold of 'medium' with batch prediction to identify proteins that are likely to be s-nitrosylated *in vivo* (Xue et al. 2010). Similiarly, the *E. huxleyi* proteome was also run through the GPS-YNO2 algorithm (threshold of

'medium') to identify potential sites of tyrosine nitration (Liu et al. 2011). Both algorithms are freely available online and can be found at http://sno.biocuckoo.org. A survey of four different programs for s-nitrosylation prediction found that the GPS-SNO software to be the best available in terms of accuracy, sensitivity, and specificity for s-nitrosylation in *Arabidopsis thaliana*. After the predictions for the entire proteome were generated, we specifically focused on both putative metacaspases as well as the putative antioxidant proteins expressed in the shared CCMP374 and CCMP379 transcriptome described in Chapter 3.

4.3.6 Western blot detection of nitrated proteins

E. huxleyi CCMP1516 biomass collected from cultures undergoing normal growth and viral infection was lysed in LDS buffer (described above) using a Microson ultrasonic cell disrupter (3 X 30 sec on ice, power setting 1; Misonix). Lysates were centrifuged (4^{o}C, 5 min, 20,000g) and the supernatant retained. Protein was quantified as described above. A total of 8 µg of protein of each sample in LDS with 100 µM DTT and 0.2% bromophenol blue was run on a Criterion TGX 4-20% gel (Bio-Rad). Rat brain extract (Santa Cruz Biotechnology, Dallas, TX) was run as a positive control for 3-nitrotyrosine. Precision Plus Dual Color Standards (Bio-Rad) was used as molecular weight ladder. Separated proteins were then transferred to a PVDF membrane. Proteins were blotted with the nitrotyrosine antiobody (Santa Cruz Biotechnology) at 1:2,000 dilution and then goat anti-rabbit HRP secondary at a dilution of 1:10,000. Protein bands were detected using ECL Select detection reagents (Sigma-Aldrich).

4.3.7 S-nitrosylated proteins

S-nitrosylated proteins were identified using the Pierce s-nitrosylation western blotting kit (Thermo Fisher), which is a modified "biotin switch" protocol using an iodo-TMT tag, according to the manufacturer's instructions. In brief, *E. huxleyi* CCMP1516 lysates were generated by lysing cells in HENS buffer and protein quantitated as described above. Protein extracts were then adjusted to 1.5 mg ml^{-1} with HENS buffer. Free cysteines in the sample were blocked using methyl methanethiosulfonate (20 mM) and s-nitrosocysteines were simultaneously reduced with sodium ascorbate (40 mM) and tagged with iodo-TMT (400 μM). For each sample, an aliquot that was not reduced with sodium ascorbate was generated to control for non-specific binding of the TMT label. Washes and reagent removal between each step were done by precipitation with pre-chilled 100% acetone. After tagging, samples were left at -20^{o}C in acetone.

Tagged proteins were enriched using an anti-TMT resin (Thermo Fisher) loaded into Pierce screw cap sin columns (Thermo Fisher). The resin was equilibrated with 1X TBS buffer (pH = 7.6) and samples were incubated with the resin for 2 hours at 4^{o}C while mixing. Bound proteins were eluted using TMT elution buffer (Thermo Fisher) and flash frozen in liquid N. Protein samples were identified by LC-MS/MS at the Rutgers Biological Mass Spectrometry Facility (Center for Advanced Biotechnology and Medicine, http://cabm-ms.cabm.rutgers.edu/index.html).

4.4 RESULTS

4.4.1 Nitrite- vs. arginine-dependent NO production in *E. huxleyi*

We detected enzymatic NO production in cell lysates of *E. huxleyi* CCMP1516 incubated with the NR substrates nitrite and NADH using a novel liposome-encapsulated spin trap (LEST) enabled EPR method (Fig 4.1 and 4.2). We also detected and quantified non-enzymatic, abiotic production in the presence of these substrates. Boiled (i.e. protein inactivated) cell lysates, as well LEST incubated with buffer and NR substrates only, displayed ~8 μM MGD2Fe(II)NO in the reaction conditions used here (Fig 4.1). This was likely due to leakage of spin trap from the LEST which reacts abiotically with nitrite to form NO. Thus 8 μM was considered as the background associated with our methodology. Furthermore, enzymatic NO production was only detected in the presence of nitrate reductase (NR) substrates (Fig. 4.2). No NOS activity was detected in our samples (Fig. 4.2). The total protein load in the reactions presented in Fig 4.1 and Fig. 4.2 ranged from 1.5 – 44.7 μg and are shown in Table 4.1.

NO production mediated by nitrate reductase (NR) activity requires high intracellular nitrite concentrations. Intracellular nitrite during infection in viral infected and uninfected cells was thus quantified. Nitrite concentrations in the control culture was 1.5 μM per million cells at the beginning of the experiment and gradually decreased over time (Fig. 4.3a). Beginning at 24 hours post infection (hpi) intracellular nitrite was ~2-fold higher in the viral infected culture than in the control. At 48 hpi the viral infected culture had an 8-fold higher nitrite signal than the control. These trends correspond to the enhanced intracellular NO production and extracellular NO concentrations observed during infection in Schieler et al. (2019).

4.4.2 *In silico* prediction of nitrated and s-nitrosylated proteins

Of the 35,608 predicted proteins in the E. huxleyi proteome, 17,827 and 20,976 (50.1% and 58.9%) of them have at least one potential amino acid that can be nitrated or nitrosylated, respectively. This is similar to what has been observed in the *A.thaliana* proteome, in which 61% of proteins were found to be candidates for s-nitrosylation using the GPS-SNO algorithm (Chaki et al. 2014).

Of the 8 full putative metacaspases (excluding 1 fragment) in the proteome, 7 have at least one cysteine that is a candidate target for s-nitrosyation (Table 4.2). In addition, 7 of the 8 have at last one tyrosine that is a candidate target for nitration (Table 4.2). Several metacaspases (6 of 8) display a possible dual regulation by nitration and s-nitrosylation.

In Chapter 3, 159 unique antioxidant genes in 17 different gene categories were identified as being expressed in a shared transcriptome of two *E. huxleyi* strains (CCMP374 and CCMP379). In this current chapter we group two types of thioredoxin reductases into one category for a total of 16 unique categories. Of the 16 ROS-related gene categories expressed in CCMP373 and CCMP374, only 11 recruited to the CCMP1516 reference proteome, totaling 52 total proteins (Table 4.3).

Proteins in these categories that were present in the CCMP516 proteome were investigated for potential s-nitrosylation and nitration targets (Table 4.3). In total, 29 proteins have at least one s-nitrosylation target and 20 have at least one nitration target. Some gene categories exhibited propensity for one PTM over the other. For example, seven of the nine thioredoxins in the proteome are candidates for s-nitrosylation and only one has a potential nitration site. Additionally, of the three peroxiredoxins in the proteome, two have a potential s-nitrosylation site and none of them have a potential

nitration site. Some proteins had few targets for both PTMS. For example, NADH-ubiquinone oxidoreductases (total of 7) had only one was a candidate for s-nitrosylation and two were candidates for nitration. On the other hand, glutathione reductases, glutathione peroxidases, glutaredoxins, thioredoxin reductases, and ascrobate peroxidase displayed propensity to be targets for both PTMs.

4.4.3 Tyrosine nitration in *E. huxleyi*

E. huxleyi cell lysates displayed a suite of proteins that are nitrated (reactive with 3-nitrotyrosine antibody) *in vivo* (Fig. 4.3). Three prominent bands occur between 10 and 15 kD. In addition, there are visible bands at 25, 50, and 60 kD. There are no differences in the patterns of 3-nitrotyrosine between infected (v) and uninfected (c) cultures, except at 48 hours post infection, when virus-infected samples distinctly lose the three small bands between 10-15 kD. In addition, the intensity of the 3 small bands increases when 1, 24, and 48 hour control samples are compared, suggesting their concentrations relative to the total intracellular protein pool accumulate over time as the cells grew from $4x10^5$ cells ml^{-1} to $2.4x10^6$ cells ml^{-1}. A biological replication of Fig 4.3 was performed and is presented as Supplementary Figure S4.1.

4.4.4 MS identification of s-nitrosylated proteins

We identified a total of 38 proteins by MS in our s-nitrosylation enrichment columns with spectral counts >10 (Supplementary Table S4.1). There were, however, no significant differences between the variety and abundance of proteins in our samples and negative controls that were incubated with the TMT tag but without ascorbate to cleave

the S-NO bond (i.e. a control for non-specific binding of TMT to cysteines). Only two proteins of these 38 were found in the reference CCMP1516 proteome, however, a core histone (protein ID 196782) and a light harvesting protein (protein ID 211477). The fact that cysteines appeared to not have been randomly tagged and pulled down by the enrichment column suggests that these proteins may indeed have been nitrosylated. However, more work needs to be done to optimize and verify our s-nitrosocysteine tagging and enrichment method.

4.5 DISCUSSION

The nitrogen-based free radical nitric oxide (NO) has been implicated in having important cellular roles during growth and viral infection in the cosmopolitan coccolithophore *Emiliania huxleyi* (Zhang et al. 2003, Schieler et al. 2019). How NO is produced in this organism, however, is still unknown. The two major NO producing pathways are the oxidation of L-arginine via nitric oxide synthase (NOS) and nitrite reduction via nitrate reductase (NR), although there are at least seven putative biosynthetic pathways of NO described for photosynthetic organisms (Mur et al. 2012). A true NOS has only been described in the small green alga *Ostreococcus tauri* among all photosynthetic protists and higher plants (Foresi et al. 2010, Frohlich & Durner 2011), leading to disagreement in the literature about how NO is produced in different model photosynthetic organisms. A putative NOS gene was initially described upon the sequencing of the *E. huxleyi* CCMP1516 genome (Read et al. 2013), although upon closer inspection this gene shows very weak homology to known NOSs and contains no conserved NOS domains.

Elucidating which of these pathways is relevant to *E. huxleyi* is vital to understanding how NO functions during different physiological processes in this organism. In addition, targeting specific genes or gene products for future study will allow for a much more nuanced and controlled investigation of NO signaling then is currently afforded by the use of pharmacological NO donors and scavengers. It will also facilitate the investigation of NO metabolism on ecosystem wide scales by enabling 'omics approaches. Here, we investigate the relative contribution of NOS and NR activity to NO production in *E. huxleyi* undergoing viral infection and normal growth using a novel EPR method utilizing a liposome-encapsulated spin trap (LEST). This *in vitro* enzymatic capacity for NO production is in stark contrast to the NO measured by Schieler et al. (2019) and in Chapter 2 and 3, which are real-time *in vivo* measurements. This method has been previously shown to be sensitive to low levels of NOS present (Hirsh et al. 2016). Our results indicate, however, that *E. huxleyi* cells do not possess NOS-like activity, at least in the conditions tested here. Enzymatic NO production only occurred in the presence of the NR substrates NADH and sodium nitrite.

Nitrite-dependent NO production was not detected in all *E. huxleyi* samples. Uninfected CCMP1516 lysates at 4 hpi did not have any detectable NO production above the background, abiotic production (~8 μM) we found to be associated with this method. Activity was found in the same culture at 48 and 72 hpi, however. Upon inspection of the total protein loads in each of the reactions performed (Table 4.1), we find that enzymatic nitrite-dependent NO production only occurred with >40 ug of total protein in the reaction. It is therefore unknown whether the lack of activity seen in viral infected samples and the early control sample was due to true reduction in NR

activity during infection or protein loads that were too dilute to detect NO above the background. These results are informative to future utilization of this method; Protein should be used at sufficient (at least >40 ug) concentrations to detect enzymatic activity.

The fact that NR-mediated NO production was detected, rather then NOS activity, has interesting implications for understanding the physiological conditions in which NO signaling is relevant in *E. huxleyi*. The main function of NR in photosynthetic organisms is in nitrogen assimilation, facilitating the two electron reduction of nitrate to nitrite using photosynthetic equivalents (NAD(P)H) for subsequent reduction to ammonia via nitrite reductase (NiR). NR has a higher affinity for nitrate then nitrite and NO production via NR is inhibited at relatively low nitrate concentrations (K_i = 50 μM) in plants (Rockel et al. 2002). It appears, therefore, that NR-dependent NO production would only be relevant under conditions in which nitrite accumulates above normal intracellular levels, such as when photosynthesis is inhibited (Sakihama et al. 2002).

Given that we detect higher NO levels infected *E. huxleyi* (Schieler et al., 2019; Chapter 2), here we quantified intracellular nitrite levels of cells undergoing infection and uninfected control cells to determine whether elevated nitrite levels for NR-mediated NO production occurs. Using the classic Griess assay for nitrite detection, we found evidence that nitrite may indeed be elevated during viral infection, further supporting our hypothesis that NO production during infection comes from NR activity. This is consistent with previous observations that photosynthetic activity is diminished during infection (Bidle et al. 2007), and is thus conceivable that nitrate reduction is decreased and nitrite accumulates. However, with n=1, the data must be interpreted with caution

and bears repeating. Since typical intracellular nitrite levels are generally quite low, our samples fell on the low end of the assay's sensitivity range (Fig. 4.3b). In the future, intracellular nitrite should be quantified in tandem with measurement of NR-activity with saturating nitrite additions in order to put the activity detected *in vitro* into physiological context.

In addition to mechanisms of production, we also aimed to elucidate the downstream targets of NO signaling, with specific focus on the two prominent NO-mediated posttranslational protein modifications (PTMs): cysteine s-nitrosylation and tyrosine nitration, using both an *in silico* prediction approach and classic biochemical approaches. Predictions for the 'global' *E. huxleyi* s-nitrosoproteome and nitroproteome were generated using the GPS-SNO and GPS-YNO2 algorithms (Xue et al. 2010, Liu et al. 2011), programs that have been shown to be fairly accurate in predicting these PTMs in *Arabidopsis thaliana* (Chaki et al. 2014). Our analysis revealed that metacaspases were likely candidates for modification by NO; these predictions were not uniform across the proteome. For example, while 50.1% and 58.9% of the total proteins represented in the *E. huxleyi* proteome were shown to be candidates for tyrosine nitration and cysteine s-nitrosylation respectively, 89% and 78% of the putative metacaspes are possibly nitrated and s-nitrosylated (8 of 9 sequences nitrated, and 7 of 9 sequences s-nitrosylated).

Antioxidant proteins have also been previously demonstrated in plants to be critically modulated by NO (Begara-Morales et al. 2016). Consistent with these models from higher plants, a number of important putative antioxidant proteins in the *E. huxleyi* proteome, shown to be expressed in the shared transcriptome of CCMP373 and CCMP374 (hereafter "transcriptome"; Chapter 3), were revealed to be candidates for

NO-mediated PTM in this study. Thioredoxins appeared in the transcriptome to be the most commonly expressed antioxidant genes in both *E. huxleyi* strains and are likely targets for s-nitrosylation (7 or 9). Glutathione reductase, glutathione peroxidases and ascorbate peroxidase are also critical antioxidant proteins that were shown to be targets of both PTMs *in silico.* That a number of these predicted genes are differntially expressed in CCMP373 and CCMP379 has important implications for interpreting expression data, as potential regulation by NO may decouple total activity from expression.

Lastly, we directly investigated patterns of protein nitration in *E. huxleyi* cell lysates undergoing infection (and uninfected controls) using an antibody raised against 3-nitrotyrosines. There were a number of proteins that reacted with anti-nitrotyrosine, confirming *in silico* predictions that this PTM is physiologically relevant to *E. huxleyi*. However, we saw no differences between 3-nitrotyrosine patterns between infected and uninfected *E. huxleyi* (except at 48-72 hpi when 3 prominent bands disappear in the infected sample), suggesting that tyrosine nitration is not a major biomarker and/or pathway during viral infection in this species, despite the routine observation of increased ROS/NO production during infection, along with other markers of oxidative stress (Evans et al. 2006, Sheyn et al. 2016, Schieler et al. 2019).

Interestingly, 3-nitrotyrosines were present in uninfected control cells and increased in concentration during normal, exponential growth. This occurred despite very low production of ROS during the same timeframe, as indicated by CM-H_2DCFDA staining, and a decrease in free intracellular NO, as indicated by DAF-FM DA staining (Chapter 2). Nitration of tyrosines is generally considered to be a marker of nitrosative and oxidative stress and facilitated by the production of peroxynitrite from the

irreversible and diffusion limited reaction of NO with superoxide (Corpas et al. 2013). However, several studies have described protein nitration during replete conditions (Chaki et al. 2009, Corpas et al. 2009a). Our data suggest that protein tyrosine nitration may also be a feature of normal growth in *E. huxleyi* as well.

4.6 CONCLUSION

In this work we aimed to shed light on two open questions about NO production in photosynthetic organisms- mechanisms of production and molecular targets- specifically for the cosmopolitan coccolithophore *Emiliania huxleyi*. Using a novel liposome-encapsulated spin trap/EPR approach, we show that enzymatic NO production occurs in *E. huxleyi* cell lysates only in the presence of sodium nitrite, suggesting that nitrate reductase- and not nitric oxide synthase- may be the main pathway of NO production in this organism. Indeed, we provide preliminary evidence that intracellular nitrite concentrations (the substrate for NR-mediated NO production) are higher during viral infection, a condition that must be met for NR-mediated NO production to occur.

We also provide for the first time direct evidence of protein tyrosine nitration in an algal species. Interestingly, tyrosine nitration was associated with basal, replete growth rather then biotic stress (specifically viral infection). *In silico* predictions suggest that a number of proteins in the *E. huxleyi* proteome are indeed candidates for modulation by NO-mediated posttranslational modification. Metcaspases and antioxidant enzymes, two classes of proteins that have been directly shown to be important during viral infection, emerge as likely targets for protein tyrosine nitration and/or s-nitrosylation. Future studies should be done to both confirm these PTMs *in vivo* and to understand their effect

on protein activity in order to get a better understanding the roles of NO production during normal growth and viral infection in *E. huxleyi.*

4.7 ACKNOWLEDGEMENTS

LC-MS/MS identification of s-nitrosylated proteins was performed by H. Zheng (Biological Mass Spectrometry Facility, Center for Advanced Biotechnology and Medicine, Rutgers, The State University of New Jersey).

4.8 REFERENCES

Alderton WK, Cooper CE, Knowles RG (2001) Nitric oxide synthase: structure, function and inhibition. Biochemical Journal 357:593-615

Begara-Morales JC, Sanchez-Calvo B, Chaki M, Valderrama R, Mata-Perez C, Lopez-Jaramillo J, Padilla MN, Carreras A, Corpas FJ, Barroso JB (2014) Dual regulation of cytosolic ascorbate peroxidase (APX) by tyrosine nitration and S-nitrosylation. Journal of experimental botany 65:527-538

Begara-Morales JC, Sanchez-Calvo B, Chaki M, Valderrama R, Mata-Perez C, Padilla MN, Corpas FJ, Barroso JB (2016) Antioxidant Systems are Regulated by Nitric Oxide-Mediated Post-translational Modifications (NO-PTMs). Frontiers in plant science 7:152

Belenghi B, Romero-Puertas MC, Vercammen D, Brackenier A, Inze D, Delledonne M, Van Breusegem F (2007) Metacaspase activity of *Arabidopsis thaliana* is regulated by S-nitrosylation of a critical cysteine residue. The Journal of biological chemistry 282:1352-1358

Besson-Bard A, Pugin A, Wendehenne D (2008) New insights into nitric oxide signaling in plants. Annual review of plant biology 59:21-39

Bidle KD (2015) The molecular ecophysiology of programmed cell death in marine phytoplankton. Annual review of marine science 7:341-375

Bidle KD, Haramaty L, Barcelos ERJ, Falkowski P (2007) Viral activation and recruitment of metacaspases in the unicellular coccolithophore, *Emiliania huxleyi*. Proceedings of the National Academy of Sciences of the United States of America 104:6049-6054

Bratbak G, Egge JK, Heldal M (1993) Viral mortality of the marine alga *Emiliania huxleyi* (Haptophyceae) and termination of algal blooms. Marine Ecology Progress Series 93:39-58

Brown CW, Yoder JA (1994) Coccolithophorid blooms in the global ocean. Journal of Geophysical Research 99:7467-7482

Brussaard CPD, Kempers RS, Kop AJ, Riegman R, Heldal M (1996) Virus-like particles in a summer bloom of *Emiliania huxleyi* in the North Sea. Aquatic Microbial Ecology 10:105-113

Chaki M, Kovacs I, Spannagl M, Lindermayr C (2014) Computational prediction of candidate proteins for S-nitrosylation in *Arabidopsis thaliana*. PloS one 9:e110232

Chaki M, Valderrama R, Fernandez-Ocana AM, Carreras A, Lopez-Jaramillo J, Luque F, Palma JM, Pedrajas JR, Begara-Morales JC, Sanchez-Calvo B, Gomez-Rodriguez MV, Corpas FJ, Barroso JB (2009) Protein targets of tyrosine nitration in sunflower (*Helianthus annuus L.*) hypocotyls. Journal of experimental botany 60:4221-4234

Chamizo-Ampudia A, Sanz-Luque E, Llamas A, Ocana-Calahorro F, Mariscal V, Carreras A, Barroso JB, Galvan A, Fernandez E (2016) A dual system formed by the ARC and NR molybdoenzymes mediates nitrite-dependent NO production in *Chlamydomonas*. Plant, cell & environment 39:2097-2107

Corpas FJ, Chaki M, Leterrier M, Barroso JB (2009a) Protein tyrosine nitration: A new challenge in plants. Plant Signaling & Behavior 4:920-923

Corpas FJ, Palma JM, Del Rio LA, Barroso JB (2009b) Evidence supporting the existence of L-arginine dependent nitric oxide synthase activity in plants. New Phytologist 184:9-14

Corpas FJ, Palma JM, Del Rio LA, Barroso JB (2013) Protein tyrosine nitration in higher plants grown under natural and stress conditions. Frontiers in plant science 4:1-4

Correa-Aragunde N, Foresi N, Lamattina L (2013) Structure diversity of nitric oxide synthases (NOS): the emergence of new forms in photosynthetic organisms. Frontiers in plant science 4:232

Crane BR, Sudhamsu J, Patel BA (2010) Bacterial nitric oxide synthases. Annual review of biochemistry 79:445-470

de Pinto MC, Locato V, Sgobba A, Romero-Puertas Mdel C, Gadaleta C, Delledonne M, De Gara L (2013) S-nitrosylation of ascorbate peroxidase is part of programmed

cell death signaling in tobacco Bright Yellow-2 cells. Plant physiology 163:1766-1775

Estevez MS, Puntarulo S (2005) Nitric oxide generation upon growth of Antarctic *Chlorella* sp. cells. Physiologia Plantarum 125:192-201

Evans C, Malin G, Mills GP, Wilson WH (2006) Viral Infection of *Emiliania Huxleyi* (Prymnesiophyceae) Leads to Elevated Production of Reactive Oxygen Species. Journal of Phycology 42:1040-1047

Foresi N, Correa-Aragunde N, Parisi G, Calo G, Salerno G, Lamattina L (2010) Characterization of a nitric oxide synthase from the plant kingdom: NO generation from the green alga *Ostreococcus tauri* is light irradiance and growth phase dependent. The Plant cell 22:3816-3830

Frohlich A, Durner J (2011) The hunt for plant nitric oxide synthase (NOS): is one really needed? Plant science : an international journal of experimental plant biology 181:401-404

Gallina AA, Brunet C, Palumbo A, Casotti R (2014) The effect of polyunsaturated aldehydes on *Skeletonema marinoi* (Bacillariophyceae): the involvement of reactive oxygen species and nitric oxide. Marine drugs 12:4165-4187

Gusarov I, Shatalin K, Starodubtseva M, Nudler E (2009) Endogenous nitric oxide protects bacteria against a wide sprectrum of antibiotics. Science 235:1380-1384

Hirsh DJ, Schieler BM, Fomchenko KM, Jordan ET, Bidle KD (2016) A liposome-encapsulated spin trap for the detection of nitric oxide. Free radical biology & medicine 96:199-210

Holligan PM, Fernández E, Aiken J, Balch WM, Boyd P, Burkill PH, Finch M, Groom SB, Malin G, Muller K, Purdie DA, Robinson C, Trees CC, Turner SM, van der Wal P (1993) A biogemical study of the coccolithophore, *Emiliania huxleyi,* in the North Atlantic Global Biogeochemical Cycles 7:879-900

Kim D, Yamaguchi K, Oda T (2006) Nitric oxide synthase-like enzyme mediated nitric oxide generation by harmful red tide phytoplankton, *Chattonella marina*. Journal of Plankton Research 28:613-620

Knowles RG, Moncada S (1994) Nitric oxide synthases in mammals. Biochemical Journal 298:249-258

Knowles RG, Palacios M, Palmer RMJ, Moncada S (1989) Formation of nitric oxide from L-arginine in the central nervous system: A transduction mechanism for stimulation of the soluble guanylate cyclase. Proc Natl Acad Sci USA 86

Kumar A, Castellano I, Patti FP, Palumbo A, Buia MC (2015) Nitric oxide in marine photosynthetic organisms. Nitric oxide : biology and chemistry 47:34-39

Laber CP, Hunter JE, Carvalho F, Collins JR, Hunter EJ, Schieler BM, Boss E, More K, Frada M, Thamatrakoln K, Brown CM, Haramaty L, Ossolinski J, Fredricks H, Nissimov JI, Vandzura R, Sheyn U, Lehahn Y, Chant RJ, Martins AM, Coolen MJL, Vardi A, DiTullio GR, Van Mooy BAS, Bidle KD (2018) *Coccolithovirus* facilitation of carbon export in the North Atlantic. Nature microbiology 3:537-547

Lehahn Y, Koren I, Schatz D, Frada M, Sheyn U, Boss E, Efrati S, Rudich Y, Trainic M, Sharoni S, Laber C, DiTullio GR, Coolen MJ, Martins AM, Van Mooy BA, Bidle KD, Vardi A (2014) Decoupling physical from biological processes to assess the impact of viruses on a mesoscale algal bloom. Current biology : CB 24:2041-2046

Liu Z, Cao J, Ma Q, Gao X, Ren J, Xue Y (2011) GPS-YNO2: computational prediction of tyrosine nitration sites in proteins. Molecular bioSystems 7:1197-1204

Ludwig J, Meixner FX, Vogel B, Förstner J (2001) Soil-air exchange of nitric oxide: An overview of processes, environmental factors, and modeling studies. Biogeochemistry 52:225-257

Mallick N, Mohn FH, Soeder CJ (1999) Studies on nitric oxide (NO) formation by the green alga *Scenedesmus obliquus* and the diazotrophic cyanobacterium *Anabaena doliolum*. Chemosphere 39:1601-1610

Mallick N, Mohn FH, Soeder CJ, Grobbelaar JU (2002) Ameliorative role of ntiric oxide on H2O2 toxicity to a chlorophycean alga *Scenedesmus obliquus*.

Martens-Habbena W, Qin W, Horak RE, Urakawa H, Schauer AJ, Moffett JW, Armbrust EV, Ingalls AE, Devol AH, Stahl DA (2015) The production of nitric oxide by marine ammonia-oxidizing archaea and inhibition of archaeal ammonia oxidation by a nitric oxide scavenger. Environmental microbiology 17:2261-2274

Moncada S (1999) Nitric oxide: discovery and impact on clinical medicine. Journal of the Royal Society of Medicine 92:164-169

Mur LA, Mandon J, Persijn S, Cristescu SM, Moshkov IE, Novikova GV, Hall MA, Harren FJ, Hebelstrup KH, Gupta KJ (2012) Nitric oxide in plants: an assessment of the current state of knowledge. AoB PLANTS 5:pls052

Olasehinde EF, Takeda K, Sakugawa H (2010) Photochemical production and consumption mechanisms of nitric oxide in seawater. Environmental science & technology 44:8403-8408

Perez S, Weis V (2006) Nitric oxide and cnidarian bleaching: an eviction notice mediates breakdown of a symbiosis. The Journal of experimental biology 209:2804-2810

Rockel P, Strube F, Rockel A, Wildt J, Kaiser WM (2002) Regulation of nitric oxide (NO) production by plant nitrate reductase *in vivo* and *in vitro*. Journal of experimental botany 53:103-110

Sakihama Y, Nakamura S, Yamasaki H (2002) Nitric oxide production mediated by nitrate reductase in the green alga *Chlamydomonas reinhardtii*: an alternative NO production pathway in photosynthetic organisms. Plant & cell physiology 43:290-297

Schieler BM, Soni MV, Brown CM, Coolen MJL, Fredricks H, Van Mooy BAS, Hirsh DJ, Bidle KD (2019) Nitric oxide production and antioxidant function during viral infection of the coccolithophore *Emiliania huxleyi.* The ISME journal

Sheyn U, Rosenwasser S, Ben-Dor S, Porat Z, Vardi A (2016) Modulation of host ROS metabolism is essential for viral infection of a bloom-forming coccolithophore in the ocean. The ISME journal 10:1742-1754

Singh A, Sharma L, Mallick N (2004) Antioxidative role of nitric oxide on copper toxicity to a chlorophycean alga, Chlorella. Ecotoxicology and environmental safety 59:223-227

Thompson SEM, Callow ME, Callow JA (2009) The effects of nitric oxide in settlement and adhesion of zoospores of the green alga *Ulva*. Biofouling 26:167-178

Thompson SEM, Taylor AR, Brownlee C, Callow ME, Callow JA (2008) The Role of Nitric Oxide in Diatom Adhesion in Relation to Substratum Properties(1). J Phycol 44:967-976

Turko IV, Murad F (2002) Protein NItration in Cardiovascular Diseases. Pharmacological Reviews 54:619-634

Tyrrell T, Merico A (2004) *Emiliania huxleyi:* bloom observations and the conditions that induce them. In: Thierstein HR, Young JR (eds) Coccolithophores: From Molecular Processes to Global Impact. Springer, Germany

Vardi A, Bidle KD, Kwityn C, Hirsh DJ, Thompson SM, Callow JA, Falkowski P, Bowler C (2008) A diatom gene regulating nitric-oxide signaling and susceptibility to diatom-derived aldehydes. Current biology : CB 18:895-899

Vardi A, Formiggini F, Casotti R, De Martino A, Ribalet F, Miralto A, Bowler C (2006) A stress surveillance system based on calcium and nitric oxide in marine diatoms. PLoS biology 4:e60

Xue Y, Liu Z, Gao X, Jin C, Wen L, Yao X, Ren J (2010) GPS-SNO: computational prediction of protein S-nitrosylation sites with a modified GPS algorithm. PloS one 5:e11290

Yang H, Mu J, Chen L, Feng J, Hu J, Li L, Zhou JM, Zuo J (2015) S-nitrosylation positively regulates ascorbate peroxidase activity during plant stress responses. Plant physiology 167:1604-1615

Zaffagnini M, De Mia M, Morisse S, Di Giacinto N, Marchand CH, Maes A, Lemaire SD, Trost P (2016) Protein S-nitrosylation in photosynthetic organisms: A comprehensive overview with future perspectives. Biochimica et biophysica acta 1864:952-966

Zhang Z, Lin C, Liu C, Sun M, Ding H (2003) The effect of nitric oxide on the growth of marine phytoplankton. Journal of Ocean University of Qingdao 2:185-188

4.9 FIGURES & TABLES

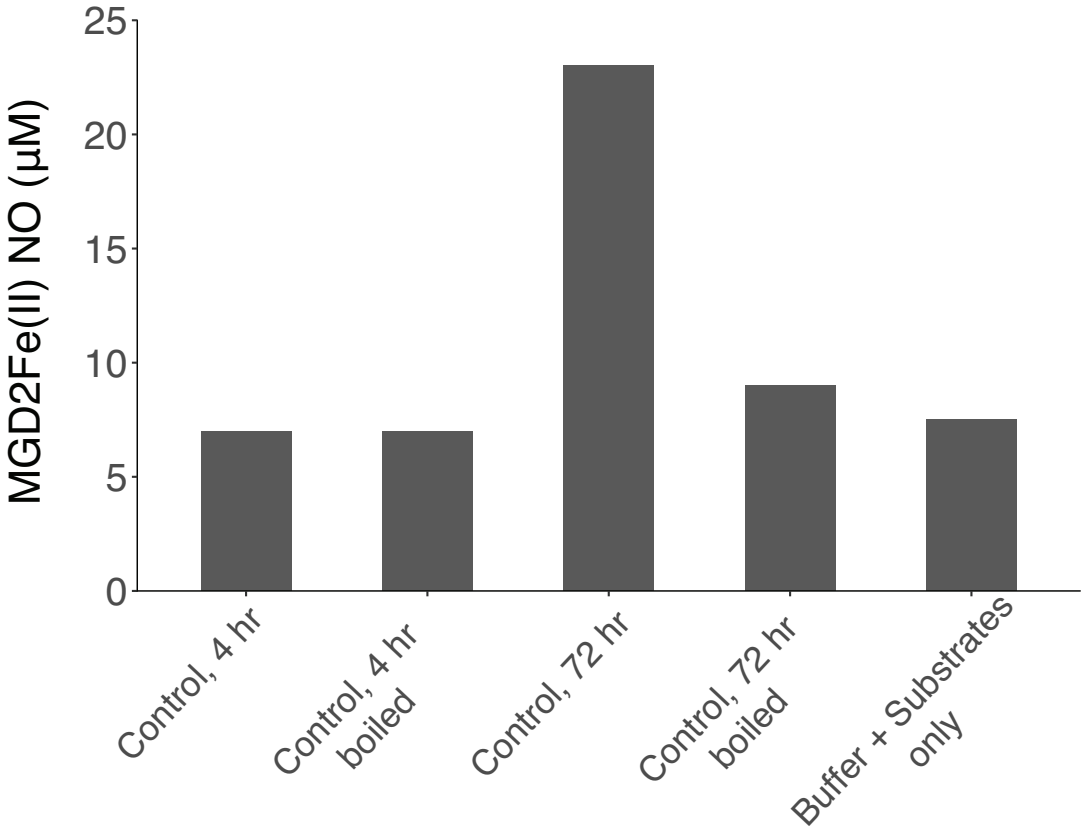

Figure 4.1 Detection of nitrite-dependent NO production in cell lysates of *E. huxleyi* CCMP1516 at two different stages of exponential growth. Boiled fractions of each sample, as well as a buffer + substrate only sample, serve as a controls for abiotic NO production from the reaction conditions. Samples are concentration of sin-trap bound NO (μM) after 3 hr incubation (n=1).

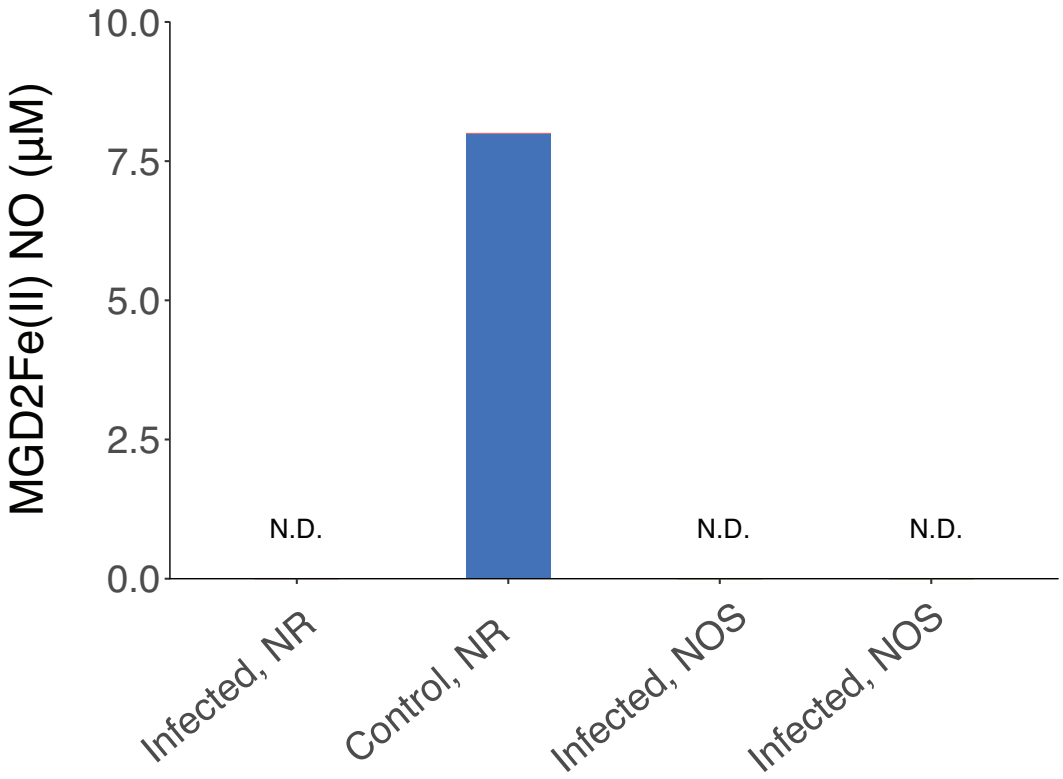

Figure 4.2 Comparison of nitrite-dependent (NR) vs. arginine dependent (NOS) NO production in lysates of *E. huxleyi* CCMP1516 undergoing viral infection and uninfected controls (48 hr post infection, n=1). Values for nitrite-dependent NO production have the abiotic, background NO production subtracted. N.D.= not detected.

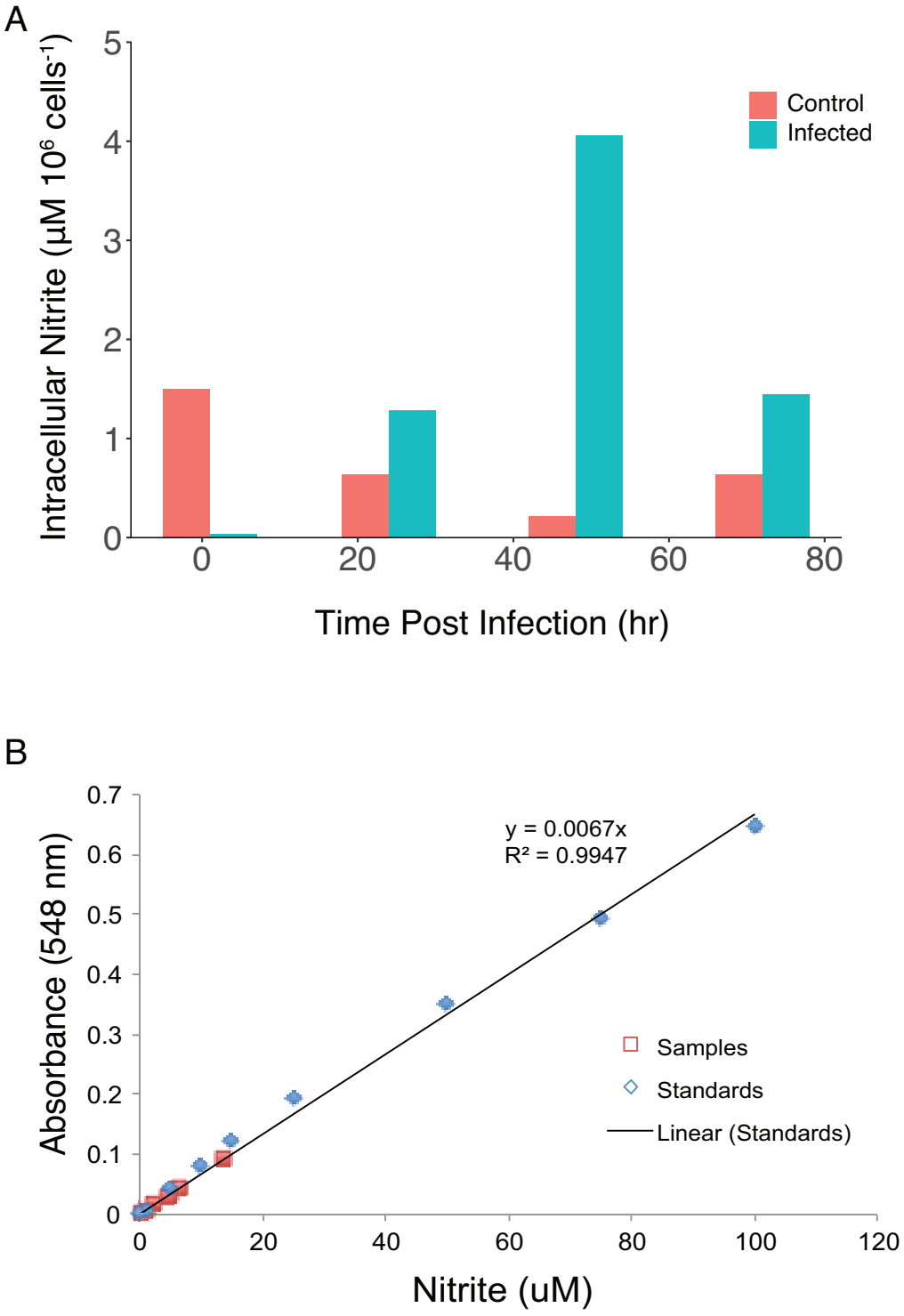

Figure 4.3 Quantification of intracellular nitrite in *E. huxleyi* CCMP1516 during viral infection with EhV201 and in uninfected control cells. (A) Intracellular nitrite displyed as µM per 10^6 cells (n=1) for infected (green) and uninfected (pink) samples. (B) Standard curve of sodium nitrite overlayed by all samples.

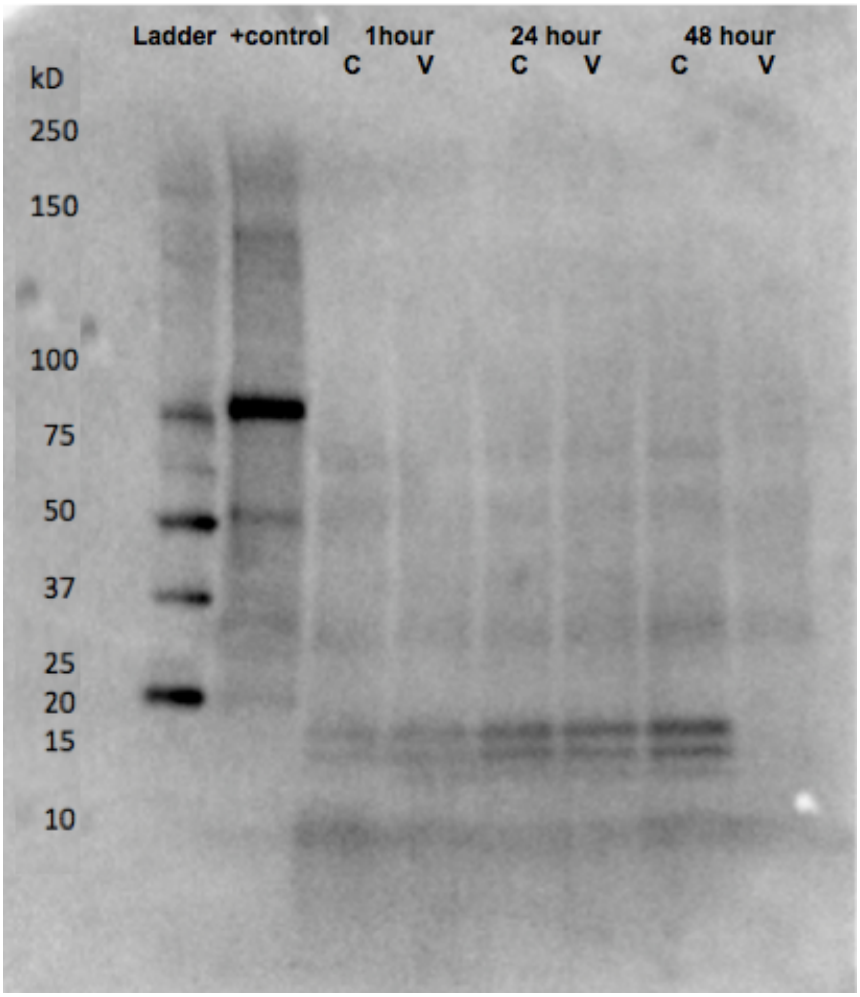

Figure 4.4 Western blot of proteins that react with 3-nitrotyrosine antibody in lysates of CCMP1516 undergoing infection (v) and uninfected control cultures (c) at 1, 24, and 48 hr post infection. "+control" is rat brain extract positive control to confirm binding of antibody. Blot is a representative of two independent experiments performed.

Table 4.1 Summary of the protein loads in the reactions presented in Fig. 4.1 and Fig 4.2 (in total ug) and whether nitrite-dependent NO production (NR activity) was detected in that sample.

Experiment #	Sample	Protein in reaction (ug)	NR activity detected? (Y/N)
1	Control, 4 hr	1.5	N
1	Control, 72 hr	44.7	Y
2	Control, 48 hr	42.8	Y
2	Virus, 48 hr	9.7	N

Table 4.2 All putatitve metacaspases described in the proteome of *E. huxleyi* CCMP1516 along with *in silico* predictions for sites of s-nitrosylated cysteines and nitrated tyrosines. Predictions generated from GPS-SNO program using the 'medium' threshold.

Protein ID	Protein Description	S-Nitrosylated Amino Acid(s)	Nitrated Amino Acid(s)
R1DPK5	Putative metacaspase protein	None	Tyr-3
R1B705	Putative metacaspase protein	Cys-4	None
R1F9V1	Putative metacaspase protein with Ca-binding EF hand domain	Cys-169	Tyr-223 Tyr-425 Tyr-474
R1EMP3	Putative metacaspase protein	Cys-163 Cys-223 Cys-379 Cys-383	Tyr-16 Tyr-215
R1FQT6	Putative metacaspase protein	Cys-198	Tyr-15 Tyr-324 Tyr-334
R1G079	Putative metacaspase protein	Cys-235 Cys-254 Cys-368	Tyr-89 Tyr-246
R1DET8	Putative metacaspase protein	Cys-363	Tyr-20 Tyr-232 Tyr-375
R1DAJ8	Putative metacaspase protein	Cys-272 Cys-474	Tyr-92
R1EEY0	Putative metacaspase protein (fragment)	None	Tyr-186 Tyr-523 Tyr-239

Table 4.3 List of 17 antioxidant gene categories identified in the shared transcriptome of 374^{S} and 379^{R} along with *in silico* predictions of which genes in these categories are candidates for s-ntirosylation of cysteines and nitration of tyrosines. Predictions generated from GPS-NO program using the 'medium' threshold. Note that 5 gene categories were not found in the annotated *E. huxleyi* CCMP1516 proteome.

Gene Type	Total Genes	Nitration Targets	S-nitrosylation Targets
Thioredoxin	9	1	7
Protein Disulfide Isomerase	1	0	1
NADH-ubiquinone Oxidoreductase	7	2	1
SOD	3	1	1
Glutathione Reductase	4	3	4
Glutathione Peroxidase	8	5	5
Glutathione Disulfide Reductase	0	0	0
Glutaredoxin	10	4	6
Ferric Reduction Oxidase	0	0	0
Thioredoxin Reductase	4	2	1
Dehydroascorbate Reductase	0	0	0
Peroxiredoxin	3	0	2
Blue-Copper Binding Protein	0	0	0
Ascorbate Peroxidase	1	1	1
Alternative Oxidase	2	1	0
5'adenylylphosphosulfate Reductase	0	0	0

4.10 SUPPLEMENTARY MATERIALS & METHODS

4.10.1 LEST preparation

Liposomes were prepared from a 9:1 molar ratio of the phospholipids 1-palmitoyl-2-oleoyl-sn-glycero-3-phosphocholine and 1,2-dipalmitoyl-*sn*-glycero-3-phospho-(1′-*rac*-glycerol), POPC and DPPG respectively, in chloroform (Avanti Polar Lipids, Alabaster, AL). A lipid film was formed by rotary evaporation and dried overnight under vacuum. The lipid film was suspended in buffer containing 10 mM of the spin trap N-methyl-D-glucamine dithiocarbamate (MGD) and 2mM ammonium iron(II) sulfate in a ratio of 1 mL buffer to 100 mg lipid mixture. The resulting multilamellar vescivles (MLVs) were freeze-thawed (x 5 cycles) in liquid nitrogen and stored in liquid nitrogen. Prior to use, the MLVs were suspended in HEPES buffer (20 mM, 140 mM NaCl, pH 7.4) and filtered through a PD-10 desalting column (GE Life Sciences, Chicago, IL) to remove extra-liposomal MGD and iron, yielding LEST.

4.11 SUPPLEMENTARY FIGURE AND TABLE

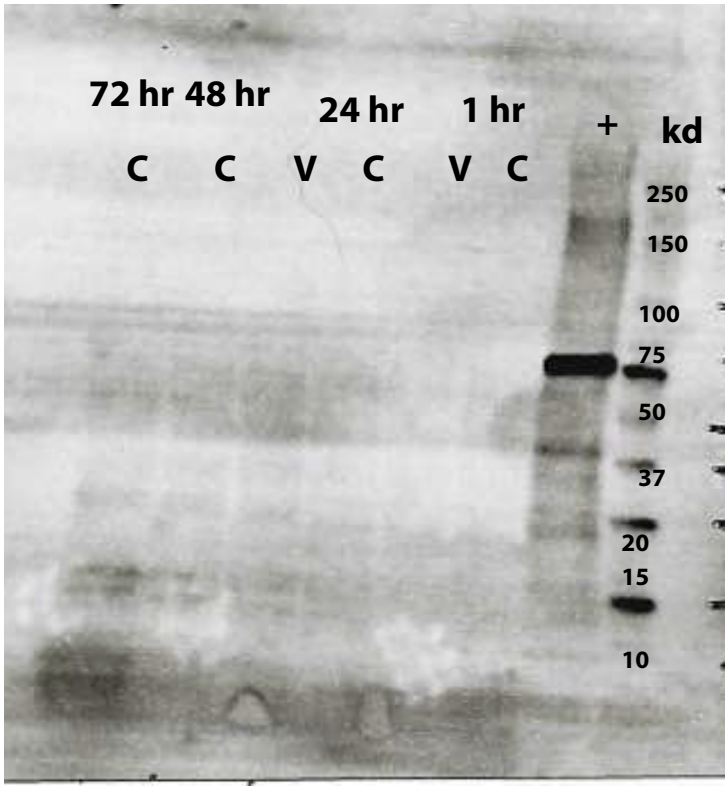

Figure S4.1 Replication (second independent experiment) of Western blot of proteins that react with 3-nitrotyrosine antibody in lysates of CCMP1516 undergoing infection (v) and uninfected control cultures (c). From right to left, lanes are: Molecular weight ladder (kD), rate brain extract positive control, uninfected control at 1hpi, infected culture at 1hpi, uninfected control at 24 hpi, infected culture at 24 hpi, uninfected control at 48 hpi, and uninfected control at 72 hpi.

Table S4.1 S-nitrosylated proteins tagged with TMT and identified by LC-MS/MS in *E. huxleyi* cell lysates. Protein ID, total spectral counts for all samples, and annotation of protein in the CCMP1516 reference proteome. Proteins that had >10 spectral counts in at least one sample were included. Total spectral counts represents the total across all samples analyzed. 'na' means no annotation found.

Protein ID	Total Spectral Counts	Annotation
jgi|Emihu1|196782|gm1.400904	161	Core Histone
jgi|Emihu1|279832|estExt_Genemark1.C_710082	141	na
jgi|Emihu1|205571|gm1.2400263	140	na
jgi|Emihu1|225399|gm1.12400092	132	na
jgi|Emihu1|265891|estExt_est_orfs.C_1670002	128	na
jgi|Emihu1|281262|estExt_Genemark1.C_1150179	114	na
jgi|Emihu1|285186|estExt_Genemark1.C_6750001	106	na
jgi|Emihu1|266533|estExt_fgeneshEH_pg.C_40311	101	na
jgi|Emihu1|196492|gm1.400614	101	na
jgi|Emihu1|41972|gw1.14.10.1	93	na
jgi|Emihu1|196256|gm1.400378	93	na
jgi|Emihu1|282640|estExt_Genemark1.C_1720058	87	na
jgi|Emihu1|195417|gm1.300468	84	na
jgi|Emihu1|88203|estExt_Genewise1.C_680019	75	na
jgi|Emihu1|406321|estExt_fgenesh_newKGs_kg.C_610016	73	na
jgi|Emihu1|409669|estExt_fgenesh_newKGs_kg.C_1580008	65	na
jgi|Emihu1|41424|gw1.401.1.1	64	na
jgi|Emihu1|70213|e_gw1.118.38.1	62	na
jgi|Emihu1|211784|gm1.5000111	59	na
jgi|Emihu1|94767|fgeneshEH_pg.1__38	58	na
jgi|Emihu1|89087|estExt_Genewise1.C_1300023	55	na
jgi|Emihu1|218361|gm1.7900023	55	na
jgi|Emihu1|402650|estExt_fgenesh_newKGs_kg.C_90061	54	na
jgi|Emihu1|230272|gm1.16200083	53	na
jgi|Emihu1|239894|gm1.29800026	52	na
jgi|Emihu1|61759|e_gw1.5.27.1	50	na
jgi|Emihu1|198687|gm1.800442	49	na
jgi|Emihu1|196337|gm1.400459	45	na
jgi|Emihu1|242418|gm1.35900025	44	na
jgi|Emihu1|285102|estExt_Genemark1.C_6030012	44	na

jgi|Emihu1|268488|estExt_fgeneshEH_pg.C_270119	42	na
jgi|Emihu1|197716|gm1.700026	41	na
jgi|Emihu1|212368|gm1.5200146	40	na
jgi|Emihu1|219315|gm1.8400164	37	na
jgi|Emihu1|353078|fgenesh_newKGs_kg.19__150__EST_ALL.fasta.Contig11938	36	na
jgi|Emihu1|211477|gm1.4800082	36	Light-harvesting protein
jgi|Emihu1|269032|estExt_fgeneshEH_pg.C_410081	35	na
jgi|Emihu1|210650|gm1.4500117	32	na

CHAPTER 5: Conclusions

Since the discovery of the free radical nitric oxide (NO) as the endothelium-derived relaxation factor in the 1980s, the list of functions it has and cellular pathways it participates in has been growing at an impressive rate. Our appreciation of the roles of NO in phytoplankton physiology and ecology, while far behind what is known in animals and higher plants, has been rapidly increasing in the past decade or so (Kumar et al. 2015). The inclusion of phytoplankton, photosynthesizing single-celled organisms (also referred to as algae) that inhabit marine and freshwater ecosystems, in the study of the biochemistry and physiology of NO is critical to addressing various aspects of this enigmatic molecule. For example, there is still extensive debate in the literature about whether photosynthetic organisms possess nitric oxide synthase (NOS)- the main NO producing enzyme in animals. Despite NOS-like activity being demonstrated in various plant models, only one true NOS in photosynthetic organisms has been identified, in the small green alga *Ostreococcus tauri* (Foresi et al. 2010). Interestingly, since this seminal discovery, the search for plant NOSs has only uncovered putative NOS sequences in algal genomes and transcripts and none in higher plants (Jeandroz et al. 2016). Therefore, algal NO biology represents an important link to understanding how NO signaling and production has evolved.

This dissertation expands the current state of knowledge of NO ecophsyiology to its function in the cosmopolitan bloom-forming coccolithophore *Emiliania huxleyi. E. huxleyi* plays fundamental roles in the environment by producing a significant portion of marine calcium carbonate, fixing inorganic carbon, influencing biogeochemical cycling of important elements, and impacting climate (reviewed in Chapter 1). *E. huxleyi* is also known for its blooms being routinely infected and terminated through infection by

viruses (*Coccoithoviruses* known as EhVs). For several reasons, *E. huxleyi* and EhVs have emerged as one of the best-described model systems for viral infection of eukaryotic marine algae. Over the passed two decades, much has been uncovered about this process, from the molecular pathways governing infection (Mackinder et al. 2009, Bidle & Vardi 2011, Bidle 2015) to its ecosystem-wide impacts (Evans et al. 2007, Lehahn et al. 2014, Laber et al. 2018).

In Chapter 2, I showed that NO production is a hallmark of viral infection. Specifically, cells that are actively undergoing viral infection exhibit an increase in intracellular NO 24 hours post infection (hpi). This work demonstrated increased NO production in both lab cultures and in natural *E. huxleyi* populations encountered in the North Atlantic during the *North Atlantic Viral Infection of Coccolithophores Expedition* (NA-VICE). Chapter 2 further placed the viral-induced production of NO into the context of what is known about the production of other reactive oxygen species, ROS (Evans et al. 2006, Sheyn et al. 2016) by exploring and supporting the hypothesis that NO production may have an antioxidant function during infection. Indeed, Chapter 2 provided strong evidence that NO has the ability to diminish toxicity of the ROS, hydrogen peroxide (H_2O_2), in cells.

Chapter 3 surveyed NO production in various strains of *E. huxleyi* that differ in their susceptibility to viral infection and, for the first time, demonstrated significant intra-species variability in the production of this critical signaling molecule. Chapter 3 leveraged these inherent NO production differences to further explore the relationship between NO, ROS, and antioxidant activity. Resistant *E. huxleyi* strains, which had the lowest NO production, also had relatively higher levels of basal oxidative stress and cell

death (and vice versa for sensitive strains). Surprisingly, these resistant strains displayed the highest levels of antioxidant activity. Chapter 3 discussed of the potential for certain molecules such as glutathione or s-nitrosylated proteins to be intracellular NO reservoirs that may artificially dampen the measured NO values in the strains. Chapter 3 concluded with a discussion of the implications of these findings for possible mechanisms and costs of resistance in *E. huxleyi.*

Finally, Chapter 4 aimed to address the potential mechanisms of NO production and protein targets of NO in *E. huxleyi*. Despite a possible NOS being formerly described in the *E. huxleyi* genome (Read et al. 2013), NOS activity was not detected in cell lysates. Instead, *E. huxleyi* lysates produced NO via nitrite/NADH and an assumed activity of nitrate reductase (NR). Lastly, Chapter 4 presented *in silico* analyses that suggested that antioxidant proteins and metacaspaes are likely important targets for NO-mediated modulation via post-translational modification. Indeed we provide biochemical evidence of nitrated tyrosines in *E. huxleyi* during normal growth conditions. This is the first time protein tyrosine nitration in non-stress conditions was demonstrated in an algal species. In addition, Chapter 4 laid out preliminary work to identify s-nitrosylated proteins in *E. huxleyi*, though more work needs to be done to optimize the method. Protein post-translational modifications, especially of antioxidant proteins and metacaspses, represent promising areas for future study of how NO functions in this species.

An important outcome of this work has been the observation that intracellular NO patterns are manifested in the extracellular milieu. Specifically, Chapter 2 showed that viral infection in *E. huxleyi* led to increases in extracellular NO concentrations compared to uninfected controls of equal cell density. In addition, Chapter 3 showed that strain-

specific variability in intracellular NO production leads to similar variability in extracellular NO concentrations. An open question in the study of NO is whether biological production can account for meaningful contributions to the environment. For example, it has been previously shown that the surface ocean may act sometimes act as a net source of NO to the atmosphere (Olasehinde et al. 2010). While this study did not find a significant contribution of biology to surface ocean NO production, it was extremely limited in the types of biological regimes examined. As is documented here, along with other previous phytoplankton NO work, NO production levels can vary considerably between and among species and in response to various biotic and abiotic stressors. Therefore, the propensity of *E. huxleyi* blooms, especially those being actively infected by viruses, to be sources of NO to the environment remains an open and provoking question. It is also timely, considering the attention the biological production of other reactive species, like superoxide, is receiving in the field (Kustka et al. 2005, Diaz et al. 2013).

This dissertation mainly focused on the intracellular roles and pathways of NO in the coccolithophore *E. huxleyi*. However, because NO is readily diffusible across biological membranes, it is conceivable that it may have a myriad of inter-cellular signaling functions in blooms and/or mixed microbial populations as well. Indeed, it has been suggest that NO plays a role in relaying stress in response to toxic aldehydes in diatoms to neighboring cells (Vardi et al. 2006). Likewise, there is intriguing data suggesting that NO may also play a inter-cellular signaling role for *E. huxleyi* in mixed microbial populations. For example, in *E. huxleyi* laboratory cultures (strain CCMP1516), removal of co-existing bacteria in the culture through multiple rounds of antibiotic

treatment led to a decrease in extracellular NO concentrations detected via the LEST/EPR method described in Chapter 2 and 3 (Fig. 5.1). However, it is not simply that the removal of NO producing cells that accounted for this reduction. Extracellular NO in the bacteria-only fraction of the cultures was not detectable. Therefore, there is some unknown effect of the presence of commensal bacteria on the physiology of *E. huxleyi* that may be mediated by NO.

In addition, epifluorescence microscopy revealed considerable spatial heterogeneity in NO production in seemingly monoclonal cultures of *E. huxleyi*. Fig. 5.2a shows a fluorescence micrograph of DAF-FM Diacetate stained *E. huxleyi* CCMP1516 cells treated with the exogenous NO donor s-nitroso-n-acetylpenicillamine (SNAP) in the red channel (showing all chlorophyll containing cells). Fig. 5.2b shows this same field-of-view but in the green channel, showing all DAF-FM DA stained cells. Interestingly, there is a subset of cells that have diminished NO production in the presence of SNAP, and these cells are also not uniformly distributed throughout the culture. This microscale variability has intriguing implications for cell-to-cell communication within a single population.

Lastly, it may also be possible that NO serves as a mediator of interspecies competition in mixed phytoplankton populations. For example, natural phytoplankton assemblages collected in a Norwegian fjord were subjected to incubations with and without the NO donor SNAP (50 μM). After three days of incubation, non-treated samples became enriched in small, pico-phytoplankton groups including S*ynechococcus* sp. and general picoeukaryotes (totaling 93% of the total phytoplankton population; Fig. 5.3). On the other hand, SNAP treated samples were enriched in larger, nano-

phytoplankton groups included cryptophytes, *Emiliania huxleyi*, and other nano-phytoplankton. Picophytoplankton only made up ~49% of the population in these experimental samples (Fig. 5.3). Whether various algal groups sense and employ NO-signaling differently remains an open question in phytoplankton ecology. This indeed does seem to be the case in diatoms; different species of diatoms respond to polyunsaturated aldehydes (PUAs) with disparate NO production dynamics (Gallina et al. 2014). Additionally, *E. huxleyi* responds to the PUA dacedienal (DD) in a drastically different manner then was shown for the model diatom *Phaeodactylum tricornutum* (Vardi et al. 2006). Instead of an increase in NO production in response to DD, *E. huxleyi* responds by decreasing intracellular NO levels (Fig. 5.4). These results expand the current understanding of the NO-based "stress surveillance" system diatoms in response to PUAs to a different genus.

These final data presented here hint that NO may have signaling functions relevant to *E.* huxleyi that extend beyond the intracellular roles described in this dissertation. They also represent exciting areas for future research in NO ecophysiology of marine microbes. NO is truly an enigmatic and important molecule that has consequences spanning the sub-micron scale (through modulation of intracellular pathways) to more far-reaching, ecosystem-wide scales (through facilitation of viral infection, mediating microbial interactions, and diffusion into the environment).

5.2 REFERENCES

Bidle KD (2015) The molecular ecophysiology of programmed cell death in marine phytoplankton. Annual review of marine science 7:341-375

Bidle KD, Vardi A (2011) A chemical arms race at sea mediates algal host-virus interactions. Current opinion in microbiology 14:449-457

Diaz JM, Hansel CM, Voelker BM, Mendes CM, Andeer PF, Zhang T (2013) Widespread production of extracellular superoxide by heterotrophic bacteria. Science 340:1223-1226

Evans C, Kadner SV, Darroch LJ, Wilson WH, Liss PS, Malin G (2007) The relative significance of viral lysis and microzooplankton grazing as pathways of dimethylsulfoniopropionate (DMSP) cleavage: An *Emiliania huxleyi* culture study Limnology and Oceanography 52:1036-1045

Evans C, Malin G, Mills GP, Wilson WH (2006) Viral Infection of *Emiliania Huxleyi* (Prymnesiophyceae) Leads to Elevated Production of Reactive Oxygen Species. Journal of Phycology 42:1040-1047

Foresi N, Correa-Aragunde N, Parisi G, Calo G, Salerno G, Lamattina L (2010) Characterization of a nitric oxide synthase from the plant kingdom: NO generation from the green alga *Ostreococcus tauri* is light irradiance and growth phase dependent. The Plant cell 22:3816-3830

Gallina AA, Brunet C, Palumbo A, Casotti R (2014) The effect of polyunsaturated aldehydes on *Skeletonema marinoi* (Bacillariophyceae): the involvement of reactive oxygen species and nitric oxide. Marine drugs 12:4165-4187

Jeandroz S, Wipf D, Stuehr DJ, Lamattina L, Melkonian M, Tian Z, Zhu Y, Carpenter EJ, Wong GK-S, Wendehenne D (2016) Occurence, structure, and evolution of nitric oxide synthase-like proteins in the plant kingdom. Science Signaling 9:re2

Kumar A, Castellano I, Patti FP, Palumbo A, Buia MC (2015) Nitric oxide in marine photosynthetic organisms. Nitric oxide : biology and chemistry 47:34-39

Kustka AB, Shaked Y, Milligan AJ, King DW, Morel FMM (2005) Extracellular production of superoxide by marine diatoms: Contrasting effects on iron redox chemistry and bioavilability. Limnology and Oceanography 50:1172-1180

Laber CP, Hunter JE, Carvalho F, Collins JR, Hunter EJ, Schieler BM, Boss E, More K, Frada M, Thamatrakoln K, Brown CM, Haramaty L, Ossolinski J, Fredricks H, Nissimov JI, Vandzura R, Sheyn U, Lehahn Y, Chant RJ, Martins AM, Coolen MJL, Vardi A, DiTullio GR, Van Mooy BAS, Bidle KD (2018) *Coccolithovirus* facilitation of carbon export in the North Atlantic. Nature microbiology 3:537-547

Lehahn Y, Koren I, Schatz D, Frada M, Sheyn U, Boss E, Efrati S, Rudich Y, Trainic M, Sharoni S, Laber C, DiTullio GR, Coolen MJ, Martins AM, Van Mooy BA, Bidle KD, Vardi A (2014) Decoupling physical from biological processes to assess the impact of viruses on a mesoscale algal bloom. Current biology : CB 24:2041-2046

Mackinder LC, Worthy CA, Biggi G, Hall M, Ryan KP, Varsani A, Harper GM, Wilson WH, Brownlee C, Schroeder DC (2009) A unicellular algal virus, *Emiliania huxleyi* virus 86, exploits an animal-like infection strategy. The Journal of general virology 90:2306-2316

Olasehinde EF, Takeda K, Sakugawa H (2010) Photochemical production and consumption mechanisms of nitric oxide in seawater. Environmental science & technology 44:8403-8408

Read BA, Kegel J, Klute MJ, Kuo A, Lefebvre SC, Maumus F, Mayer C, Miller J, Monier A, Salamov A, Young J, Aguilar M, Claverie JM, Frickenhaus S, Gonzalez K, Herman EK, Lin YC, Napier J, Ogata H, Sarno AF, Shmutz J, Schroeder D, de Vargas C, Verret F, von Dassow P, Valentin K, Van de Peer Y, Wheeler G, Emiliania huxleyi Annotation C, Dacks JB, Delwiche CF, Dyhrman ST, Glockner G, John U, Richards T, Worden AZ, Zhang X, Grigoriev IV (2013) Pan genome of the phytoplankton *Emiliania* underpins its global distribution. Nature 499:209-213

Sheyn U, Rosenwasser S, Ben-Dor S, Porat Z, Vardi A (2016) Modulation of host ROS metabolism is essential for viral infection of a bloom-forming coccolithophore in the ocean. The ISME journal 10:1742-1754

Vardi A, Formiggini F, Casotti R, De Martino A, Ribalet F, Miralto A, Bowler C (2006) A stress surveillance system based on calcium and nitric oxide in marine diatoms. PLoS biology 4:e60

5.3 FIGURES

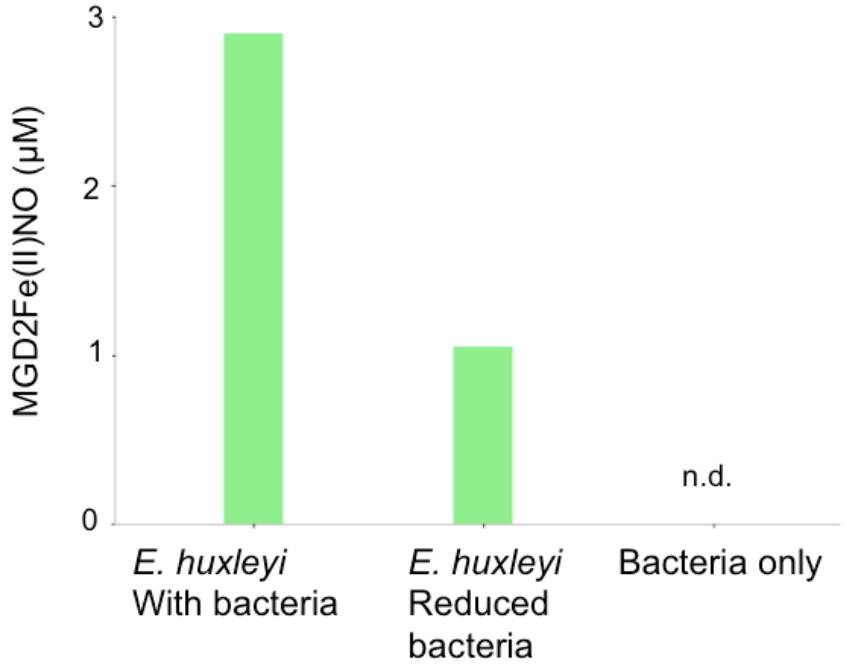

Figure 5.1 Extracellular NO concentration (µM) in *E. huxleyi* CCMP1516 cultures with typical bacterial loads (about 4x the concentration of *E. huxleyi* cells), an 80% reduction in total bacterial load, as well as a bacteria-only fraction (n=1). n.d.= not detected.

A

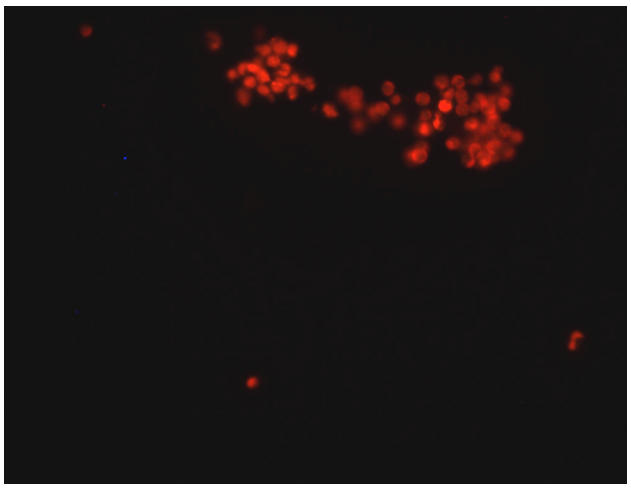

B

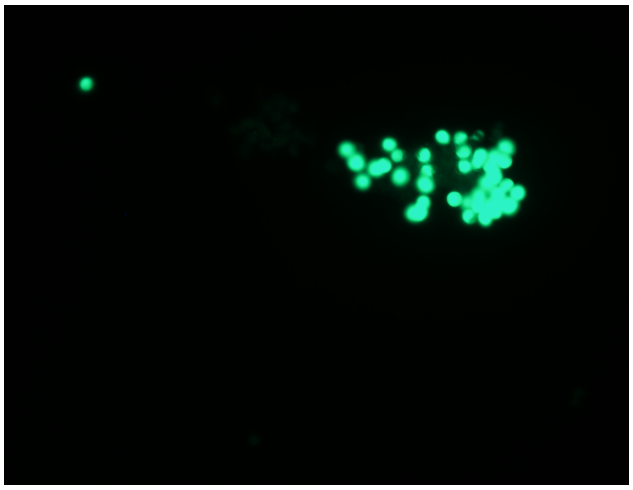

Figure 5.2 Epifluorescence micrographs of *E. huxleyi* CCMP1516 cells stained with the NO probe DAF-FM Diacetate and treated with the NO donor SNAP (250 μM) with the same field-of-view in the (A) red channel, excited by a green laser and (B) green channel, excited by a blue laser.

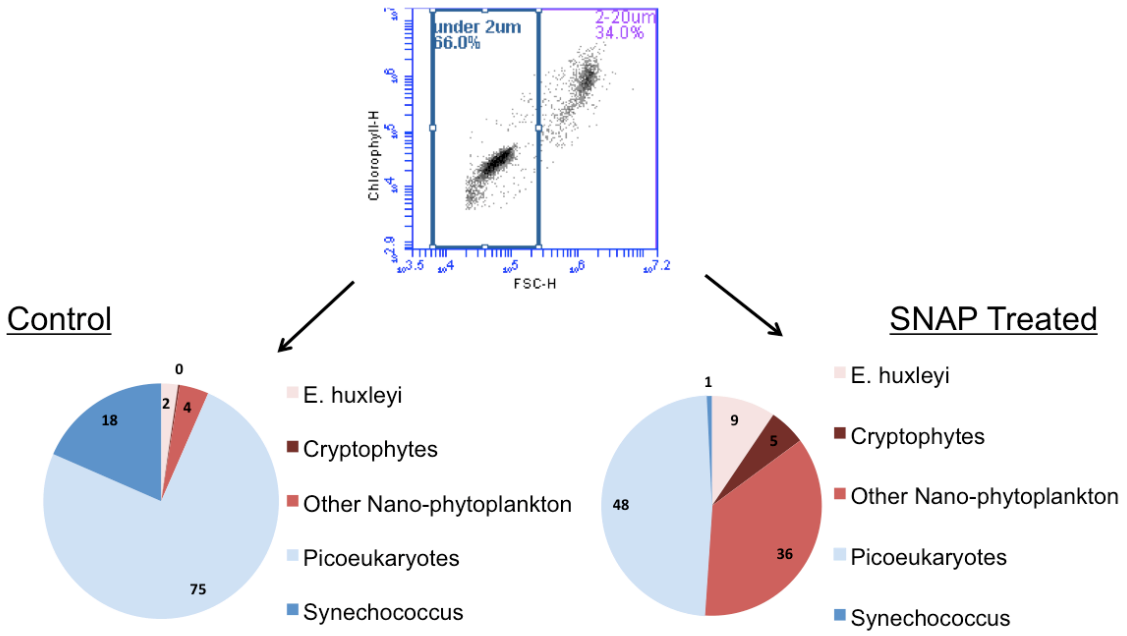

Figure 5.3 Effect of incubation with the NO donor SNAP on a natural phytoplankton assemblage collected from a Norwegian fjord. Top panel shows a bivariate flow cytogram of chlorophyll fluorescence vs. forward scatter of the initial assemblage. The control pie chart shows the relative proportions of various phytoplankton groups in the sample after three days of incubation in *in situ* temperature and light conditions. The SNAP treated pie chart shows the relative proportions of various phytoplankton groups in the sample amended with 50 µM SNAP after the same time frame. Values represent the mean abundance of n=2. Phytoplankton groups were identified by flow cytometry using a BD Accuri C6 with autosampling arm.

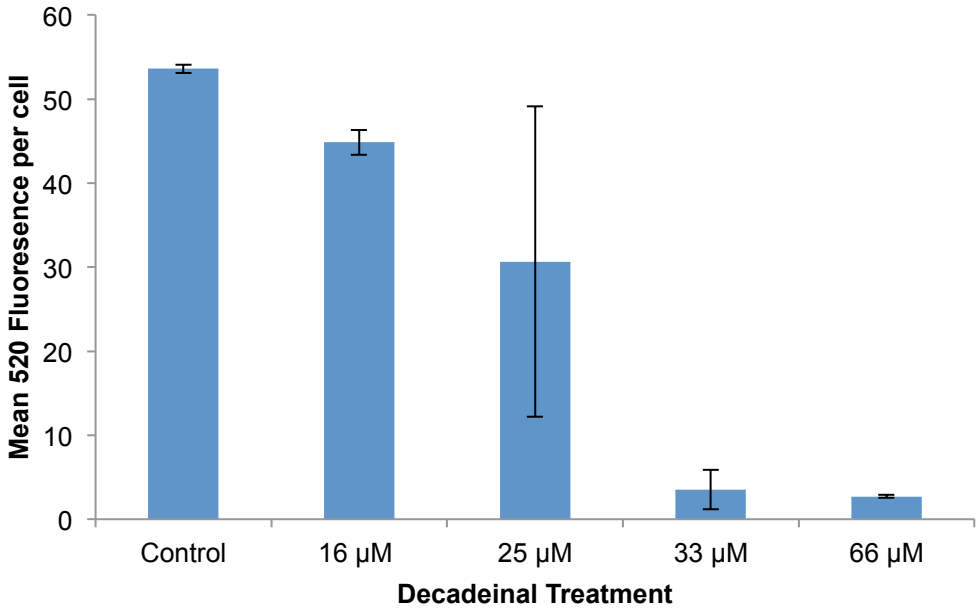

Figure 5.4 DAF-FM DA fluorescence (mean per cell) of *E. huxleyi* CCMP1516 cells treated with various concentrations of the PUA decadienal and an untreated control culture. Values are the mean of n=2 (± s.e.).